Role of glucose and glutamine in lipogenesis in the VM-M3 glioblastoma cell line and the inheritance of brain cardiolipin fatty acid abnormality in the VM/Dk mice

Author: Nathan Ta

Boston College

The Graduate School of Arts and Sciences

Department of Biology

Dissertation

Role of glucose and glutamine in lipogenesis in the VM-M3 glioblastoma cell line and the inheritance of brain cardiolipin fatty acid abnormality in VM/Dk mice

by

Nathan Linh Ta

Submitted in partial fulfillment of the requirements
for the degree of
Doctor of Philosophy

Date

10/28/2014

ABSTRACT

Role of glucose and glutamine in lipogenesis in VM-M3 glioblastoma cell line and the inheritance of brain cardiolipin fatty acid abnormality in VM/DK mice

Nathan L. Ta

Thesis Advisor: Thomas N. Seyfried

Lipids, in all their forms from structural components of the membranes (phosphoglycerides, glycolglycerolipids) to signaling molecules (IP_3, DAG, prostaglandins, etc.,) post-translational modification of proteins (palmitoylated, farnesylated, prenylated, and GPI anchoring) play an essential role in cancer cell survival, proliferation, and metastasis. Alteration in structural lipids can impair transport, and signaling cascades. Abnormalities in lipids, such as cardiolipin (Ptd_2Gro), impair mitochondrial function, bioenergetics, and could play a role in precipitatting the high incidence of spontaneous tumors in VM/Dk mice. This thesis explores the role of glucose and glutamine in their incorporation into lipids in the VM-M3 murine glioblastoma cell line as well as the inheritance of brain cardiolipin fatty acids abnormalities in VM/Dk mice. I used labeled [^{14}C]-U-D-glucose and [^{14}C]-U-L-glutamine to examine the profile of *de novo* lipid biosynthesis in the VM-M3 cell line. The major lipids synthesized included phosphatidylcholine (PtdCho), phosphatidylethanolamine (EtnGpl), phosphatidylinositol (PtdIns), phosphatidylserine (PtdSer), sphingomyelin

(CerPCho), bis(monoacylglycero)phosphate (BMP) / phosphatidic acid (PtdOH), cholesterol (C), Ptd_2Gro, and the gangliosides. The data show that the incorporation of labeled glucose and glutamine into synthesized lipids was dependent on the type of growth environment, and that the VM-M3 glioblastoma cells could acquire lipids, especially cholesterol, from the external environment for growth and proliferation.

In addition, this thesis also explores and evaluates the abnormality of Ptd_2Gro fatty acid composition in VM mice in comparison to B6 mice. Although previously reported, I confirmed the finding in the abnormal cardiolipin fatty acid composition in the VM mice. The abnormal brain cardiolipin fatty acid composition was found to be inherited as an autosomal dominant trait in reciprocal B6 x VM F_1 hybrids for both male and female. Impaired cognitive awareness under hypoxia observed for the VM mice and reciprocal F1 hybrids is associated with abnormalities in neural lipid composition.

Ye shall eat no fat, of ox, or sheep, or goat. And the fat of that which dieth of itself, and the fat of that which is torn of beasts, may be used for any other service; but ye shall in no wise eat of it. For whosoever eateth the fat of the beast, of which men present an offering made by fire unto the Lord, even the soul that eateth it shall be cut off from his people" (Leviticus ***7:23-25).***

DEDICATION

To my parents Peter Ta and Lily Pham for their never ending support not just in my graduate career, but throughout my educational procurement. It was their long hard work and many sacrifices to bring my siblings and me here in America for a better education. I humbly dedicate this work for their love, strength, and sacrifices to make this arduous task a more manageable one. To my brothers and sister, thank you for your support and encouragement through this entire endeavor.

ACKNOWLEDGMENTS

I would like to acknowledge those who have made this possible. First and foremost, I would like to acknowledge Dr. Thomas N. Seyfried for being a mentor and providing guidance in research topics. In his lab, I have learned invaluable skills and techniques that will help me in my future work. I would also like to acknowledge the primary members of my committee: Dr. Thomas Chiles and Dr. Daniel Kirschner for helpful discussion, Dr. Mary Roberts, and Dr. Marc Gubbels for being the additional members of the committee. Additionally, I like to thank Dr. Michael Kiebish in his assistance in the mass spectrometry analysis. Lastly, I would like to thank current and former members of the Seyfried Laboratory, including Dr. Purna Mukherjee, Dr. Rena Baek, Dr. Michael Kiebish, Dr. John Mantis, Karie Heinecke, Jeremy Marsh, Roberto Flores, Zeynep Akgoc, Joshua Meidenbauer, Kevin Santos, and Ashley Brown, as well as many of undergraduates for their friendship and helpful discussion.

TABLE OF CONTENTS

LIST OF TABLES

LIST OF FIGURES

Supplemental Figures

LIST OF ABBREVIATIONS

AA	antimycin
ACLY	ATP citrate lyase
ACC	acetyl CoA carboxylase
AKT	protein kinase B
AL	*ad libitum*
B6	C57BL/6J mouse
BCL-2	B-cell lymphoma 2
BMP	bismonoacylglycerolphosphate
BNIP3	BCL2/adenovirus E1B 19 kDa protein-interacting protein 3
C16:0	palmitoyl or palmitate or palmitic acid
C18:1	oleoyl
C18:2	linoleoyl
C22:6	docosahexaenoyl
CDP-DAG	cytidine diphosphate diacylglycerol
CerPCho	sphingomyelin
$CHCl_3$	chloroform
CH_3OH	methanol
C	cholesterol
CD36	fatty acid translocase
Cer	ceramide
CoA	coenzyme A
CTP	cytidine triphosphate
CDP-DAG	cytidine diphosphate diacylglycerol
DAG	diacylglycerol
DEAE-Sephadex	diethylaminoethanol linked sepharose
DGAT	diacylglycerol acyltransferase
DPM	disintegration per minute
ERK	extracellular signal regulated kinase
ESI/MS	electrospray ionization mass spectrometry
ETC	electron transport chain
EtnGpl	phosphatidylethanolamine
FAME	fatty acid methyl esters
FASN	fatty acid synthase
FBS	fetal bovine serum
FFA	free fatty acid
G-3-P	glycerol-3-phosphate
GD3	alphaNeu5Ac(2-8)aNeu5Ac(2-3)bDGalp(1-4)bDGlcp(1-1)Cer
GBM	glioblastoma multiforme
GLC	gas liquid chromatography
GM3	alphaNeu5Ac(2-3)bDGalp(1-4)bDGlcp(1-1)Cer
GPCR	G-protein coupled receptors
GPI	glycosylphosphatidylinositol

HIF1-alpha	hypoxia inducible factor alpha
HPTLC	high performance thin-layer chromatography
IP3	inositol triphosphate
LC/MS	liquid chromatography/mass spectrometry
LCPUFA	longer chain polyunsaturated fatty acids
LDH-A	lactate dehydrogenase A
LDL	low density lipoprotein
LPL	lipoprotein lipases
lysoPtdOH	lysophosphatidic acid
lysoPtdCho	lysophosphatidyl choline
MAGL	monoacylglycerol lipase
MUFA	monounsaturated fatty acid
NeuAc	N-acetylneuraminic acid
NeuGc	N-glycolyl neuraminic acid
PGC	peroxisome proliferator-activated receptor coactivator
PGE2	prostaglandin E2
PtdOH	phosphatidic acid
PtdCho	phosphatidylcholine
PtdGro	phosphatidylglycerol
Ptd_2Gro	cardolipin
PtdIns	phosphatidylinositol
PL	phospholipids
PPP	pentose phosphate pathway
PtdSer	phosphatidylserine
PUFA	polyunsaturated fatty acid
S1P	sphingosine-1-phosphate
SA	saturated fatty acid
s.c	subcutaneous
SCD-1	steroyl coA desaturase - 1
SCID	severe combined immunodeficient mice
SREPB	sterol regulatory element-binding proteins
TAG	triacylglycerol
UFA	unsaturated fatty acid
uPA	urokinase-type plasminogen activator
uPAR	urokinase-type plasminogen activator receptor
VEGF	vascular epidermal growth factor
VM/DK	VM/DK mouse

CHAPTER ONE

Introduction

Lipids and their metabolism in cancer

Lipids, derived from the Greek word *lipos,* are among the four essential components that make up a cell. Unlike nucleic acids and proteins, lipids do not form secondary or tertiary structures and are not polymeric as seen in polysaccharides. However, the amphipathic properties, of phospholipids, form the lipid bilayers of plasma and organelle membranes. The saturation, unsaturation and chain lengths determine physicochemical properties of the fatty acids. The long hydrocarbon chains can serve as the major energy stores. They also play a major role in cellular signaling and post-translational modification of proteins. Sterols, such as cholesterol, play a major role in the fluidity of the lipid bilayer. All animal and plant cells contain cholesterol in their membranes. Cholesterol and phospholipids are critical for processes such as cell division, besides DNA synthesis, replication, and protein synthesis. Lipid composition of various membranes (plasma, mitochondria, ER, nuclear, lysosomal, etc.) consists of a particular lipid : cholesterol ratio. Moreover, there is specificity to inner or outer leaflets of the membrane or higher content of particular lipids or

cholesterol for a particular membrane type. For instance, plasma and lysosomal membranes consist of the highest content of cholesterol while mitochondria have the least amount of cholesterol, particularly the inner mitochondrial membrane (Colbeau *et al.* 1971, Hackenbrock *et al.* 1980). However, the inner membrane of mitochondria consists of higher mole percentage of Ptd_2Gro in comparison to other membranes (Daum 1985).

There are three principle classes of lipids: glycerophospholipids (Figure 1a), sphingolipids (including glycosphingolipids) (Figure 1b), and sterols (Figure 1c). *De novo* lipid synthesis begins from the transport of mitochondrial citrate to the cytosol to be converted to acetyl CoA. The bifurcation of acetyl CoA into either malonyl CoA or acetoacetyl CoA leads to fatty acid or cholesterol synthesis, respectively (Figure 2). The committed step in the conversion of acetyl CoA to malonyl CoA is carried out by acetyl CoA carboxylase (ACC). Condensation of malonyl CoA with acetyl CoA and repeated condensations with acetyl CoA is carried out by fatty acid synthase (FASN) in the formation of palmitic acid (C16:0). Palmitic acid can either be elongated and/or desaturated to make longer unsaturated fatty acids. Fatty acyl CoA can then be transferred to glycerol-3-phosphate (G-3-P) to form lysophosphatidic acid (lysoPtdOH), and then phosphatidic acid (PtdOH). Although PtdOH is only found in small quantities in the membrane, it represents the precursors for all phospholipid synthesis, as well as triacylglycerol (TAG). PtdOH can either react with cytidine

triphosphate (CTP) to form cytidine diphosphate diacylglycerol (CDP-DAG) or dephosphorylated to diacylglycerol (DAG). DAG serves as the precursor for neutral glycerophospholipids: phosphatidylcholine (PtdCho), and phosphatidylethanolamine (EtnGpl). CDP-DAG serves as the precursor for acidic, anionic glycerophospholipids: phosphatidylserine (PtdSer), phosphatidylinositol, (PtdIns), phosphatidylglycerol, (PtdGro), and cardiolipin (Ptd_2Gro). Sphingolipid synthesis begins with the condensation of serine and palmitoyl CoA to form 3-ketosphingosine. This is the precursor for ceramide (Cer), sphingomyelin (CerPCho), and glycosphingolipids (gangliosides). Alternatively, acetyl CoA can be diverted for cholesterol (C) biosynthesis via the mevalonate pathway (Figure 2).

Structural lipids, such as Ptd_2Gro, located in the inner membrane of the mitochondria membrane, can directly associate with electron transport chain (ETC) enzymes and influence the enzymatic activities. Aberrant Ptd_2Gro content and fatty acid (FA) composition were found in all the tumors that were analyzed (Kiebish *et al.* 2007). Ether lipids, i.e. plasmalogens, are linked to cancer pathogenicity, motility, and growth (Benjamin *et al.* 2013). The bioactive sphingosine-1-phosphate (S1P) stimulates motility, and proliferation through activation of ERK1,2, neovascularization, and the Bcl-2 family (Pyne *et al.* 2010, Abuhusain *et al.* 2013). Ceramides have been shown to be reduced in some cancer cells and they are a critical mediator in tumor cell resistance to apoptosis

(Morad *et al.* 2013) Signaling molecules such as IP_3, and DAG have been widely shown in signaling pathways involving PKC, and G-protein coupled receptors (GPCR). Post-translational modification (i.e. prenylation of Ras GTPases, or GPI anchored of urokinase-type plasminogen activator (uPA) and its receptor (uPAR)) anchors designated proteins to the membranes and is associated with protein activation status and signal transduction (Bergum *et al.* 2012, Gorfe 2010). Glycosphingolipids are components of the cellular membrane that can be shed to the tumor microenvironment and that can influence angiogenesis. On the one hand, GD3 (alphaNeu5Ac(2-8)aNeu5Ac(2-3)bDGalp(1-4)bDGlcp(1-1)Cer) can promote tumor angiogenesis in human gliomas (Alessandri *et al.* 1987, Koochekpour *et al.* 1996), but on the other hand GM3 (alphaNeu5Ac(2-3)bDGalp(1-4)bDGlcp(1-1)Cer) can repress the angiogenic response (Tagami *et al.* 2002, Fujimoto *et al.* 2005, Seyfried *et al.* 2010a) and tumor progression (Song *et al.* 1991, Rebbaa *et al.* 1996, Choi *et al.* 2006, Nakatsuji *et al.* 2001). Levels of expression and distribution of particular glycosphingolipids are associated with the tumor angiogenic properties (Ziche *et al.* 1992, Jennemann *et al.* 1994).

Deregulation of lipid metabolism in cancer is often involved with high expression activity of enzymes involved in the lipid synthesis pathway, i.e., ATP citrate lyase (ACLY), ACC, FASN, and steroyl CoA desaturase –1 (SCD-1) (Menendez *et al.* 2007, Santos *et al.* 2012, Fritz *et al.* 2010, Mason *et al.* 2012, Roongta *et al.*

2011). Overexpression of fatty acid synthase (FASN) and ACLY is considered important in the pathogenesis and the proliferative capacity of the neoplastic cells (Pizer *et al.* 1998b, Pizer *et al.* 1996). Hence, inhibition or silencing of ACLY has been shown to be effective in reducing tumor growth (Hatzivassiliou *et al.* 2005, Bauer *et al.* 2005). Hochkacha proposed the lipogenic benefit of the cancer cells was to improve the redox balance due to the aerobic fermentation phenomenon in cancer cells (Hochachka *et al.* 2002). Lipid oxidative enzymes and pathways have also been linked to the characteristics of cancer phenotypes (Liu 2006, Nomura *et al.* 2010). Monoacylglycerol lipase (MAGL) was found to be higher in the aggressive tumors and thought to maintain the malignant properties by liberating free fatty acid (FFA) from glycerophospholipids in generating lipid mediators, such as prostaglandin E2 (PGE_2) and lysoPtdOH (Nomura *et al.* 2010, Mills *et al.* 2003).

Hypoxia and its influences on lipid metabolism

Typically, non-cancerous proliferating cells, i.e., regenerating liver cells or hematopoietic stem cells proliferate or differentiate in a well defined manner with controlled regulations of their growth. On the other hand, tumor cells proliferate in an uncontrolled manner in such that it can lead to their own demise. The uncontrolled growth can distance the central core of the tumor mass from

oxygen, and nutrients from blood vessels. The limitation of oxygen and nutrients often result in necrotic cell death in the inner core of a tumor mass. Yet, the unintended self-imposed hypoxic environment initiates a major adaptation to the deficient environment by activating hypoxia inducible factor – alpha (HIF1-alpha). Activation of HIF1-alpha mediates transcription of genes to ensure their survival. Among the obvious and well-known activated genes are AKT, glycolytic enzymes, lactate dehydrogenase A (LDH-A) and vascular endothelium growth factor (VEGF) to further enhance the glycolytic activities, formation of new blood vessels and prevention of apoptosis (Semenza *et al.* 1996, Mathupala *et al.* 2001, Alvarez-Tejado *et al.* 2001). HIF1-alpha activation also leads to the reduction of mitochondrial biogenesis via the suppression of peroxisome proliferator-activated receptor coactivator (PGC) and induction of autophagy through a BNIP3 - Beclin-1 dependent mechanism (Zhang *et al.* 2008, Zhang *et al.* 2007, Mazure *et al.* 2009). Hypoxia also induces alteration in glycolyl attachment to E-cadherin that may aide in tumor cell extravasation for metastasis (Koike *et al.* 2004). Other, less well known, but as important effects, are enzymes involving lipid metabolism. Hypoxia induces the activation of FASN through SREPB-1 and AKT dependent mechanisms (Furuta *et al.* 2008). Hypoxia induces the transcription of the sialin gene and enhances the attachment of NeuGc (N-glycolyl neuraminic acid) sialic acid (acquired from the external milieu) to gangliosides in human tumors which are normally attached with NeuAc (N-

acetylneuraminic acid). The ceramide moiety of the ganglioside portion was also found to be modified with decreased level of unsaturation (Yin *et al.* 2010).

Figures

Figure 1.

Three principle classes of lipids: glycerophospholipids (a), sphingolipids (b), and sterols (c). Adapted from the AOCS Lipid Library.

Figure 1

a.

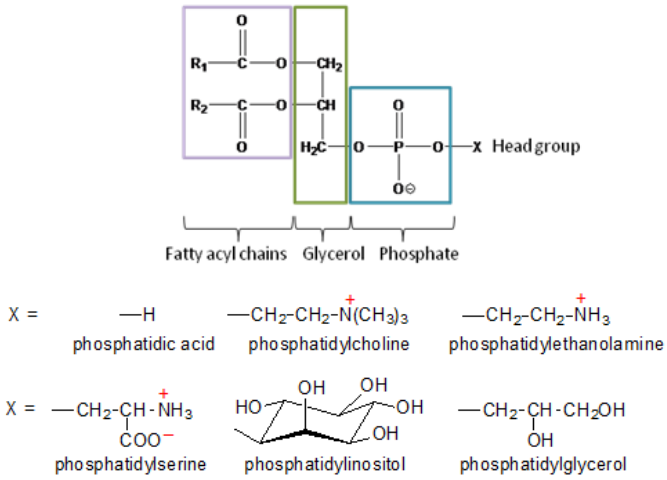
Head group
Fatty acyl chains
Glycerol
Phosphate
X =
—H
phosphatidic acid
—CH2-CH2-N(CH3)3
phosphatidylcholine
—CH2-CH2-NH3
phosphatidylethanolamine
—CH2-CH-NH3
COO−
phosphatidylserine
phosphatidylinositol
—CH2-CH-CH2OH
OH
phosphatidylglycerol

b.

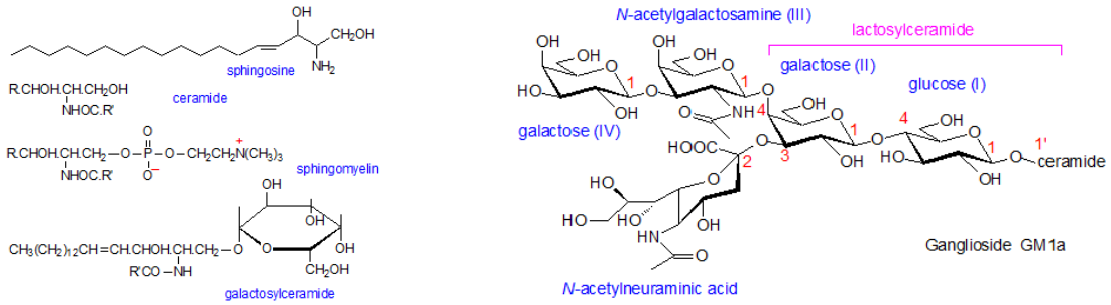
sphingosine
ceramide
sphingomyelin
galactosylceramide
N-acetylgalactosamine (III)
lactosylceramide
galactose (II)
glucose (I)
galactose (IV)
ceramide
Ganglioside GM1a
N-acetylneuraminic acid

c.

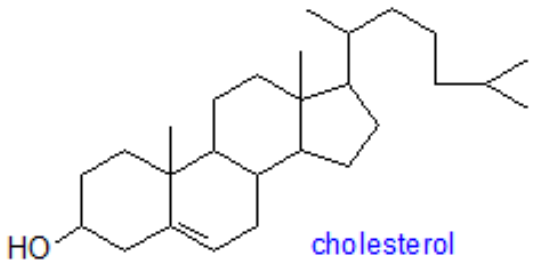
HO
cholesterol

Figure 2.

Schematic diagram of acetyl Co-A derived citrate bifurcated route into synthesis of fatty acid or cholesterol biosynthesis

Figure 2

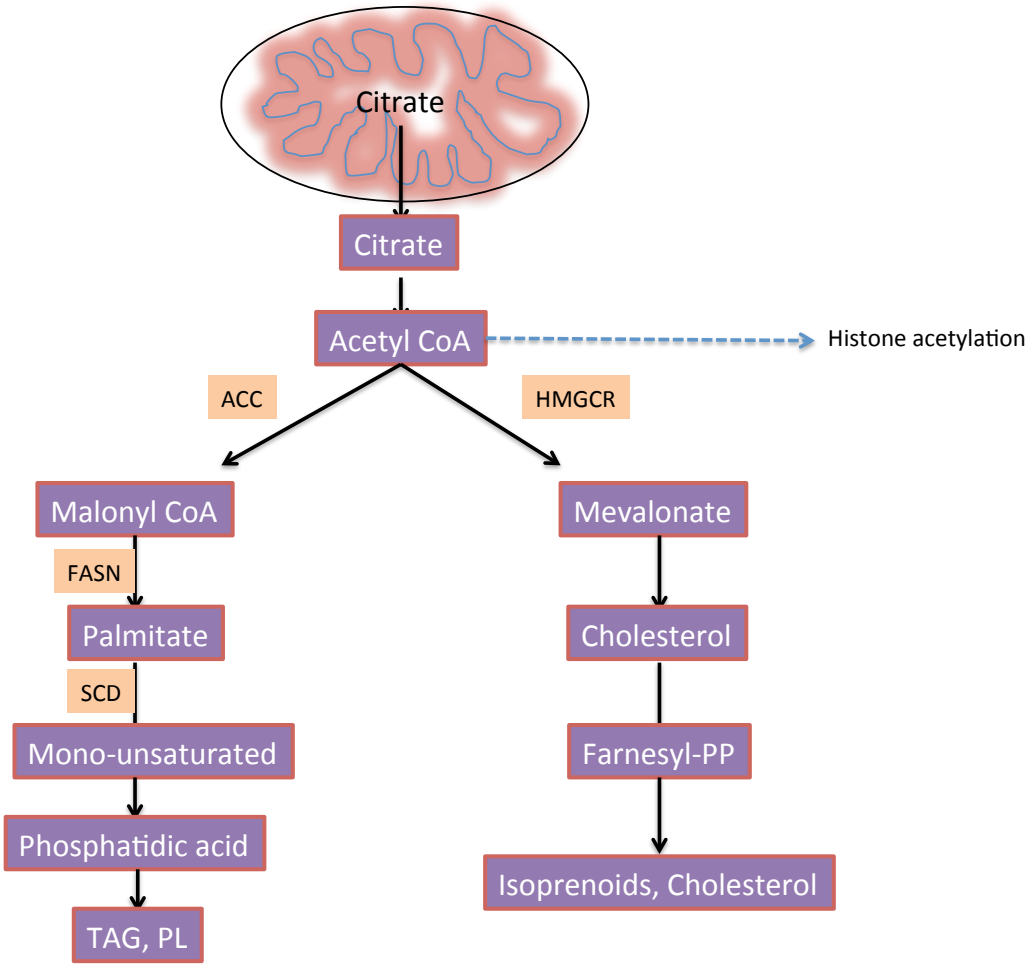
Citrate
Citrate
Acetyl CoA
Histone acetylation
ACC
HMGCR
Malonyl CoA
Mevalonate
FASN
Palmitate
Cholesterol
SCD
Mono-unsaturated
Farnesyl-PP
Phosphatidic acid
Isoprenoids, Cholesterol
TAG, PL

CHAPTER TWO

Influence of serum and hypoxia on incorporation of [^{14}C]-U-D-glucose or [^{14}C]-U-L-glutamine into lipids and lactate in murine glioblastoma cells

Introduction

Glioblastoma multiforme (GBM) is among the most aggressive of all brain tumors that often leads to morbidity and death within 12-15 months despite the best available treatments (Wen *et al.* 2008, Seyfried *et al.* 2014). Malignant gliomas, similar to other tumor types, have aberrant metabolism of glucose and glutamine (Portais *et al.* 1996, DeBerardinis *et al.* 2007). Enhanced glycolytic fermentation in the presence of oxygen (Warburg effect) and glutamine utilization are common metabolic features of glioma cells whether grown *in vitro or in vivo* (DeBerardinis *et al.* 2007, Wolf *et al.* 2010, Maher *et al.* 2012, Qu *et al.* 2012, Gambhir 2002). The conversion of glucose into lactate rather than complete oxidation through the TCA cycle helps in regenerating the NAD+ that is required for production of anabolic intermediates and ATP through glycolysis (Vander Heiden *et al.* 2009, Lunt *et al.* 2011). These metabolic substrates are also involved in the anabolic requirement of lipid biosynthesis in proliferating glioma cells (DeBerardinis *et al.* 2007).

Lipids play an essential role in the survival, proliferation, and metastasis of tumor cells (Park *et al.* 2012, Mills *et al.* 2003, Karmali 1986, Wang *et al.* 2006, Rolin *et al.* 2011, Kamphorst *et al.* 2013, Chang *et al.* 2004, Clendening *et al.* 2010). *Ex vivo* culture of human gliomas showed significant synthesis of choline and ethanolamine plasmalogens, with less synthesis of the structurally complex gangliosides (Yates *et al.* 1979). More recently, tracer studies using [^{13}C] glucose and [^{13}C] glutamine with LC/MS have only evaluated palmitate synthesis (DeBerardinis *et al.* 2007, Scott *et al.* 2011), but not to the synthesis of individual phospholipids or glycosphingolipids (gangliosides).

Lipogenesis in cancer is coupled to glucose and glutamine metabolism

Endogenously synthesized fatty acids can be derived from one of the three precursors: glucose, glutamine, and acetate. Enhanced glucose uptake, first posited by Warburg in 1927 (Warburg *et al.* 1927), has long been accepted and the principle is still being used at the present time to detect tumors *in vivo* by 2-deoxy-2(^{18}F)fluoro-D-glucose – PET imaging. Aerobic glycolysis exhibited in tumor cells is considered as one of the major hallmarks in tumor cell metabolism. The conversion of glucose into lactate rather than coupling it to TCA and ETC, helps in regenerating the NAD+ that is required for continued glycolytic activity (Figure 3). Enhanced glycolytic flux satisfies the demand of ATP due to the

suppression of mitochondria. In addition, it also provides anabolic intermediates for macromolecules synthesis through the generation of nucleotides from the pentose phosphate pathway (PPP) or glycerol-3-P for lipid biosynthesis. As Costello and Franklin pointed out "if bioenergetics were the important metabolic concern of the tumour cells as is often proposed, the 'anoxic glycolytic' pathway would be a costly adaptation (Costello *et al.* 2005). They proposed the enhanced aerobic glycolytic flux could be due to supplying the pool of acetyl CoA for lipogenesis in demand for tumor cells to proliferate

Glutamine can serve as an anaplerotic substrate, in replenishing the TCA cycle intermediates particularly α-ketoglutarate, and oxaloacetate, or be oxidized in generation of ATP. Alternatively, glutamine is not fully oxidized to CO_2, but converted to lactate or alanine by malic enzymes in producing NADPH. This metabolic flux of glutamine metabolism is what considered as glutaminolysis, as proposed by Mckeehan (McKeehan 1982). As early as 1979, Reitzer et al demonstrated that glutamine was used as a major energy source for Hela cells, and not sugar (Reitzer *et al.* 1979). The authors also found a significant portion of glutamine was converted to lactate. Similar observations were put forth by DeBerardinis that 60% of glutamine was metabolized to lactate in SF188 human glioblastoma cell line (DeBerardinis *et al.* 2007). The conversion of glutamine to lactate through cytosolic malic enzymes was hypothesized to synthesize ample

of NADPH to support lipid biosynthesis. Alternatively, glutamine can enter the truncated TCA cycle in which α-ketoglutarate generates and sequentially in generating citrate. Exported citrate to the cytosol is converted to acetyl CoA for FA synthesis and the generation of extramitochondrial malate. This pool of malate can re-enter the mitochondria and be converted back to pyruvate via mitochondrial malic enzyme. Pyruvate is then converted to acetyl CoA and condensed with oxaloacetate to citrate (Figure 3) (Kovacevic *et al.* 1983, Moreadith *et al.* 1984, Piva *et al.* 1998). This also allows the generation of GTP via substrate level phosphorylation. Hence, it is still unclear how glutamine is being fluxed through which pathway.

The misconception: Cancer cells synthesize all their lipids endogenously

The thematic interest in the dependency of tumor cells to endogenously synthesize their own lipids for the sake of proliferation has been misconstrued and misinterpreted. For instance, Weljie et al. express this in their statement referencing a paper from Medes et al. (1953), “Although normal cells (other than in liver and adipose tissue) rarely use *de novo* synthesis, instead acquiring fatty acids from dietary sources, the majority of fatty acids produced by tumor cells are not derived from dietary sources. Indeed, an important observation in this area was made as a result of labeling studies that indicated that *de novo* fatty acid

synthesis was the primary source of tumor lipids, in spite of the availability of exogenous FA pools" (Weljie *et al.* 2011). Similarly, in a Nature Review article published in 2007, Menendez and Lupu cited the same paper, stating "practically all esterified FAs in tumor models were derived from *de novo synthesis"* (Menendez *et al.* 2007). The direct quote in the summary of Medes et al. paper in 1953 concludes otherwise: "A study of lipogenesis in neoplastic tissues has shown that acetate and glucose carbon can be utilized for synthesis of fatty acid chain. However, the data indicate that this process is probably too slow to supply the lipid needs of a rapidly growing tumor, and the tumor must therefore obtain its lipids preformed from the host" (Medes *et al.* 1953). Lipids preformed from the host are primarily triglycerides, free fatty acids, and lipoprotein complexes (cholesterol, cholesteryl esters, and triglycerides). There are tumors, arising from liver, breast, ovary, prostate that exhibit lipogenic phenotype with enhanced lipogenic gene signatures (Beckers *et al.* 2007, Swinnen *et al.* 2006, Milgraum *et al.* 1997, Pizer *et al.* 1996). Inhibition of *de novo* lipogenesis with FASN, ACC inhibitors *in vivo* exerts antitumor effect in rodent models for these tumor types (Alli *et al.* 2005, Kridel *et al.* 2004, Chen *et al.* 2012, Pizer *et al.* 1998a). Ironically, even some of these lipogenic tumor types also have increased expression of lipoprotein lipases (LPL), and CD36. These are enzymes that are related to the uptake of lipids into the cells (Kuemmerle *et al.* 2011). Efficient utilization of FA or LDL requires the expression of CD36 and LPL. CD36

expression was found to be positive in 80% of breast and liposarcoma tumor tissues, and 50% for prostate tumor tissues (Kuemmerle *et al.* 2011).

Our goal here was to examine the influence of fetal bovine serum (FBS), which contains large amounts of lipids (Stoll *et al.* 1984, Rothblat *et al.* 1976) on lipid biosynthesis derived from [^{14}C]-U-D-glucose and [^{14}C]-U-L-glutamine in the metastatic murine glioblastoma cell line (Huysentruyt *et al.* 2008a). Additionally, we evaluated the influence of hypoxia on lipid biosynthesis using uniformly labeled glucose and glutamine. The current study identified an increase in lipid biosynthesis when cells were deprived of FBS. This study also confirmed the high rate of aerobic glycolysis, with high lactate derived from glucose. However, minimal lactate was derived from labeled glutamine. The attenuation of glucose entering the TCA cycle under hypoxia leads to a compensatory increase of glutamine utilization for lipid biosynthesis. In addition, hypoxia induced accumulation of triglycerides and increased the level of saturated and monounsatured fatty acids.

Materials and Methods

Chemicals

[^{14}C]-U-D-glucose was purchased from MP Biomedicals (Fountain parkway, OH), and [^{14}C]-U-L-glutamine was from Perkin Elmer (Boston, Ma). Lipid standards were either purchased from Matreya (Pleasant Gap, PA), Sigma (St. Louis, MO), or from Nu-Chek Prep (Elysian, MN). Antimycin A, Oil Red O, acetyl chloride were from Sigma. Primulin and lipoprotein were from MP Biomedicals. DEAE Sephadex (A-25) for column chromatography was obtained from GE Healthcare (Uppsala, Sweden). HPTLC plates (10 x 20 cm and 20 x 20 cm) were from Merck kGaA (Darmstadt, Germany). All developing solvents are of ACS and HPLC reagent grade, and purchased either from Sigma, or Fisher Scientific (Fair Lawn, NJ).

Origin of VM tumors

VM-M3 microglial tumor cell line arose spontaneously from VM/Dk (VM) mice after routine examination of the colony over a period of 7 years. Specifically, VM-M3 was derived from the cerebrum of an adult VM mouse.

Cell culture and treatment

The VM-M3 glial tumor cell line was established from a mouse of the VM/Dk inbred strain as previously described (Huysentruyt *et al.* 2008b). Cells were grown in Dulbecco's modified Eagle medium (DMEM) (Sigma, St. Louis MO) with glucose (25 mM) and glutamine (4 mM) and 50 µg/ml penicillin/streptomycin (Sigma). 10% fetal bovine serum (FBS) (Hyclone Thermo Scientific, Waltham, MA) was supplemented where indicated. All cells were cultured in a humidified incubator containing 5% CO_2 at 37^0C. Cells were either grown in the presence or absence of 10% FBS as well as under normoxia (21% O_2) or under 0.1% O_2 (hypoxia) using hypoxic chamber (Biospherix) equilibrated with N_2. Cells were seeded equally in 150 x 25 mm culture dishes and were cultured for 48 hrs in medium containing either 0.15 mCi/mL [^{14}C]-U-D-glucose or [^{14}C]-U-L-glutamine, both at final concentration of 0.05 µmol/ml. The cells were collected, rinsed with PBS, and counted by trypan blue dye exclusion before lipid extraction.

Lipid isolation, purification, and quantification

Neutral lipids, acidic lipids, and gangliosides were isolated and purified from lyophilized cell pellets by modified procedures previously described (Seyfried *et al.* 1978, Baek *et al.* 2004). Briefly, total lipids were extracted with chloroform ($CHCl_3$) and methanol (CH_3OH) 1:1 vol/vol. Neutral and acidic lipids were

separated using DEAE-Sephadex column chromatography as previously described (Macala *et al.* 1983, Kasperzyk *et al.* 2005). The total lipid extract, suspended in $CHCl_3$:CH_3OH:dH_20, 30:60:8 by volume (solvent A), was applied to a DEAE-Sephadex column (1.2 mL bed volume) that had been equilibrated prior with solvent A. Neutral lipids were eluted with two 20 ml washes of solvent A. The acidic lipids and gangliosides were eluted from the column with 35 mL $CHCl_3$:CH_3OH: 0.8 M sodium acetate, 30:60:8 by volume (solvent B). Gangliosides were separated from acidic lipids as previously described (Seyfried *et al.* 1978, Kasperzyk *et al.* 2004, Macala *et al.* 1983).

Individual lipids were separated by high performance thin-layer chromatography (HPTLC) according to previously described methods (Macala *et al.* 1983). For neutral and acidic phospholipids, the plates were developed to a height of 4.5 cm or 6.0 cm, respectively with chloroform: methanol: acetic acid: formic acid: water (70:30:12:4:2 by volume), and developed to the top with hexanes: diisopropyl ether: acetic acid (65:35:2 by volume). For gangliosides, the plates were developed using chloroform: methanol: 0.02% aqueous calcium chloride (55:45:10 by volume). Radiolabeled lipids were developed using Kodak Phosphor screen and visualized using Phosphoimager STORM 820 (GE Healthcare) and quantitated by densitometric determination with ImageQuant TL software. Total non-labeled lipids were visualized by charring with 3% cupric acetate in 8% phosphoric acid solution, followed by heating in an oven at 165^0 C

for 7 min for neutral and acidic lipids. Total non-labeled gangliosides were visualized by spraying the plates with resorcinol-HCL reagent, followed by heating at 100^0 C for 10 min.

Distribution and quantification of total and radiolabeled lipids

The distribution of total and radiolabeled lipids was determined after densitometric determination of individual lipids that has been resolved by HPTLC using ImageQuant TL. The percent distribution of an individual lipid was calculated and displayed as the mole percent of that lipid to the entire compilation of lipids in neutral, acidic lipids, and ganglioside fractions. The disintegration per minute (dpm) value of newly synthesized lipids was determined by liquid scintillation counting in 7 mls of Ecosint A with the Tri-Carb liquid scintillation counter (Perkin Elmers). The amount of ^{14}C incorporation into each individual lipid was determined by applying the PhosphorImager determined percentage distributions mulitiply by the total scintillation counter estimations of total radioactivity present in the neutral, acidic, or ganglioside fractions.

Preparative HPTLC, gas liquid chromatography (GLC) and ESI/MS analysis of triacylglycerols (TAG)

Neutral lipid fractions were isolated as described above. The entire neutral lipid fraction was used for preparative high performance thin-layer chromatography (10 x 20 cm) to separate triglycerides from phospholipids, and cholesterol. The plate was developed in a single solvent system containing hexanes: diethyl ether: acetic acid (70:30:1). A purified TAG standard (Sigma) was used to identify the TAG band from samples. Lipids were visualized by spraying the plate with 0.05% primulin (80:20 acetone: water vol/vol). The TAG fraction was scraped from the plate and trans-esterified with acetyl chloride in methanol (1:50 by volume) for 45 min in a sealed boriscilicated glass tube under nitrogen at 90^0 C. Gas chromatography (HP 6890) equipped with flame ionization detector and splitless injector was used for the quantitative analysis of the fatty acid methyl esters. The fatty acids were resolved using a 30 m x 0.25 mm x 0.25 μm Omegawax 250 fused silica capillary column (Supelco). The temperature program increased from 150^oC to 220^0C at 2^oC per minute and was held constant at 220^0C for 20 min.

ESI tandem mass spectrometry was carried out with the help of Dr. Kiebish at Berg Diagnostics. Briefly, lipids were extracted with a modified Bligh and Dyer procedure, and analyzed using AB SCIEX 5600+ TripleTOF mass spectrometry.

Lactate measurement

Lactate was analyzed from the culture media. L-lactate (Sigma) was used to confirm the lactate band by visualizing it with bromocresol green. An equal amount of media (250 µl) was lyophilized and re-suspended in 60 µl of methanol and spotted on HPTLC (20 x 20 cm). The plate was developed in a single solvent system with butanol: acetic acid: water (50:11:25 by volume) for 5 hours. Autoradiography visualization and densitometric scanning were performed as previously described.

Oil Red O staining for triacylglycerols

A 0.7% solution of Oil Red O in a 2-propanol stock solution was diluted with water (3:2, v/v) and filtered before use. Cells were grown directly on slide cover slips embedded inside a culture dish (100 x 20 mm) (BD Falcon). Cells were either grown in atmospheric oxygen (21% O_2), 0.1% O_2, or 0.1 µM antimycin (AA). Cells were then washed with PBS, fixed for 5 min with 3.7% paraformaldehyde in PBS, and incubated with Oil Red O for 20 min. Cells were rinsed 3 x with PBS before visualization using phase contrast microscopy (Zeiss Axioplan 2.)

Determination of triacylglyerol content in subcutaneous implanted VM tumor

VM-M3 tumor fragments were diced in cold PBS at pH 7.4. VM male mice (3 months of age) were anesthesized with isoflurane (Halocarbon, NJ) and 0.1 ml of the diced tumor tissue was implanted subcutaneously (s.c.) in the left flank using a 1 cc tuberculin syringe and 18-gauge needle. The inoculated mice were housed together with free access to food and water. After a period of 30 days, tumors were removed from the flank and sliced into three distinct areas of the tumor designated as inner, middle, and outer core of the tumor. Each of the three regions of the tumors from three different mice was subjected to lipid isolation in determining the triacylglycerol content.

Statistical analysis

Interquartile range was used as error bars in experiments with only two samples. Otherwise, the two-tailed *t* test or ANOVA was used to calculate statistical significance using SPSS version 21. A *p* value of less than 0.02 was considered to be significant.

Results

Influence of FBS on lipid distribution and incorporation of [^{14}C]-U-D-glucose and [^{14}C]-U-L-glutamine in VM-M3 glioblastoma cells

Neutral Lipids

The influence of FBS on the relative distribution of total neutral lipids in the VM-M3 cells, visualized with HPTLC charring, is shown in Table 1 and Figure 3 (the charring of the HPTLC was done after visualization of radioactive lipids). The data showed that the relative distribution of all major lipids was similar with two samples from either labeled glucose or labeled glutamine. Hence the data was combined to only show FBS as the experimental factor.

The relative distribution of all neutral lipids was similar in the presence or absence of FBS (Table 1, Figure 4). Cholesterol comprised ~ 27% of the total lipids. EtnGpl, and PtdCho, represented ~ 21% individually of the total lipids, while CerPCho was at ~ 10%, Cer, and TAG ~ 6% each. LysoPtdCho was only minimally detected.

FBS had a major influence on *de novo* neutral lipid biosynthesis and distribution using labeled carbons from either glucose or glutamine (Table 2, Figure 5, Figure 6).

The incorporation of either glucose or glutamine carbons into the neutral lipids was markedly greater in the absence (8100 ± 931 dpm, and 4574 ± 44 dpm) than in the presence of FBS (4574 ± 44 dpm and 2557 ± 131 dpm, respectively) (Table 2). While cholesterol comprised ~ 27% of the total neutral lipids in the presence or absence of FBS (Table 1), cholesterol comprised only ~ 8% and 10% of the neutral lipids synthesized from labeled glucose or glutamine, respectively, in the presence of FBS (Figure 4, Figure 5). Cholesterol synthesis increased to about 14% and 12%, respectively, in the absence of FBS. These findings indicate that cholesterol could be obtained exogenously from the FBS and that cholesterol synthesis increased in the absence of FBS. PtdCho represented ~ 21% of the total neutral lipid distribution (Table 1), but increased to ~ 38% of the radiolabeled neutral lipids (Figure 4, Figure 5). The relative distribution of the other radiolabeled neutral lipids was similar to their distribution in the total neutral lipid fraction, but overall synthesis was greater in the absence than in the presence of FBS using either glucose or glutamine carbons.

Acidic Lipids

Similar to neutral lipids, relative distribution of total acidic lipids was similar in the presence or absence of FBS (Table 3, Figure 7). PtdSer comprised of c.a. 38.0% of the total acidic lipids, while PtdIns was comprised at c.a. 32%, Ptd_2Gro at c.a. 10%, followed by BMP/PtdOH at c.a. 8%, and PtdGro at c.a. 4%. FBS also had a major influence on *de novo* acidic lipid biosynthesis using labeled carbons from either glucose or glutamine (Table 4, Figure 8, Figure 9). The incorporation of either glucose or glutamine carbons into the acidic lipids was markedly greater in the absence (4721 ± 337 dpm, and 3077 ± 128 dpm,) than in the presence of FBS (3247 ± 301 dpm and 1667 ± 71 dpm, respectively) (Table 4). Similar to total lipids, PtdIns and PtdSer were the major acidic phospholipids expressed in the VM-M3 cells (Figure 8). Lower amounts of Ptd_2Gro, BMP/PtdOH, and PtdGro were also synthesized. Despite the overall increased synthesis of the individual acidic lipids in the absence of FBS, the relative distribution of these lipids was similar in the presence or absence of FBS, with a minor reduction of PtdOH/BMP, and PtdSer in the absence of FBS (Figure 8).

Overall, the incorporation of either glucose and glutamine carbons into both neutral and acidic lipids was greater in the absence than in the presence of FBS. In addition, lipid biosynthesis using glucose carbons is about 2-fold greater than biosynthesis using glutamine carbons (Figure 10).

Gangliosides

The relative distribution of total gangliosides was similar in the presence or absence of FBS (Table 5, Figure 11). Gangliosides GD1a, GM1, and GM2 were the three major species present in both the non-labeled and the labeled lipid fractions (Figure 11, Figure 13). The distribution of these gangliosides was similar in the presence or absence of FBS for both total and radiolabeled lipids (Table 5, Figure 12) but total radiolabeling was greater using carbons from glucose than from glutamine (Table 6). This observation is expected in gangliosides since the carbons from glucose can be incorporated into the carbohydrate, sphingosine, and fatty acids of gangliosides, whereas the carbons from glutamine will be incorporated largely into the fatty acyl components of these lipids.

Influence of FBS on lactate production from radiolabeled glucose or glutamine carbons

The lactate produced in the VM-M3 cells was derived largely from glucose in either the presence or absence of FBS (Figure 14 A, B). However, lactate production from glucose was less in the absence than presence of FBS suggesting a diversion of glucose carbons from lactate synthesis to lipid

synthesis. Only minor amounts of lactate were derived from labeled glutamine carbons in either the presence or absence of FBS. These findings indicate that glutamine carbons contributed very little to the lactate pool in these cells.

Influence of hypoxia on lipid distribution and incorporation of [^{14}C]-U-D-glucose and [^{14}C]-U-L-glutamine in VM-M3 glioblastoma cells

Neutral Lipids

The influence of hypoxia on total neutral lipids in the VM-M3 cells is shown in Figure 15. In order to visualize qualitative changes of lipids, particularly triacylglycerols and cholesterol, under hypoxia, an equal amount of disintegration per minute (dpm) were spotted on the HPTLC plate for comparison. Here, approximately 3000 dpm were spotted for the neutral lipids, rather than equal number of cells. However the calculated dpm as shown in Table 7 is normalized to the same number of cells.

The incorporation of carbons from labeled glucose into neutral lipids was significantly lower under hypoxia (0.1% O_2) (4038 ± 43 dpm) than under normoxia (21% O_2) (6904 ± 370 dpm) (Table 7). However, the opposite was seen for the synthesis of neutral lipids from labeled glutamine under hypoxia. The incorporation of carbons from glutamine increased two folds (from 3154 ± 92 dpm to 6258 ± 338 dpm).

Hypoxia induced accumulation of triacylglycerols (TAG) in the neutral lipid fraction, which represented a significant amount of the lipid distribution (Figure

16). TAG accumulation was seen in both total lipids (Figure 15), and the labeled lipids (Figure 17) derived from either glucose or glutamine. Additionally, hypoxia significantly reduced the incorporation of carbons into cholesterol derived from both labeled glucose and glutamine (Table 7, Figure 16). Incorporation of carbons from either labeled glucose or glutamine into PtdCho and EtnGpl was noticeably lower under hypoxia than normoxia (Figure 16).

Acidic Lipids

The influence of hypoxia on total acidic lipids in the VM-M3 cells is shown in Figure 18. Similar to the neutral lipids, approximately 3000 dpm was spotted on the HPTLC plate for acidic lipids, and the calculated dpm in Table 8 is normalized to same number of cells. The incorporation of carbons from labeled glucose into acidic lipids was significantly lower under hypoxia (313 ± 8 dpm) than under normoxia (1568 ± 94 dpm) (Table 8). Again, the opposite was seen for the synthesis of acidic lipids from labeled glutamine under hypoxia. The incorporation of carbons from glutamine increased not to the extent seen in neutral lipids but still significantly higher from 717 ± 13 dpm to 829 ± 38 dpm. Hypoxia induced a reduction in the distribution of PtdSer, and BMP/PtdOH, but slightly increased PtdGro and PtdIns. No changes were observed under hypoxia for Ptd_2Gro using either labeled glucose or glutamine (Figure 19, Figure 20).

Overall, the incorporation glucose carbons into both neutral and acidic lipids were significantly less under hypoxia in comparison to normoxia. Conversely, the incorporation of glutamine carbons into both neutral and acidic lipids was significantly higher under hypoxia (Figure 21).

Gangliosides

The influence of hypoxia on total gangliosides in the VM-M3 cells is shown in Figure 22. For gangliosides approximately 2000 dpm was spotted on HPTLC plate. The incorporation of carbons from labeled glucose into gangliosides was significantly lower under hypoxia (2115 ± 45 dpm) than under normoxia (3341 ± 82 dpm) (Table 9). There was no change in the incorporation of carbons from glutamine. Hypoxia may have influenced the biosynthesis and distribution of either GM1 or GM2, but it is unclear which species was being modified due to poor separation (Figure 23). Future analysis using [^{14}C] galactose could resolve this issue since galactose can be better incorporated into gangliosides.

Influence of hypoxia on lactate production from radiolabeled glucose or glutamine carbons

Hypoxia enhanced the incorporation of glucose carbons into lactate. Minimal lactate was derived from glutamine under hypoxia even though there was enhanced glutamine utilization for lipid biosynthesis (Figure 24 A, B). The increase of glutamine utilization for lipid biosynthesis could be a compensatory response to the enhanced conversion of glucose into lactate.

Hypoxia induced accumulation of triacylglycerols with increased saturated fatty acids

Significant accumulation of TAG was seen in both total and labeled lipids for cells grew in hypoxia (Figure 15, Figure 17, Figure 25). Oil red O staining confirmed the accumulation of lipid droplets in the cells (Figure 26 C, D). Re-oxygenation of the cells for 24 hrs reduced the TAG that had accumulated during the 24hrs incubation under hypoxia (Figure 25). The respiratory inhibitor antimycin A (AA) also induced TAG accumulation (Figure 25) and the appearance of lipid droplets (Figure 26 E, F) similar to those seen under hypoxia. Although both hypoxia and AA treatment induced TAG accumulation, the FA composition of TAG differed under the two conditions. The TAG that accumulated under hypoxia migrated as

double bands on HPTLC plate, whereas the TAG that accumulated under AA treatment migrated only as a singlet (Figure 25). Longer and/or saturated FA migrated with higher Rf distance while shorter and/or unsaturated FA migrates with smaller Rf distance on HPTLC plate. Further analysis using ESI tandem mass spectrometry further confirmed triglyceride accumulation in cells treated with hypoxia (Suppl. S1). Data from ESI/MS also indicated a higher preponderance of shorter, saturated FA. However, we were unable to identify the specific fatty acids that were elevated. Henceforth, preparative HPTLC and GLC analysis were used to analyze the fatty acid composition of the lower (slower) and upper (faster) migrating bands of the TAG that accumulated under hypoxia. FA accumulation was greater in the upper than in the lower TAG band (Table 10). The proportion of saturated FA (C16:0, and C18:0) was greater in the upper TAG band than in the lower TAG band, whereas the proportion of unsaturated FA (C16:1) was less in the upper band than in the lower band, as indicated in Table 11. Interestingly, the molar percent distribution of C18:1 was similar in the upper and lower bands.

The relative distribution of the upper and lower TAG bands under hypoxia differed depending whether TAG was evaluated from the total lipids (Figure 15) or from the radiolabeled lipids (Figure 17). In contrast to the higher intensity of the lower TAG band in comparison to the upper TAG band in the total lipids (Figure 15), the intensity of the lower bands were either similar or higher than the

upper bands in the TAG derived from radiolabeled lipids (Figure 17). This finding suggested that saturated FA (derived from labeled glucose or labeled glutamine) were preferentially synthesized under hypoxia. On the other hand, the TAG FA composition obtained from the total lipids contained more of the unsaturated species, as indicated by the higher intensity in the lower band of the doublet

In vivo accumulation of triacylglycerol in subcutaneous implanted VM tumor

VM-M3 tumor was implanted subcutaneously (s.c.) in VM mice for the duration of 30 days. A small tumor fragment from three sagital cross sections were obtained for triacylglycerol determination. The outer section of the tumor comprised the least amount of TAG (1.5 ± 0.3 ug lipid/ 100 mg of dry tumor weight) in comparison to the middle region (2.1 ± 0.6 ug lipid/ 100 mg of dry tumor weight). The most inner region of the tumor accumulated the most TAG (3.5 ± 0.5 ug lipid/ 100 mg of dry tumor weight) (Figure 27).

Lipoprotein is required for VM-M3 cell viability and growth in the absence of FBS and under hypoxia

Preliminary assessment of viability and growth was analyzed for VM-M3 cells growing in the presence or absence of FBS under hypoxia (Suppl. S2). In the

presence of FBS and under hypoxia, cell viability and proliferation was higher compared to cells grown in the absence of FBS and under hypoxia. In addition, there was an increase in ceramide in cells growing in media without FBS and under hypoxia (Suppl. S3). The increase in ceramide has been implicated in a variety of physiological conditions including apoptosis and cell growth arrest. The supplementation of media with 5 mg/dL of lipoproteins, which primarily contain cholesteryl esters and cholesterol (data not shown), allowed cells to proliferate under hypoxia at a rate similar to cells growing in media containing 10% FBS under hypoxia.

Discussion

Interest is growing in the role of glucose and glutamine in cancer metabolism. These energy metabolites are thought to contribute to anabolic growth, and synthesis of ribonucleotides, nonessential amino acids, and NADPH. (Cairns *et al.* 2011, Yuneva 2008, Teicher *et al.* 2012, Vander Heiden 2011, Dang *et al.* 2011, Rodriguez-Enriquez *et al.* 2009, Piva *et al.* 1998, Souba 1993, Moreadith *et al.* 1984, Lu *et al.* 2010, Meng *et al.* 2010). Although prior studies have evaluated the contribution of glucose and glutamine to palmitate synthesis (C16:0) (DeBerardinis *et al.* 2007, Scott *et al.* 2011), no prior studies have examined the contribution of glucose and glutamine carbons to the total lipid profile in cancer cells. In the current study, I conducted a full analysis of the lipid profile in a murine glioblastoma cell line using uniformly labeled [^{14}C]-U-D-glucose and [^{14}C]-U-L-glutamine. Both the total lipids and radiolabeled lipids were evaluated.

Previous studies suggested that neoplastic cells synthesize all of their FA endogenously, even in the presence of an exogenous source of dietary lipids (Ookhtens *et al.* 1984). Various hypotheses posited that the dependency of cancer cells on lipogenesis was due to heightened expression of ACLY, ACC, and FASN lipids (Weljie *et al.* 2011, Menendez *et al.* 2007, Zhang *et al.* 2012, Vazquez-Martin *et al.* 2008, Hatzivassiliou *et al.* 2005). There is accumulating

evidence, however, showing that tumor cells do not rely solely on endogenous FA biosynthesis for growth and proliferation.

Our findings show that FBS, an exogenous lipid source, has a major impact on the incorporation of glucose and glutamine into lipids. Lipids derived from exogenous sources can be as important for tumor cell growth as are those synthesized endogenously. It was previously reported that mouse derived NeuGc containing gangliosides were found in U87 human glioma cell line, when grown as a xenograft in a SCID mouse and only minimally found when grown *in vitro* (Ecsedy *et al.* 1999). The authors concluded that the NeuGc containing gangliosides were obtained from the host. Recently, Normura's group showed that multiple cancer cell lines could incorporate palmitate into phospholipids and signaling lipids (LPA, DAG, ceramide-1-P) (Louie *et al.* 2013). In addition, Kuemmerle et al. described high expression of CD36 and LPL *in vivo* in multiple tumor cell types. CD36 and LPL facilitate the uptake of extracellular FA into the cell (Kuemmerle *et al.* 2011). In light of this confusion surrounding the contribution of endogenous and exogenous sources to cancer cells, it is important to delineate the contribution of exogenous FA sources to cancer cell lipid metabolism. Furthermore, this confusion will require a re-examination and re-evaluation of the therapeutic strategies that target lipid biosynthesis (e.g. ACLY) for tumor management.

My data showed that glucose was the preferred substrate under normoxia for lipid biosynthesis in comparison to glutamine even though a significant amount of glucose was being converted to lactate. Whereas in hypoxia, the utilization of glutamine into lipid biosynthesis is increased by 2 fold, nearing the level of glucose incorporation into lipids under normoxia. This is in agreement with previous reports showing enhanced utilization of glutamine for lipid biosynthesis under hypoxia. This may occur through the reductive carboxylation of glutamine derived α-ketoglutarate to citrate (Metallo *et al.* 2012, Filipp *et al.* 2012, Wise *et al.* 2011).

There are also suggestions that glutamine can be converted to lactate through malic enzyme to also produce NADPH for lipid biosynthesis (DeBerardinis *et al.* 2007). However, we detected only minimal amounts of lactate being derived from glutamine. My findings are consistent with the previous reports (Portais *et al.* 1996, Scott *et al.* 2011). Enhanced glutaminolysis in generating NADPH can still occur through the conversion of pyruvate to alanine through the transamination reaction. However, Scott et al. have investigated the flux of [^{13}C]-U-D-glucose and [^{13}C]-U-D-glutamine to lactate and alanine, and found only one of six melanoma samples analyzed produced an excess of alanine with minimal production of lactate (Scott *et al.* 2011). Inherently, this could be a cell line specific phenomenon similar to that of Hela cells, where it is estimated that 13% of glutamine was converted to lactate (Reitzer *et al.* 1979). Although glutamine is

a major metabolite for some cell lines including lung, ERB2+ breast or AKT transformed cancer cell lines (van den Heuvel *et al.* 2012, Fan *et al.* 2013, McGuirk *et al.* 2013), it is unclear if the lactate produced in these cells is derived largely from glutamine. It appears that glutamine carbons are not likely a major contributor to lactate production in tumor cells

It is well documented that hypoxia can increase glycolysis (Semenza 2007, Semenza *et al.* 2001, Dang *et al.* 1999). However, the increase in triglyceride accumulation under hypoxia was unexpected. Under hypoxia, FAs cannot be oxidatively metabolized and therefore accumulate as triacylglycerol (TAG). TAG accumulation was present in both total lipid and labeled lipids derived from [^{14}C]-U-D-glucose and [^{14}C]-U-D-glutamine when cells were grown under hypoxia. The diversion of FA into triglycerides under hypoxia is presumably an adaptation for cells to prevent toxic accumulation of free fatty acid. Free fatty acids accumulation in non-adipogenic cell types can lead to lipotoxicity and cell death. Cytoplasmic palmitate can inhibit lipophagy and induce apoptosis (Liu *et al.* 2013, Singh *et al.* 2012). Indeed, palmitate represents approximately 50 mole percentage of FA in the TAG that was accumulated inside cells grown under hypoxia. The presence of TAG was also confirmed in the inner region of the tumor when VM-M3 was grown subcutaneously in the VM/Dk mice. *Ex vivo* ^{1}H-NMR and *in vivo* ^{1}H MRS revealed the presence of TAG in high-grade glioblastomas whereas it was absent in normal brain spectra, and high levels of

lipid droplets are associated with tumor aggressiveness in human brain tumors (Tugnoli *et al.* 2001, Opstad *et al.* 2007).

Interestingly, there was no difference in the mole percent distribution of C18:1 from the upper band to the lower band in the accumulated TAG under hypoxia. Since 18:1 is one of the predominant FA in glycerophospholipids, and is also the predominant FA in FBS (personal observation), it is possible that much of the C18:1 that was accumulated in the TAG was derived from the serum used in the media. It also has been shown recently that Ras transformed cells scavenge predominantly C18:1 LPC to support growth (Kamphorst *et al.* 2013).

In addition, hypoxia also reduced *de novo* synthesis of cholesterol. Cholesterol, synthesized through the mevalonate pathway, similar to SCD-1, requires oxygen as the electron acceptor (Figure S4) (Bloch 1965, Nguyen *et al.* 2007, Summons *et al.* 2006). Cholesterol was also observed to have the highest fold increase when serum was absent from the media. My preliminary data also indicated that cholesterol supplementation in the form of lipoprotein is crucial for cellular viability and proliferation under hypoxia when FBS is absent from the media. It can therefore be concluded that cholesterol becomes the essential component for tumor cells to proliferate both under normoxia and hypoxia and it can be acquired from the extracellular environment.

Hypoxia also influences the distribution of gangliosides. Although due to poor HPTLC separation of the gangiosides, there was a consistent reduced intensity in the lower band of the GM1/GM2 gangliosides. In addition, narrowing of the GD1a bands can also suggest an alteration in gangliosides. Yin et al. have also found changes in mobility of gangliosides under hypoxia in Caco-2M colonic cancer cells and attributed it to the decrease of unsaturated very long chain fatty acid in the ceramide moiety. Further studies using [^{14}C] galactose will help resolve this issue, since it is readily incorporated into gangliosides

In view of our findings and others showing that exogenous fatty acids can be obtained from the FBS (*in vitro)* or host serum (*in vivo)*, it is unlikely that mono-therapeutic targeting of FASN or ACLY alone will be an effective therapy for managing tumor cell growth. A more effective approach would be to target availability of glucose and glutamine. The restriction of these metabolites would not only inhibit synthesis of NADPH and nucleotides through the PPP pathway, but would also inhibit ATP production through glycolysis. The inhibition of lipogenic processes provides an additional layer of protection of other metabolite contributions into lipid biosynthesis, i.e. acetoacetate. The involvement of lipin and diacylglycerol acyltransferase (DGAT) in triglyceride biosynthesis could be a potential target for solid tumors with hypoxic regions. Hypoxia also enhances import of unsaturated FA and cholesterol due to the cell's inability to synthesize

those molecules. This property can also be further exploited for tumor management.

My findings would also question the use of statins and cholesterol targeting as a cancer therapy, as the tumor cells will likely acquire cholesterol from the microenvironment thereby circumventing cholesterol-lowering drugs. Therapeutic approaches should be aimed at both the endogenous and the import pathways. The effectiveness of statins *in vitro* may be related to the inhibition of isoprenoid biosynthesis and protein modifications of Ras or Rho (prenylation, farnesylation, geranylgeranylation) in cancer, and not likely because of the inhibition of cholesterol biosynthesis (Bouterfa *et al.* 2000, Bifulco 2005, Zhong *et al.* 2005). However, human clinical trials using statins as anticancer treatment were largely heterogeneous, inconclusive, and produced little evidence of a real efficacy as adjuvant therapy (Thibault *et al.* 1996, Larner *et al.* 1998, Kim *et al.* 2001, Lersch *et al.* 2004). My results can provide insight on these issues.

In conclusion, cancer therapeutic interventions that target lipid biosynthesis must take into consideration not only the endogenous pathway, but also the import pathway of acquiring exogenous lipids.

Summary

Overall, my findings indicated that the murine VM-M3 glioblastoma cell line could acquire lipids from the extracellular environment. This is in agreement with the original work done by Medes et. al in the 1950's and is in opposition to the popular view of lipogenesis in cancer, which considers lipid synthesis in cancer cells as self sufficient. In other words, cancer cells preferentially synthesize their own fatty acids even in the presence of exogenous lipids. The data shown here indicate that the VM-M3 glioblastoma cells could acquire lipids, especially cholesterol, from the external environment for growth and proliferation, particularly under hypoxia where a limited amount of cholesterol is synthesized.

While glucose carbons are preferentially used and incorporated into lipids under normoxia, glutamine carbons are preferentially incorporated into lipids under hypoxia. This is due to the enhanced conversion of glucose into lactate rather than entering the TCA cycle. The enhanced incorporation of glutamine carbons into lipids under hypoxia corroborates other methods of analysis using ^{13}C labeled substrates in human glioblastoma and melanoma cell lines.

Current work described here also provides a better overview of endogenously synthesized lipids including glycerophospholipid, cholesterols, triacylglycerols, and gangliosides derived from [^{14}C]-U-D-glucose and [^{14}C]-U-D-glutamine. The

unnatural cell culture environment can also significantly influence the amounts and types of lipids synthesized from glucose and glutamine carbons.

In addition, in the model of murine glioblastoma that was examined in this study, lactate is largely derived from glucose and not from glutamine. A brief summary depicting the relative incorporation of glucose and glutamine into lipids and lactate is presented in Figure 28 A, B.

Tables and Figures

Figure 3.

Glucose and glutamine metabolism converge at citrate for lipid synthesis.

Figure 3.

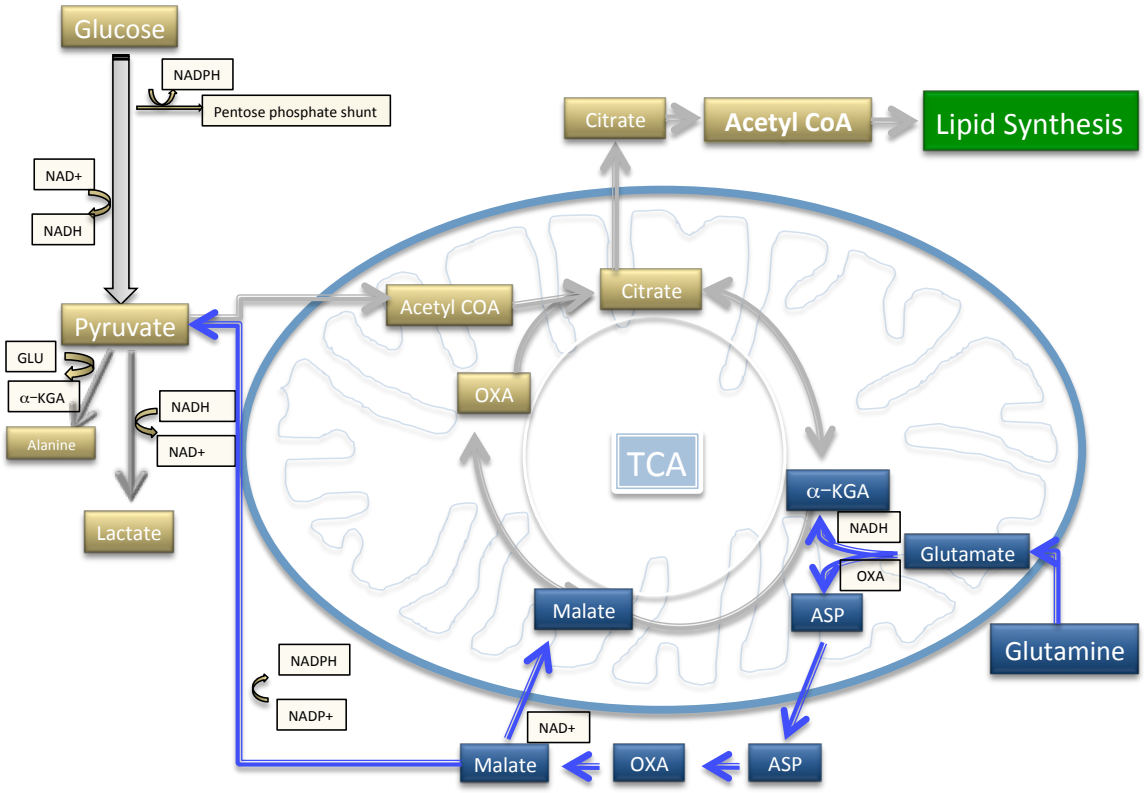
Glucose
NADPH
Pentose phosphate shunt
NAD+
NADH
Pyruvate
GLU
α−KGA
Alanine
Lactate
NADH
NAD+
Citrate
Acetyl CoA
Lipid Synthesis
Acetyl COA
Citrate
OXA
TCA
α−KGA
NADH
Glutamate
OXA
ASP
Glutamine
Malate
NADPH
NADP+
NAD+
Malate
OXA
ASP

Table 1. Influence of FBS on total neutral lipids molar percent distribution in VM-M3 cells[a]

FBS[b]	+	-
Neutral Lipids[c]		
TAG	6.1 ± 0.9	7.3 ± 0.6
C	27.8 ± 2.1	26.5 ± 0.9
Cer	6.5 ± 0.7	7.3 ± 0.2
EtnGpl	21.8 ± 0.4	20.6 ± 0.2
PtdCho	21.8 ± 1.4	21.3 ± 0.7
CerPCho	9.6 ± 1.1	10.4 ± 0.8
LysoPtdCho	trace	trace

[a] Values represent percentage distribution generated from scanning of HPTLC plate similar to that seen in Figure 3, and are expressed as means ± SEM of 4 independent samples. Two samples from both radiolabled glucose and glutamine were combined in calculating total lipid distribution since no changes were observed in the lipid distribution in either the presence or absence of FBS.

[b] Fetal bovine serum at 10% of media.

[c] The amount of lipid spotted was equivalent to 3 x 10^6 cells. Abbreviations for lipids are as followed: TAG, triacylglycerol; C, cholesterol; Cer, ceramide; EtnGpl, phosphatidylethanolamine; PtdCho, phosphatidylcholine; CerPCho, sphingomyelin; LysoPtdCho, lyso-phosphatidylcholine.

Figure 4.

High performance thin-layer chromatography (HPTLC) analysis of total neutral (non-labeled and labeled) lipids in VM-M3 tumor cell line grown in DMEM in the presence or absence of FBS. The amount of lipid spotted was equivalent to 3 x 10^6 cells. The abbreviations used are as indicated: lysoPtdCho, lysophosphatidylcholine; CerPCho, sphingomyelin; PtdCho, phosphatidylcholine; EtnGpl, phosphatidylethanolamine; Cer, ceramide; C, cholesterol; TAG, triglycerides; MB, mouse brain; STD, standard. The plates were developed to the initial solvent front (SF) with chloroform: methanol: acetic acid: formic acid: water (70:30:12:4:2 by volume) and to the top with hexanes: diisopropyl ether: acetic acid (65:35:2 by volume). Lipids were visualized by charring with 3% cupric acetate in 8% phosphoric acid solution, followed by heating in an oven at 165^0C for 7 min. Since an equal number of cells was spotted on the HPTLC plate, there were no differences in the distribution of the total lipids in experiment using either labeled glucose or labeled glutamine. Hence, only representative samples were presented.

Figure 4.

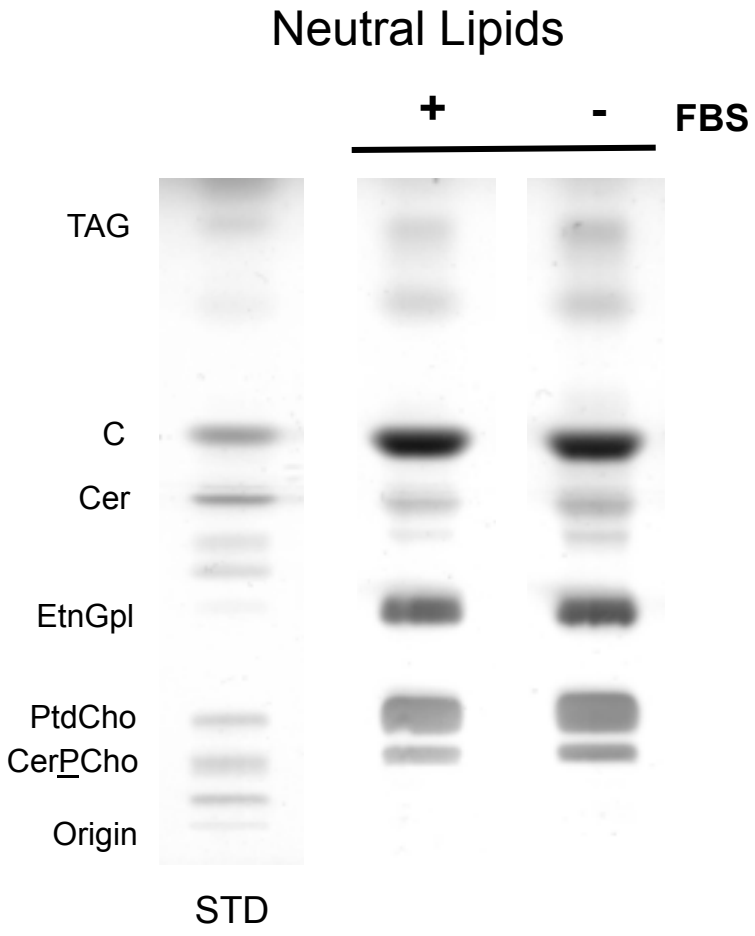
Neutral Lipids
+
-
FBS
TAG
C
Cer
EtnGpl
PtdCho
CerPCho
Origin
STD

Table 2. Influence of FBS on incorporation of carbons from [^{14}C] glucose and [^{14}C] glutamine into neutral lipids in VM-M3 cells[a]

	[^{14}C] Glucose		[^{14}C] Glutamine	
FBS	**+**	**-**	**+**	**-**
Neutral Lipids[b]				
TAG	228 ± 5	76 ± 2	112 ± 17	138 ± 7
C	400 ± 31	1127 ± 126	254 ± 3	575 ± 22
Cer	268 ± 31	251 ± 12	163 ± 4	264 ± 17
EtnGpl	1045 ± 87	2008 ± 276	427 ± 42	920 ± 9
PtdCho	2002 ± 156	3604 ± 405	900 ± 50	1647 ± 16
CerPCho	542 ± 47	686 ± 67	329 ± 28	520 ± 4
LysoPtdCho	112 ± 2	55 ± 14	88 ± 7	125 ± 12
Total DPM	**5075 ± 92**	**8100 ± 931**	**2557 ± 131**	**4574 ± 44**

Values represent calculated disintegration per minute (dpm), expressed as means ± interquartile range (IQR) of two independent samples. Individual lipids dpm are calculated from the percent distribution (as seen in figure 4) x total dpm.

[a] Fetal bovine serum at 10% of media. Cells were grown in either the presence of absence of FBS with either [^{14}C] glucose and [^{14}C] glutamine for 48hrs as described in the methods section.

[b] The amount of lipid spotted is as described in Table 1.

Abbreviations for lipids are as indicated in Table 1.

Figure 5.

Influence of FBS on radiolabeled neutral lipids molar percent distribution. Values represent mole percent distribtion and expressed as the means ± IQR of two independent samples as represented in Figure 6. Cells were grown in either the presence or absence of FBS with either [^{14}C]-U-D-glucose and [^{14}C]-U-D-glutamine for 48 hrs. as described in the Method section. Abbreviations are as indicated in Figure 4.

Figure 5.

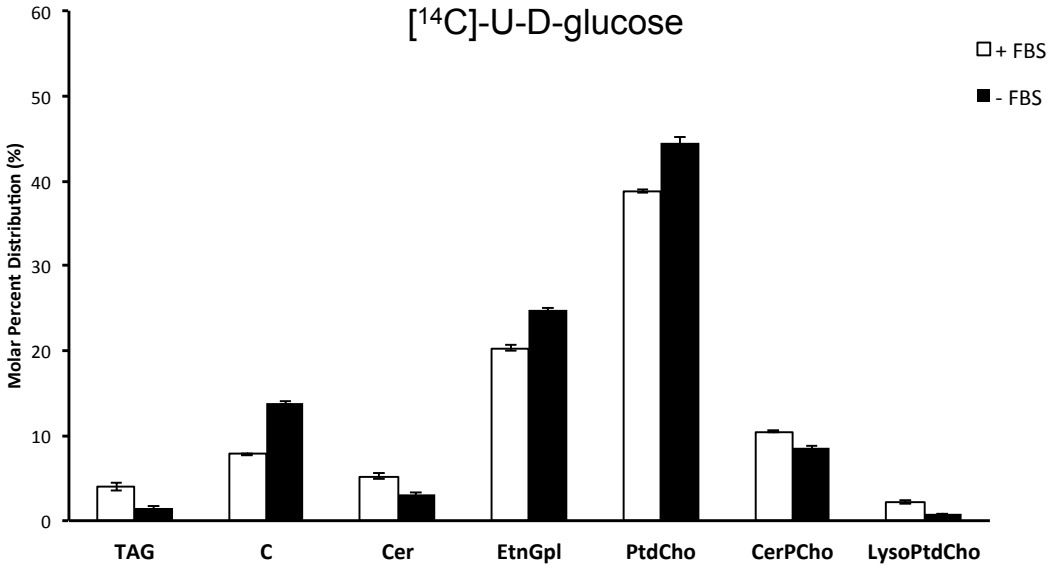
[14C]-U-D-glucose
+ FBS
- FBS
Molar Percent Distribution (%)
60
50
40
30
20
10
0
TAG
C
Cer
EtnGpl
PtdCho
CerPCho
LysoPtdCho

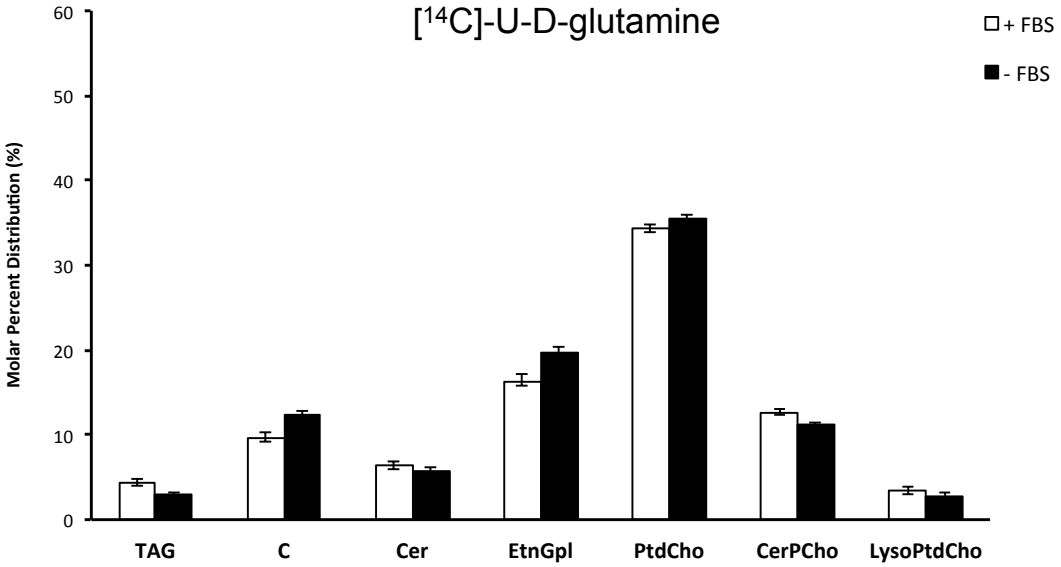
[14C]-U-D-glutamine
+ FBS
- FBS
Molar Percent Distribution (%)
60
50
40
30
20
10
0
TAG
C
Cer
EtnGpl
PtdCho
CerPCho
LysoPtdCho

Figure 6.

HPTLC analysis of endogenously synthesized (radiolabeled) neutral lipids in VM-M3 tumor cell line grown in DMEM in the presence or absence of FBS using uniformly labeled [^{14}C] glucose or [^{14}C] glutamine. The amount of lipid spotted was equivalent to 3 x 10^6 cells. Radiolabeled lipids were visualized with PhosphoImager. Abbreviations are as indicated in Figure 4.

Figure 6.

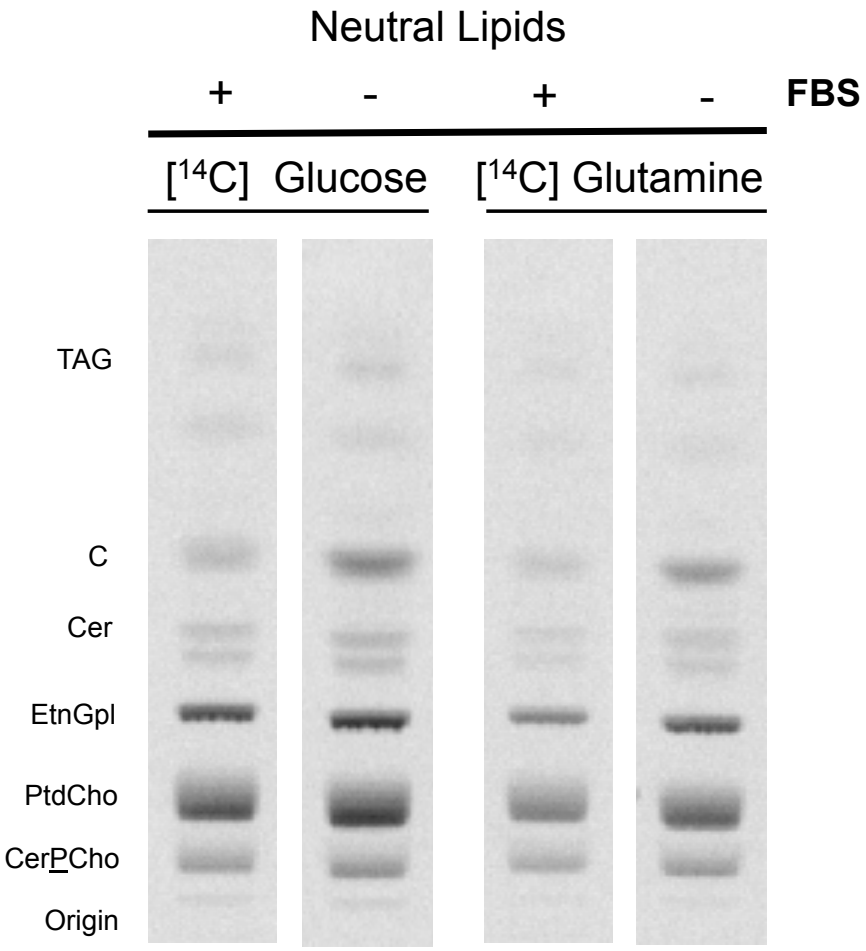
Neutral Lipids
+
-
+
-
FBS
[14C] Glucose
[14C] Glutamine
TAG
C
Cer
EtnGpl
PtdCho
CerPCho
Origin

Table 3. Influence of FBS on total acidic lipids molar percent distribution in VM-M3 cells[a]

FBS[b]	+	-
Acidic Lipids[c]		
Ptd_2Gro	9.2 ± 0.7	10.5 ± 1.0
BMP/PtdOH	7.8 ± 0.5	8.8 ± 0.7
PtdGro	3.4 ± 0.3	5.0 ± 0.9
PtdSer	38.0 ± 1.1	37.3 ± 0.9
PtdIns	32.2 ± 1.1	31.7 ± 1.9

[a] Values represent percentage distribution generated from scanning of HPTLC plate similar to that seen in Figure 6, and are expressed as means ± SEM of 4 independent samples. Two samples from both radiolabled glucose and glutamine were combined in calculating total lipid distribution since no changes were observed in the lipid distribution in either the presence or absence of FBS.

[b] Fetal bovine serum at 10% of media.

[c] The amount of lipid spotted was equivalent to 6×10^6 cells.

Abbreviations for lipids are as followed: Ptd2Gro, cardiolipin; PtdOH, phosphatidic acid; BMP, bis(monoacylglycero)phosphate; PtdGro, phosphatidylglycerol; PtdSer, phosphatidylserine; PtdIns, phosphatidylinositol

Figure 7.

HPTLC analysis of total acidic (non-labeled and labeled) lipids in VM-M3 tumor cell line grown in DMEM in the presence or absence of FBS. The amount of lipid spotted was equivalent to 6 x 10^6 cells. The abbreviations used are as indicated: PtdIns, phosphatidylinositol; PtdSer, phosphatidylserine; PtdGro, phosphatidylglycerol; PtdOH, phosphatidic acid; BMP, bis(monoacylglycero)phosphate; Ptd_2Gro , cardiolipin; MB, mouse brain; STD, standard. Developing solvents, and lipid visualization is as indicated in Figure 4.

Figure 7.

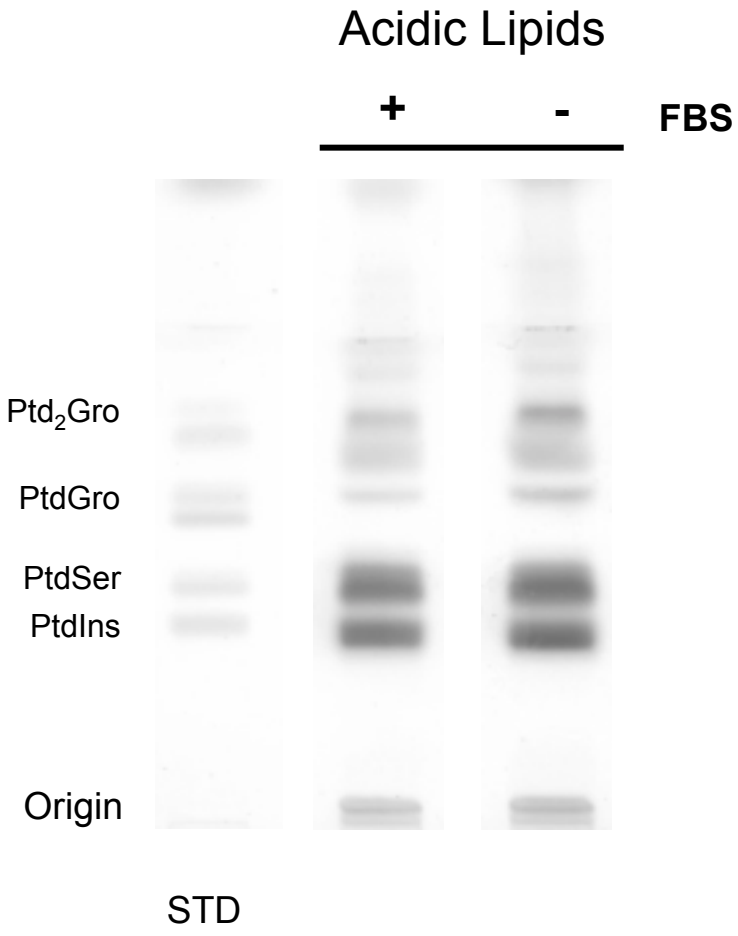

Table 4. Influence of FBS on incorporation of carbons from [^{14}C] glucose and [^{14}C] glutamine into acidic lipids in VM-M3 cells[a]

	[^{14}C] Glucose		[^{14}C] Glutamine	
FBS	**+**	**-**	**+**	**-**
Acidic Lipids[b]				
Ptd_2Gro	271 ± 26	368 ± 19	167 ± 10	283 ± 7
BMP/PtdOH	350 ± 15	593 ± 10	200 ± 14	378 ± 1
PtdGro	256 ± 16	489 ± 9	159 ± 16	268 ± 3
PtdSer	959 ± 92	1352 ± 140	505 ± 2	923 ± 73
PtdIns	1276 ± 150	1762 ± 213	519 ± 20	1094 ± 67
Total DPM	**3247 ± 301**	**4721 ± 337**	**1667 ± 73**	**3077 ± 128**

Values represent calculated disintegration per minute (dpm), expressed as means ± interquartile range (IQR) of two independent samples. Individual lipids dpm are calculated from the percent distribution (as seen in figure 7) x total dpm.

[a] Fetal bovine serum at 10% of media. Cells were grown in either the presence of absence of FBS with either [^{14}C] glucose and [^{14}C] glutamine for 48hrs as described in the methods section.

[b] The amount of lipid spotted is as described in Table 3.

Abbreviations for lipids are as indicated in Table 3.

Figure 8.

Influence of FBS on radiolabeled acidic lipids molar percent distribution. Values represent mole percent distribtion and expressed as the means ± IQR of two independent samples as represented in Figure 9. Cells were grown in either the presence or absence of FBS with either [^{14}C]-U-D-glucose and [^{14}C]-U-D-glutamine for 48hrs as described in the Method section. Abbreviations are as indicated in Figure 7.

Figure 8.

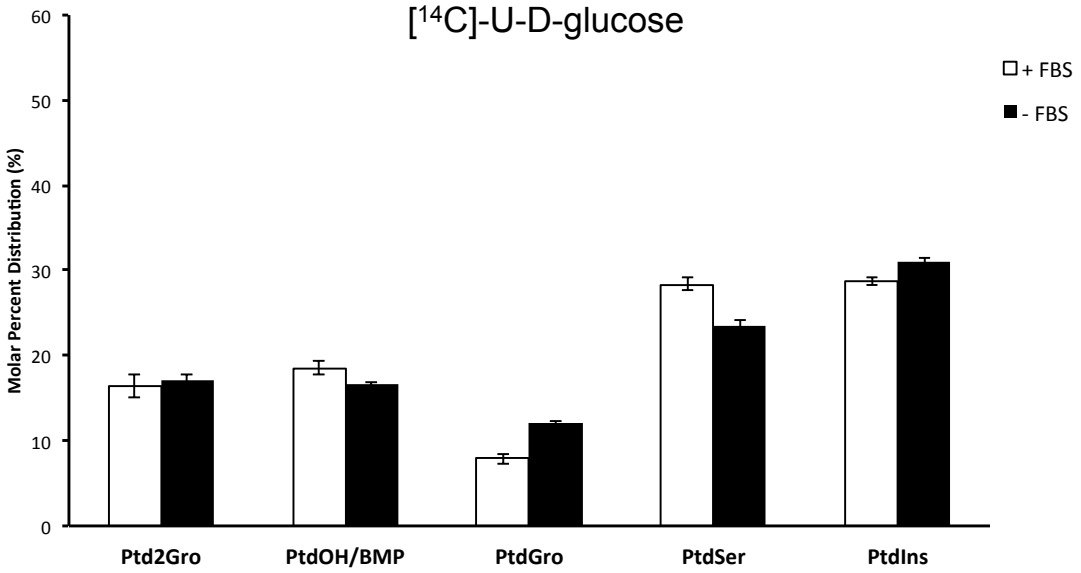
[14C]-U-D-glucose
+ FBS
- FBS
Molar Percent Distribution (%)
60
50
40
30
20
10
0
Ptd2Gro
PtdOH/BMP
PtdGro
PtdSer
PtdIns

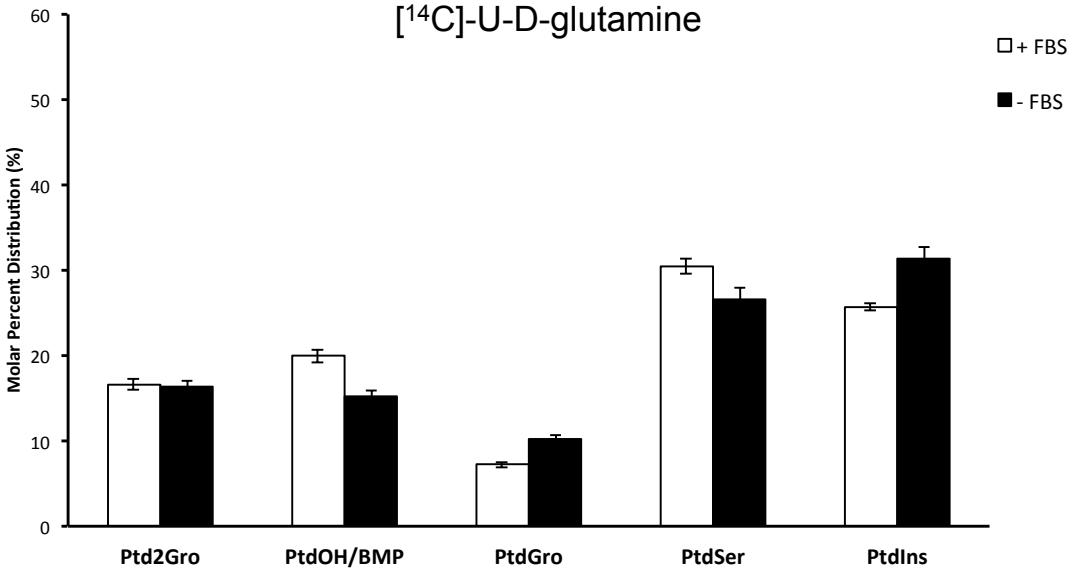
[14C]-U-D-glutamine
+ FBS
- FBS
Molar Percent Distribution (%)
60
50
40
30
20
10
0
Ptd2Gro
PtdOH/BMP
PtdGro
PtdSer
PtdIns

Figure 9.

HPTLC analysis of endogenously synthesized (radiolabeled) acidic lipids in VM-M3 tumor cell line grown in DMEM in the presence or absence of FBS using uniformly labeled [^{14}C] glucose or [^{14}C] glutamine. The amount of lipid spotted was equivalent to 6 x 10^6 cells. Radiolabeled lipids were visualized with PhosphoImager. Abbreviations are as indicated in Figure 7.

Figure 9.

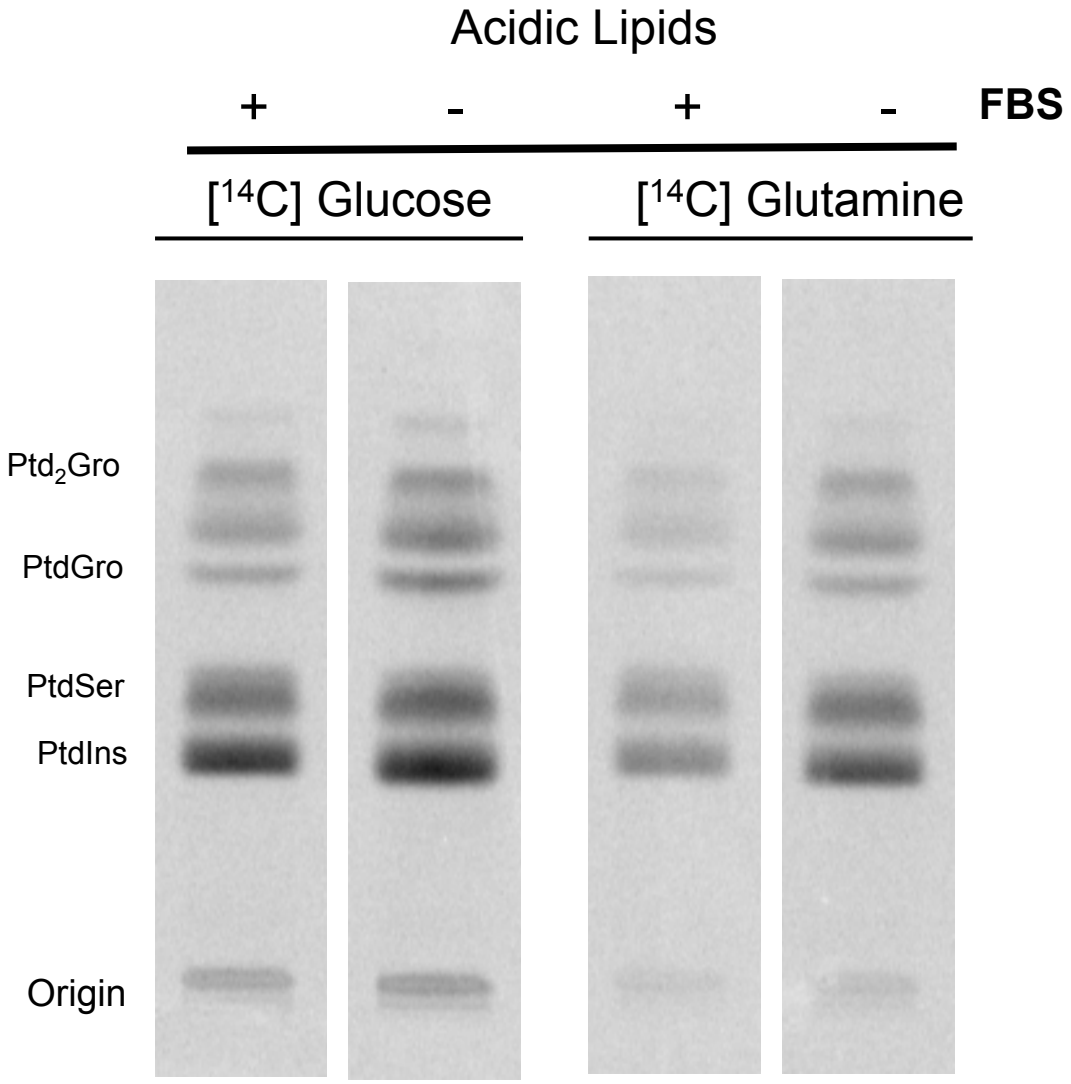
Acidic Lipids
+
-
+
-
FBS
[14C] Glucose
[14C] Glutamine
Ptd2Gro
PtdGro
PtdSer
PtdIns
Origin

Figure 10.

The influence of FBS on incorporation of carbons from [^{14}C] glucose or [^{14}C] glutamine on total dpm from neutral and acidic lipids. The calculated total dpm is the sum of the dpm of the neutral lipids (Table 2) plus dpm of the acidic lipids (Table 4). Values represent as mean ± IQR of two independent samples.

Figure 10.

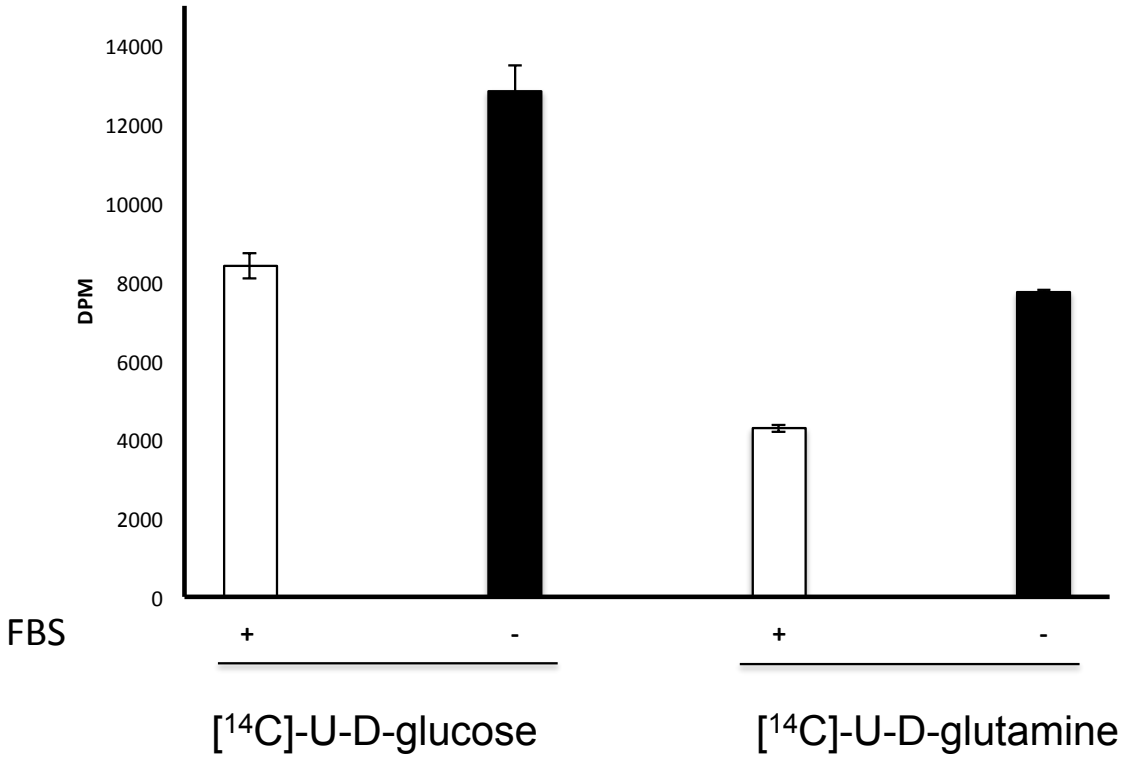
14000
12000
10000
8000
6000
4000
2000
0
DPM
FBS
+
-
+
-
[14C]-U-D-glucose
[14C]-U-D-glutamine

Table 5. Influence of FBS on total ganglioside molar percent distribution in VM-M3 cells[a]

FBS[b]	+	-
Gangliosides[c]		
GM2	25.4 ± 0.6	24.4 ± 0.5
GM1	28.2 ± 0.5	28.5 ± 0.4
GD1a	46.1 ± 1.1	47.1 ± 1.2

[a] Values represent percentage distribution generated from scanning of HPTLC plate similar to that seen in Figure 10, and are expressed as means ± SEM of 4 independent samples. Two samples from both radiolabled glucose and glutamine were combined in calculating total lipid distribution since no changes were observed in the lipid distribution in either the presence or absence of FBS.

[b] Fetal bovine serum at 10% of media.

[c] The amount of lipid spotted was equivalent to 15 x 10^6 cells. The individual gangliosides were labeled according to the nomenclature system of Svennerholm.

Figure 11.

HPTLC analysis of total gangliosides (non-labeled and labeled) in VM-M3 tumor cell line grown in DMEM in the presence or absence of FBS. The amount of lipid spotted was equivalent to 15 x 10^6 cells. The plate was developed with a single solvent system with chloroform: methanol: 0.02% (55:45:10 by volume). Lipids were visualized by spraying with resorcinol-HCL reagent, followed by heating at 100^0C for 10 min. The individual gangliosides were labeled according to the nomenclature system of Svennerholm. MB indicates mouse brain.

Figure 11

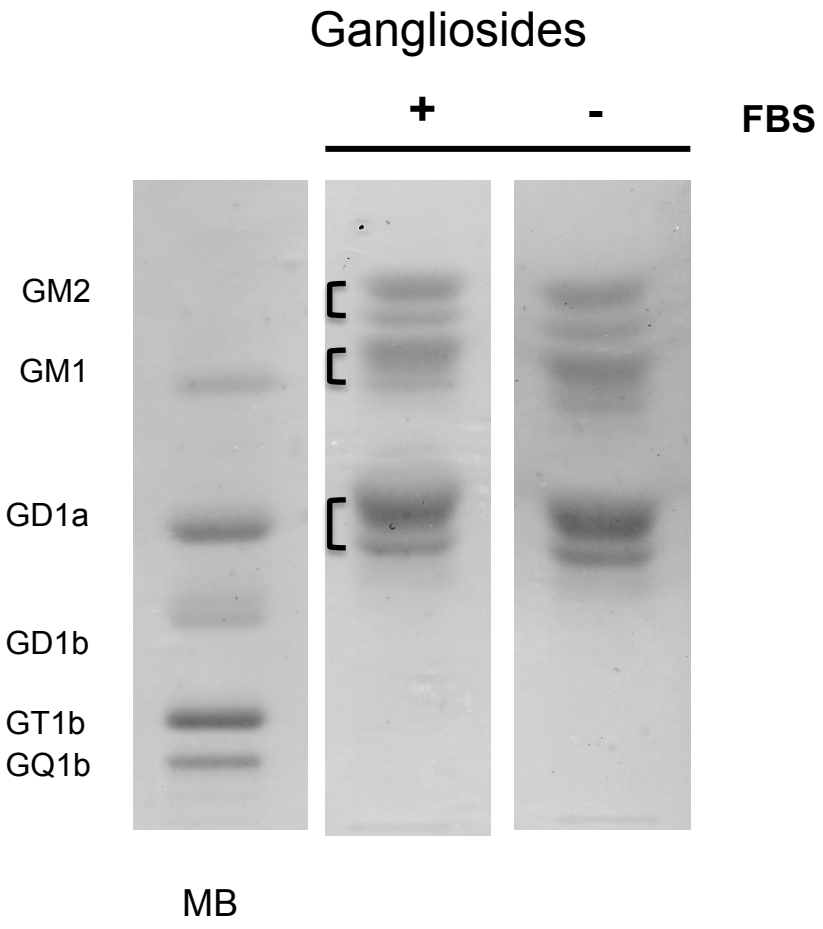

Table 6. Influence of FBS on incorporation of carbons from [^{14}C] glucose and [^{14}C] glutamine into ganglioside in VM-M3 cells[a]

	[^{14}C] Glucose		[^{14}C] Glutamine	
FBS	**+**	**-**	**+**	**-**
Gangliosides[b]				
GM2	699 ± 138	632 ± 25	491 ± 8	514 ± 23
GM1	927 ± 229	693 ± 33	603 ± 18	569 ± 30
GD1a	1188 ± 247	1036 ± 141	557 ± 24	517 ± 47
Total DPM	**2815 ± 615**	**2360 ± 240**	**1650 ± 168**	**1600 ± 100**

Values represent calculated disintegration per minute (dpm), expressed as means ± interquartile range (IQR) of two independent samples. Individual lipids dpm are calculated from the percent distribution (as seen in figure 11) x total dpm.

[a] Fetal bovine serum at 10% of media. Cells were grown in either the presence of absence of FBS with either [^{14}C] glucose and [^{14}C] glutamine for 48hrs as described in the methods section.

[b] The amount of lipid spotted is as described in Table 5.

Abbreviations for lipids are as indicated in Table 3.

The individual gangliosides were labeled according to the nomenclature of Svennerholm.

Figure 12.

Influence of FBS on radiolabeled ganglioside molar percent distribution. Values represent mole percent distribtion and expressed as the means ± IQR of two independent samples as represented in Figure 13. Cells were grown in either the presence or absence of FBS with either [^{14}C]-U-D-glucose and [^{14}C]-U-D-glutamine for 48hrs as described in the Method section. The individual gangliosides were labeled according to the nomenclature system of Svennerholm.

Figure 12.

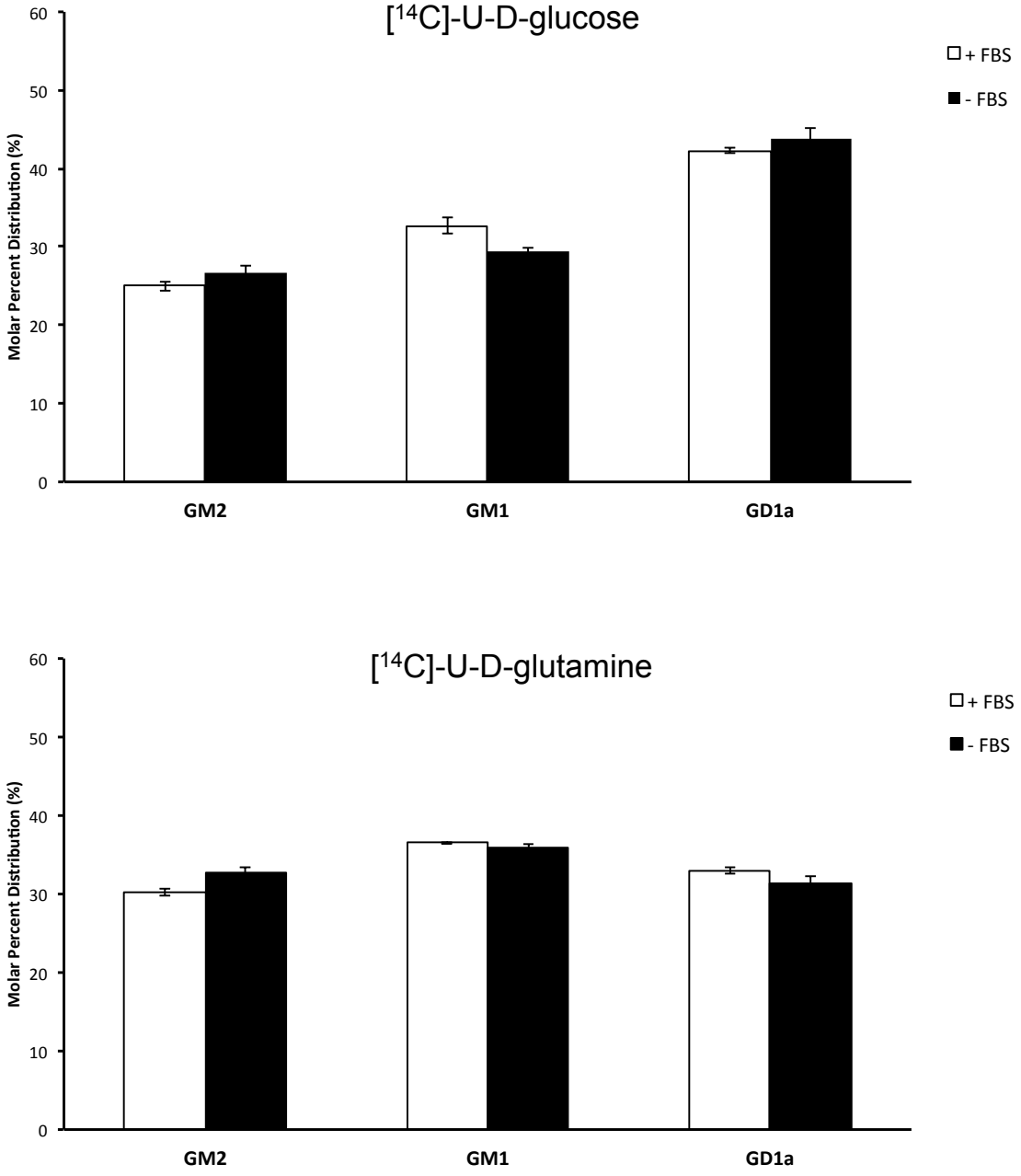
[14C]-U-D-glucose
+ FBS
- FBS
Molar Percent Distribution (%)
60
50
40
30
20
10
0
GM2
GM1
GD1a
[14C]-U-D-glutamine
+ FBS
- FBS
Molar Percent Distribution (%)
60
50
40
30
20
10
0
GM2
GM1
GD1a

Figure 13.

HPTLC analysis of endogenously synthesized (radiolabeled) gangliosides in VM-M3 tumor cell line grown in DMEM in the presence or absence of FBS using uniformly labeled [^{14}C] glucose or [^{14}C] glutamine. The amount of lipid spotted was equivalent to 15 x 10^6 cells. Radiolabeled lipids were visualized with PhosphoImager. The individual gangliosides were labeled according to the nomenclature system of Svennerholm.

Figure 13.

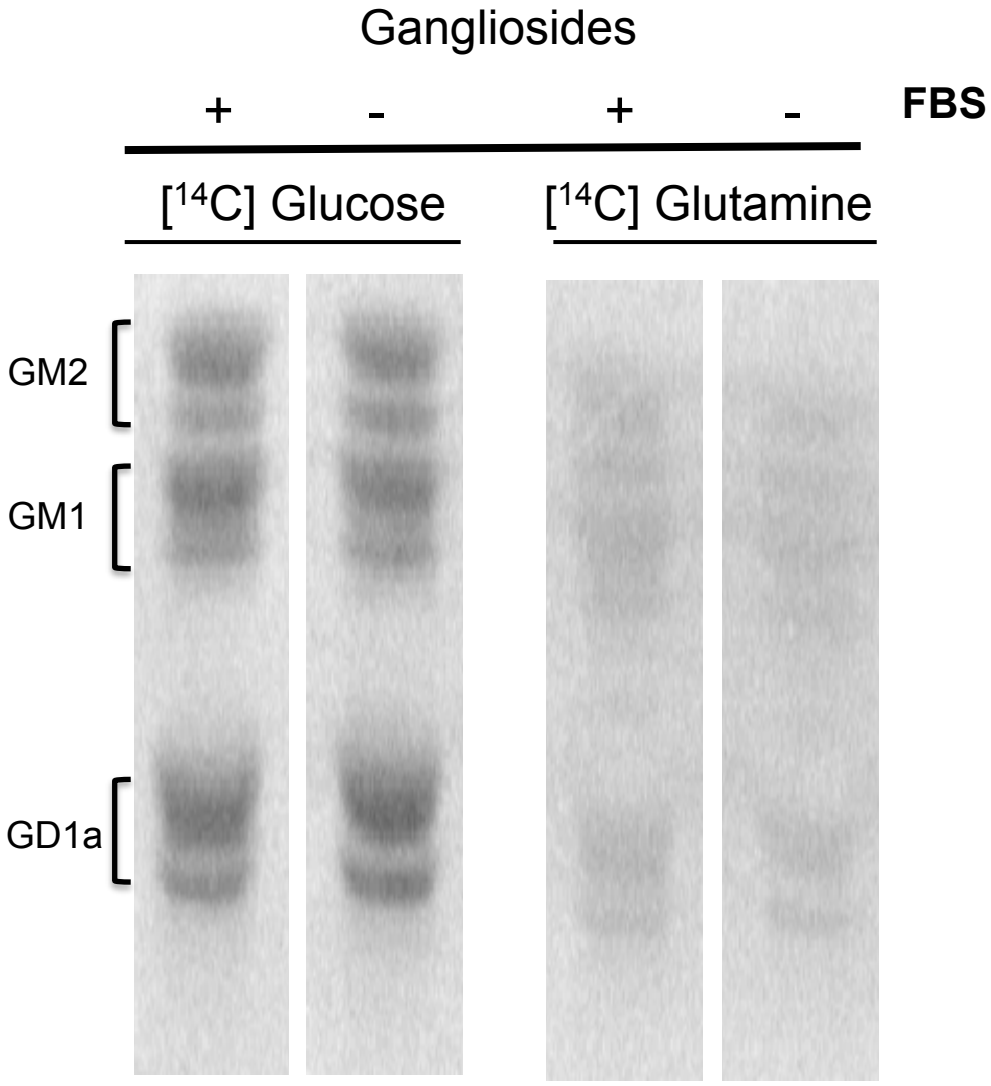

Figure 14.

HPTLC analysis of lactate derived from the media of VM-M3 grown in DMEM in the presence or absence of FBS using uniformly labeled [^{14}C] glucose and [^{14}C] glutamine. Equal amount of 250ul of the media was spotted (a) and data analysis was normalized to equal number of cells (b). The plate was developed in a single ascending solvent with butanol: acetic acid: water (50:11:25 by volume) for 5 hrs. Values shown in (b) represent two independent samples and are expressed as means ± IQR.

Figure 14.

A.

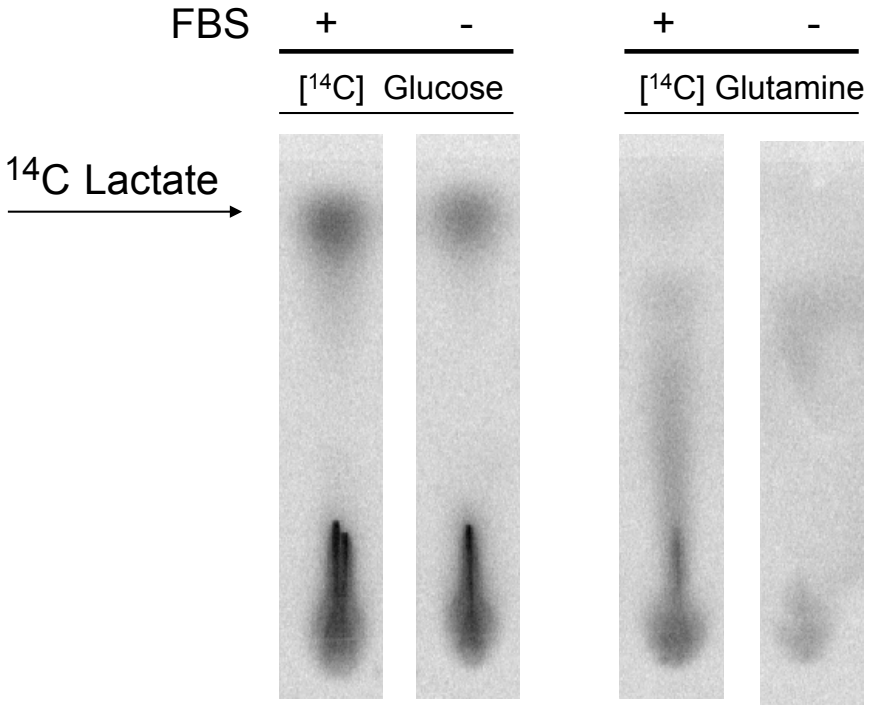
FBS
+
-
+
-
[14C] Glucose
[14C] Glutamine
14C Lactate

B.

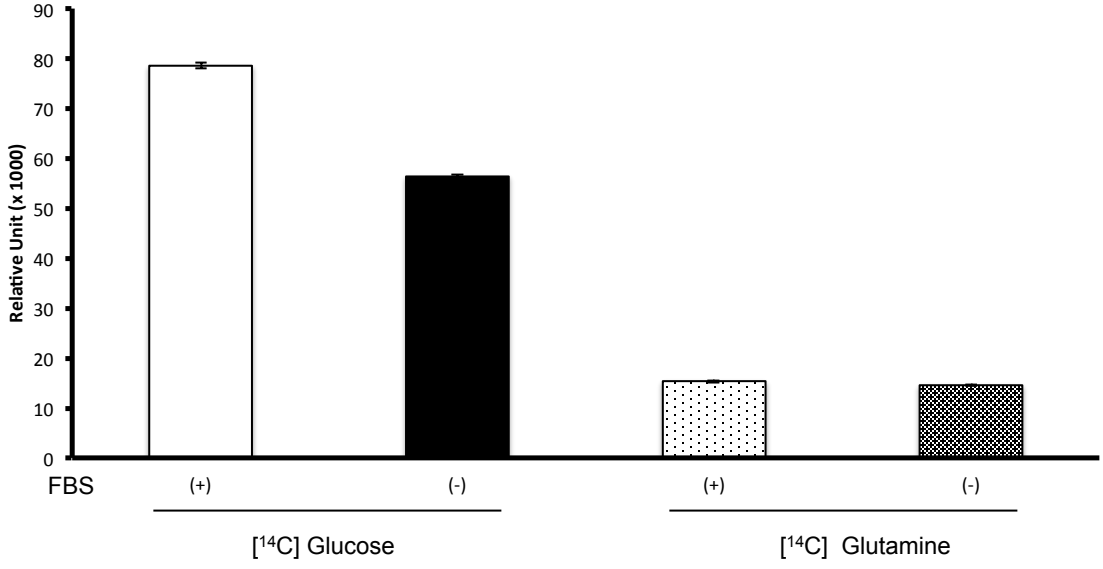
90
80
70
60
50
40
30
20
10
0
Relative Unit (x 1000)
FBS
(+)
(-)
(+)
(-)
[14C] Glucose
[14C] Glutamine

Figure 15.

HPTLC analysis of total neutral (non-labeled and labeled) lipids in VM-M3 tumor cell line grown under the influence of oxygen. The amount of lipid spotted was equivalent to 3000 dpm. Same amount of dpm were spotted here on HPTLC plate to show qualitative changes in lipids under the influence of hypoxia. This corresponded to different number of cells spotted as represented by the different intensity of the bands in total lipids. Developing solvents, and lipid visualization is as indicated in Figure 4. The abbreviations used are as indicated in Figure 4.

Figure 15.

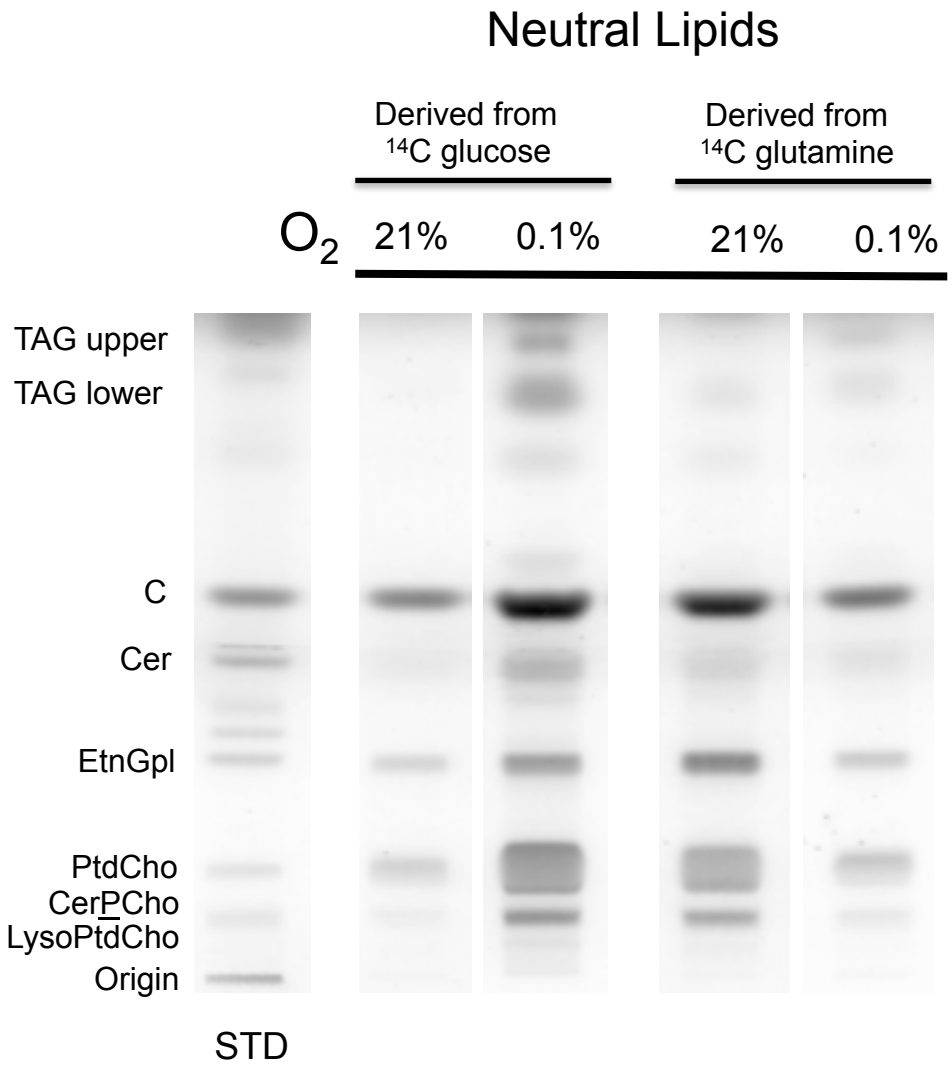
Neutral Lipids
Derived from
14C glucose
Derived from
14C glutamine
O2
21%
0.1%
21%
0.1%
TAG upper
TAG lower
C
Cer
EtnGpl
PtdCho
CerPCho
LysoPtdCho
Origin
STD

Table 7. Influence of O_2 on incorporation of carbons from [^{14}C] glucose and [^{14}C] glutamine into neutral lipids in VM-M3 cells[a]

	[^{14}C] Glucose		[^{14}C] Glutamine	
O_2	21%	0.1%	21%	0.1%
Neutral Lipids[b]				
TAG upper	N.D.	332 ± 13	N.D.	827 ± 84
TAG lower	Trace	306 ± 21	Trace	828 ± 28
C	822 ± 82	262 ± 14	525 ± 24	450 ± 31
Cer	385 ± 5	174 ± 7	201 ± 6	344 ± 24
EtnGpl	967± 40	324 ± 5	530 ± 26	550 ± 25
PtdCho	3171 ± 219	1761 ± 49	1822 ± 78	1962 ± 113
CerPCho	661 ± 40	226 ± 24	454 ± 19	476 ± 22
LysoPtdCho	330 ± 45	148 ± 16	182 ± 4	217 ± 16
Total DPM	**6904 ± 370**	**4038 ± 43 ***	**3154 ± 92**	**6258 ± 338 ***

Calculated dpm were normalized to same number of cells, and expressed as means ± SEM of three independent samples. Individual lipids dpm are calculated from the percent distribution (as seen in figure 15) x total dpm. * indicates significant differences from 21% O_2 at $p < 0.02$.

[a] Cells were grown in DMEM with 10% FBS in the presence of 21% O_2 or 0.1% O_2 with either [^{14}C] glucose and [^{14}C] glutamine for 48hrs.

[b] The amount of lipid spotted was equivalent to 3000 dpm.

N.D - None detected.

Abbreviations of lipids are as indicated in Table 1.

Figure 16.

Influence of hypoxia on radiolabeled neutral lipids molar percent distribution. Values represent mole percent distribtion of lipids as represented in Figure 17 and expressed as the means ± SEM of three independent samples. Mole percent distribution for upper TAG and lower TAG (as seen in Figure 17) is combined to represent one nominal value. Cells were grown in either normoxia (21% O_2) or hypoxia (0.1% O_2) with either [^{14}C]-U-D-glucose and [^{14}C]-U-D-glutamine for 48hrs as described in the Method section. Asterisk indicates significant difference from 21% O_2 at $p < 0.02$. Abbreviations are as indicated in Figure 4.

Figure 16.

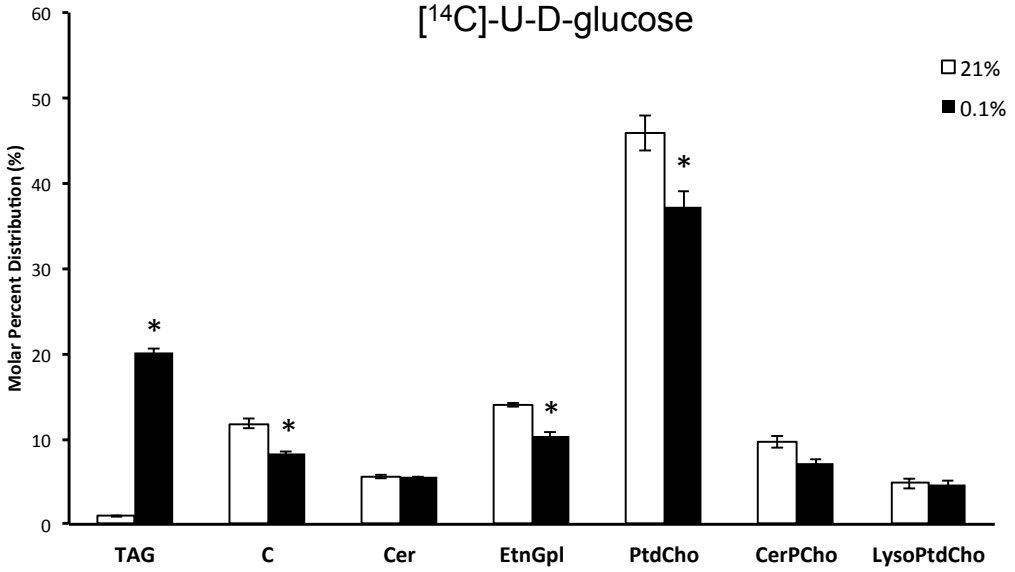
[14C]-U-D-glucose
21%
0.1%
Molar Percent Distribution (%)
60
50
40
30
20
10
0
TAG
C
Cer
EtnGpl
PtdCho
CerPCho
LysoPtdCho

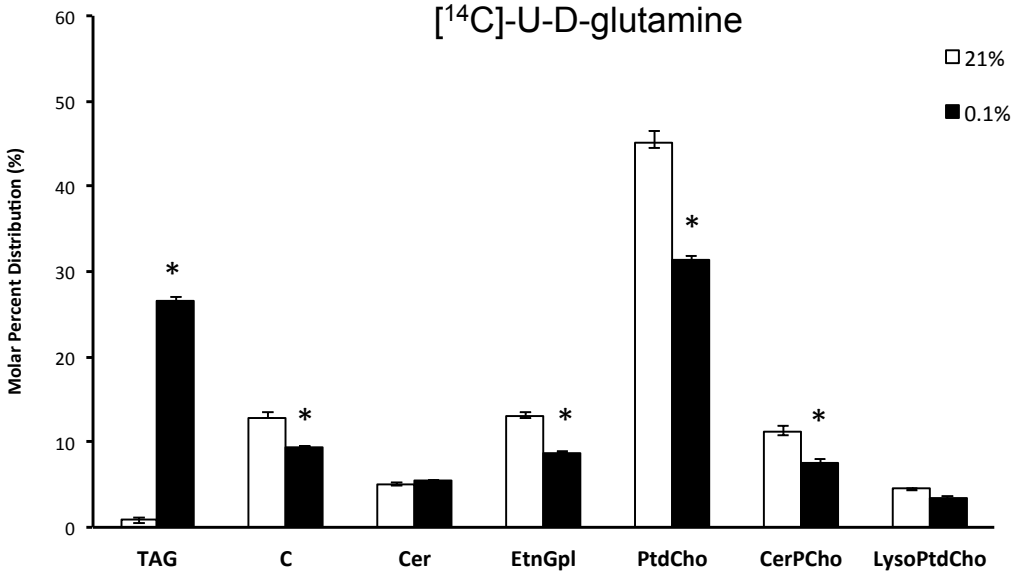
[14C]-U-D-glutamine
21%
0.1%
Molar Percent Distribution (%)
60
50
40
30
20
10
0
TAG
C
Cer
EtnGpl
PtdCho
CerPCho
LysoPtdCho

Figure 17

HPTLC analysis of endogenously synthesized (radiolabeled) neutral lipids in VM-M3 tumor cell line grown in either normoxia (21% O_2) or hypoxia (0.1% O_2) using uniformly labeled [^{14}C] glucose or [^{14}C] glutamine. The amount of lipid spotted was equivalent to 3000 dpm. Radiolabeled lipids were visualized with PhosphoImager. Abbreviations are as indicated in Figure 4.

Figure 17.

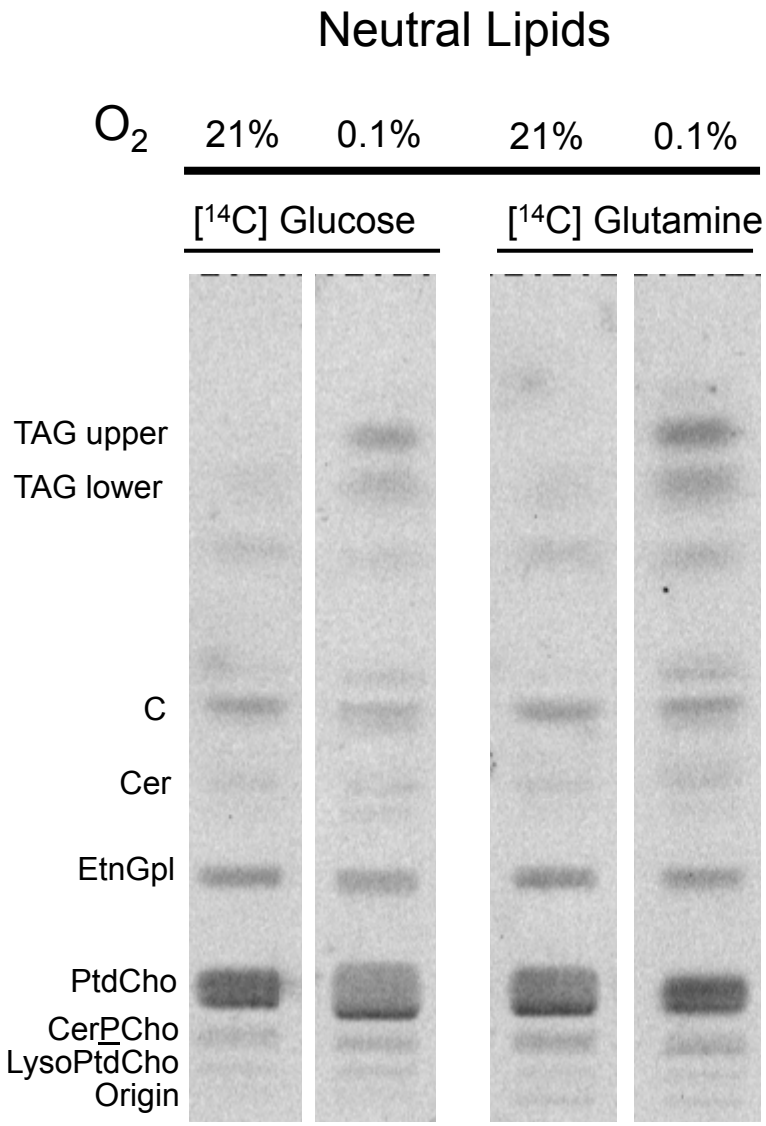
Neutral Lipids
O_2
21%
0.1%
21%
0.1%
[14C] Glucose
[14C] Glutamine
TAG upper
TAG lower
C
Cer
EtnGpl
PtdCho
CerPCho
LysoPtdCho
Origin

Figure 18.

HPTLC analysis of total acidic (non-labeled and labeled) lipids in VM-M3 tumor cell line grown under the influence of oxygen. The amount of lipid spotted was equivalent to 3000 dpm. Same amount of dpm were spotted here on HPTLC plate to show qualitative changes in lipids under the influence of hypoxia. This corresponded to different number of cells spotted as represented by the different intensity of the bands in total lipids. Developing solvents, and lipid visualization is as indicated in Figure 7. The abbreviations used are as indicated in Figure 7.

Figure 18.

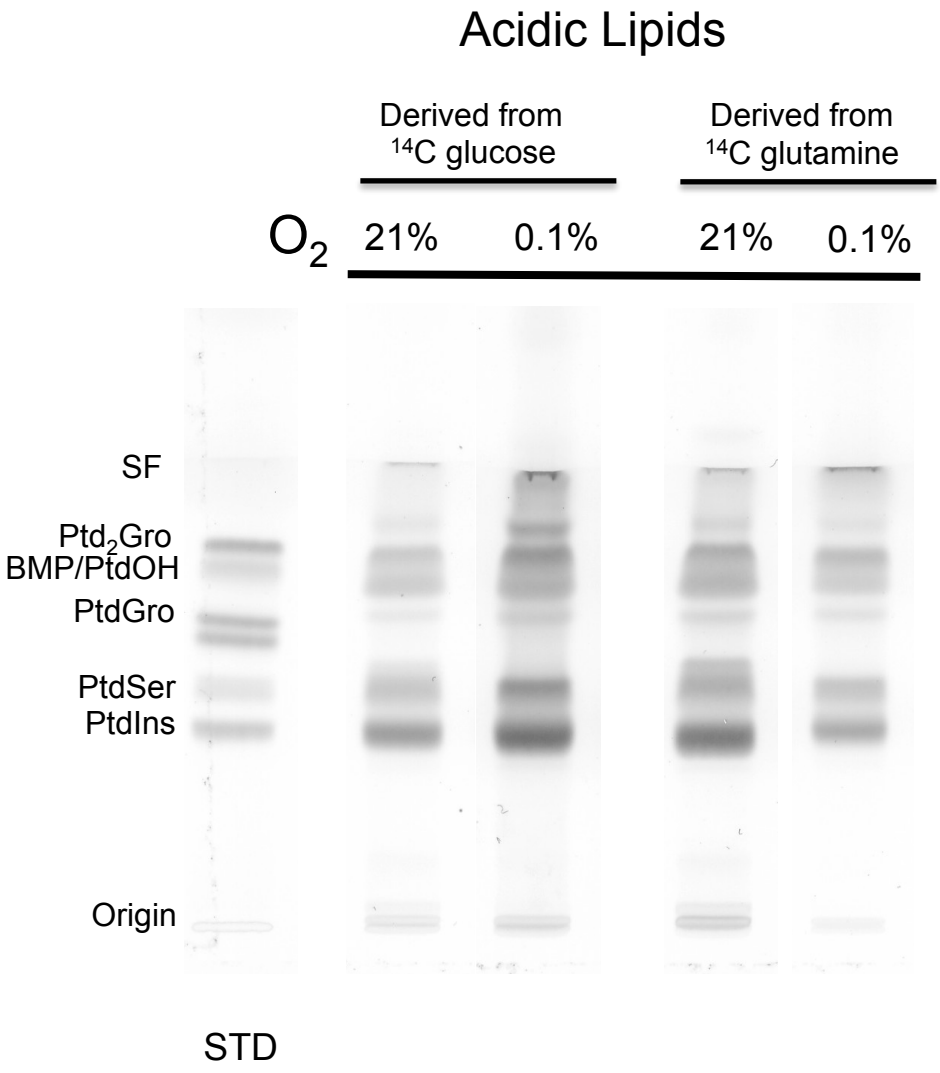
Acidic Lipids
Derived from ^{14}C glucose
Derived from ^{14}C glutamine
O_2
21%
0.1%
21%
0.1%
SF
Ptd_2Gro
BMP/PtdOH
PtdGro
PtdSer
PtdIns
Origin
STD

Table 8. Influence of O_2 on incorporation of carbons from [^{14}C] glucose and [^{14}C] glutamine into acidic lipids in VM-M3 cells[a]

	[^{14}C] Glucose		[^{14}C] Glutamine	
O_2	**21%**	**0.1%**	**21%**	**0.1%**
Acidic Lipids[b]				
Ptd_2Gro	260 ± 33	53 ± 4	119 ± 3	135 ± 3
PtdOH/BMP	291 ± 27	52 ± 1	143 ± 8	127 ± 11
PtdGro	123 ± 3	37 ± 2	52 ± 3	85 ± 2
PtdSer	444 ± 16	73 ± 1	219 ± 3	222 ± 20
PtdIns	450 ± 29	97 ± 2	185 ± 7	260 ± 9
Total DPM	**1568 ± 94**	**313 ± 8 ***	**717 ± 13**	**829 ± 38 ***

Calculated dpm were normalized to same number of cells, and expressed as means ± SEM of three independent samples. Individual lipids dpm are calculated from the percent distribution (as seen in figure 18) x total dpm. * indicates significant differences from 21% O_2 at $p < 0.02$.

[a] Cells were grown in DMEM with 10% FBS in the presence of 21% O_2 or 0.1% O_2 with either [^{14}C] glucose and [^{14}C] glutamine for 48hrs.

[b] The amount of lipid spotted was equivalent to 3000 dpm

Abbreviations of lipids are as indicated in Table 3.

Figure 19.

Influence of hypoxia on radiolabeled acidic lipids molar percent distribution. Values represent mole percent distribtion of lipids as represented in Figure 20 and expressed as the means ± SEM of three independent samples. Cells were grown in either normoxia (21% O_2) or hypoxia (0.1% O_2) with either [^{14}C]-U-D-glucose and [^{14}C]-U-D-glutamine for 48hrs as described in the Method section. . Asterisk indicates significant difference from 21% O_2 at $p < 0.02$. Abbreviations are as indicated in Figure 7.

Figure 19.

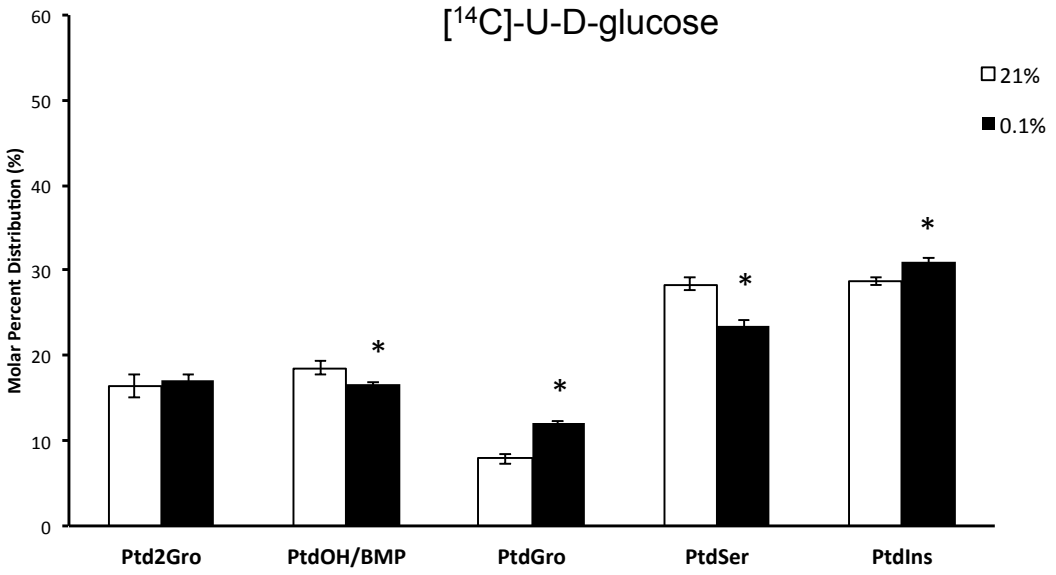
[14C]-U-D-glucose
21%
0.1%
Molar Percent Distribution (%)
60
50
40
30
20
10
0
*
Ptd2Gro
PtdOH/BMP
PtdGro
PtdSer
PtdIns

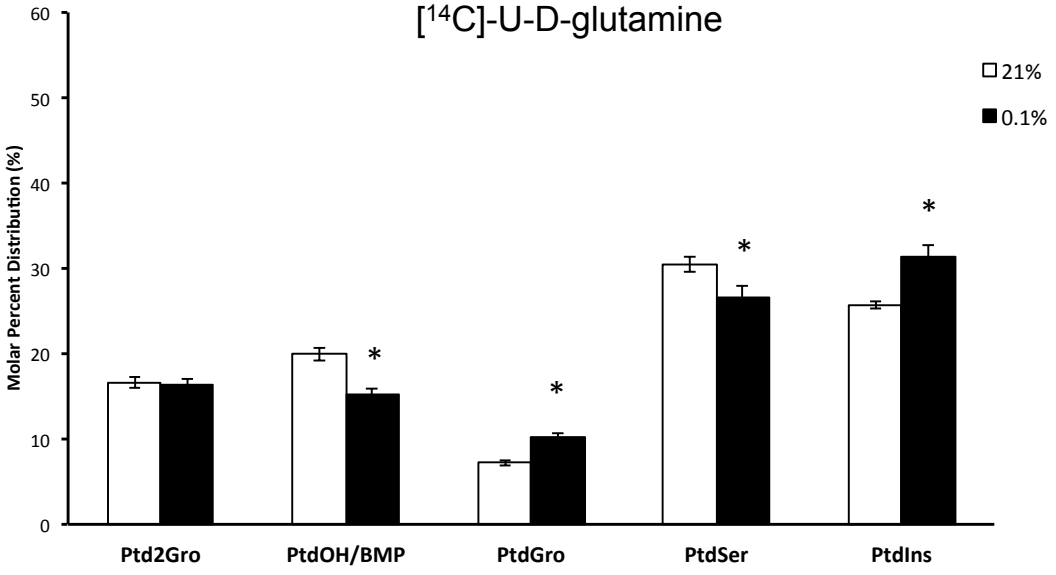
[14C]-U-D-glutamine
21%
0.1%
Molar Percent Distribution (%)
60
50
40
30
20
10
0
*
Ptd2Gro
PtdOH/BMP
PtdGro
PtdSer
PtdIns

Figure 20.

HPTLC analysis of endogenously synthesized (radiolabeled) acidic lipids in VM-M3 tumor cell line grown in either normoxia (21% O_2) or hypoxia (0.1% O_2) using uniformly labeled [^{14}C] glucose or [^{14}C] glutamine. The amount of lipid spotted was equivalent to 3000 dpm. Radiolabeled lipids were visualized with PhosphoImager. Abbreviations are as indicated in Figure 4.

Figure 20.

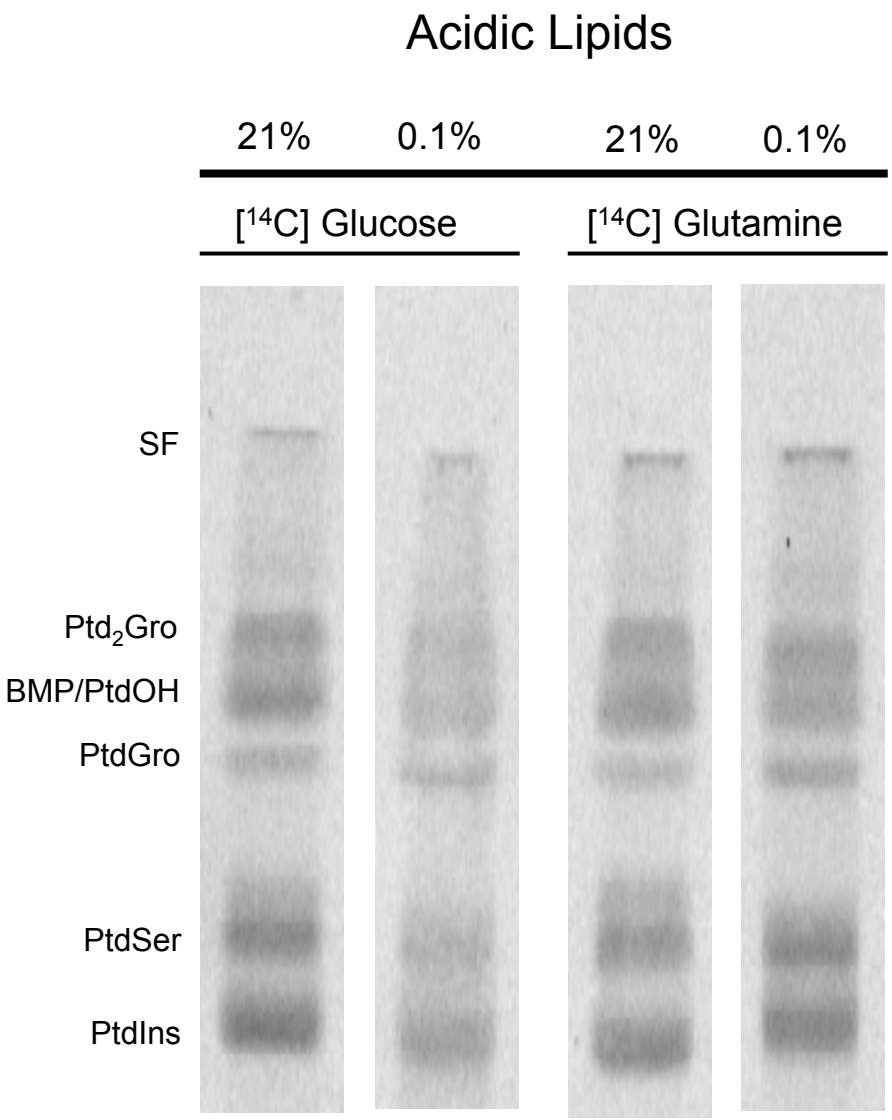
Acidic Lipids
21%
0.1%
21%
0.1%
[14C] Glucose
[14C] Glutamine
SF
Ptd2Gro
BMP/PtdOH
PtdGro
PtdSer
PtdIns

Figure 21.

The influence of hypoxia on incorporation of carbons from [^{14}C] glucose or [^{14}C] glutamine on total dpm from neutral and acidic lipids. The calculated total dpm is the sum of the dpm of the neutral lipids (Table 7) plus dpm of the acidic lipids (Table 8). Values represent as mean ± SEM of three independent samples. Asterisk indicates significant difference from 21% O_2 at $p < 0.01$.

Figure 21.

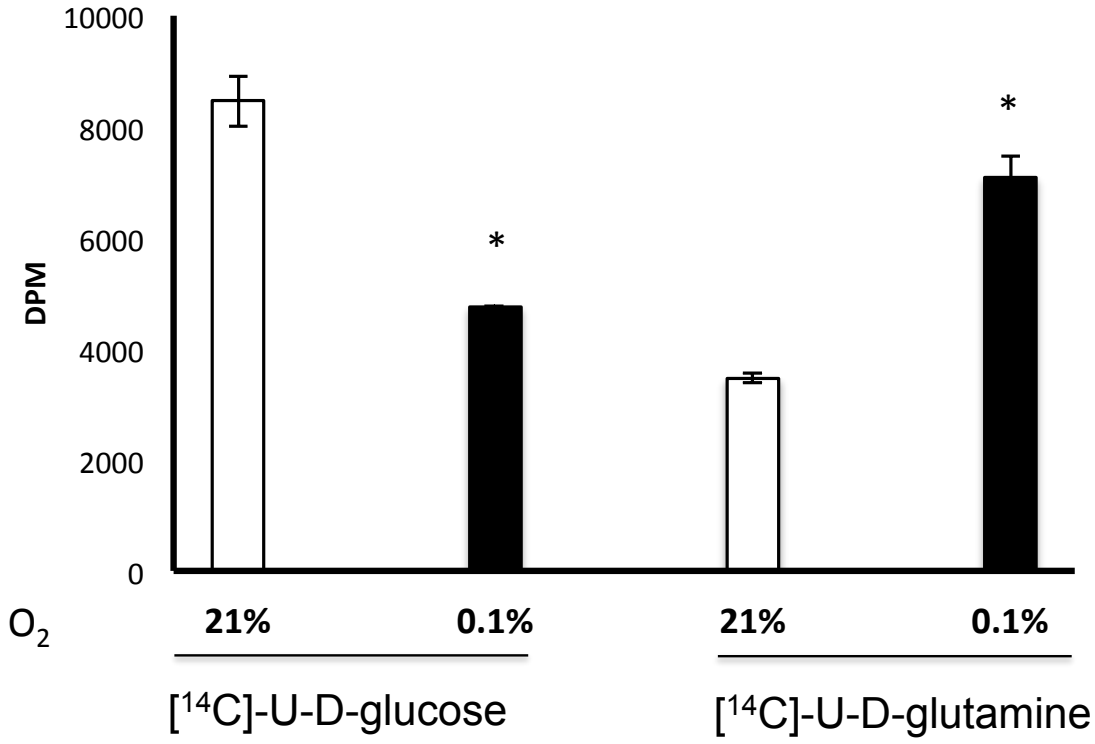
10000
8000
6000
4000
2000
0
DPM
*
*
O2
21%
0.1%
21%
0.1%
[14C]-U-D-glucose
[14C]-U-D-glutamine

Figure 22.

HPTLC analysis of total gangliosides (non-labeled and labeled) in VM-M3 tumor cell line grown under the influence of oxygen. The amount of lipid spotted was equivalent to 2000 dpm. Developing solvents, and lipid visualization is as indicated in Figure 11. The individual gangliosides were labeled according to the nomenclature system of Svennerholm. MB indicates mouse brain.

Figure 22.

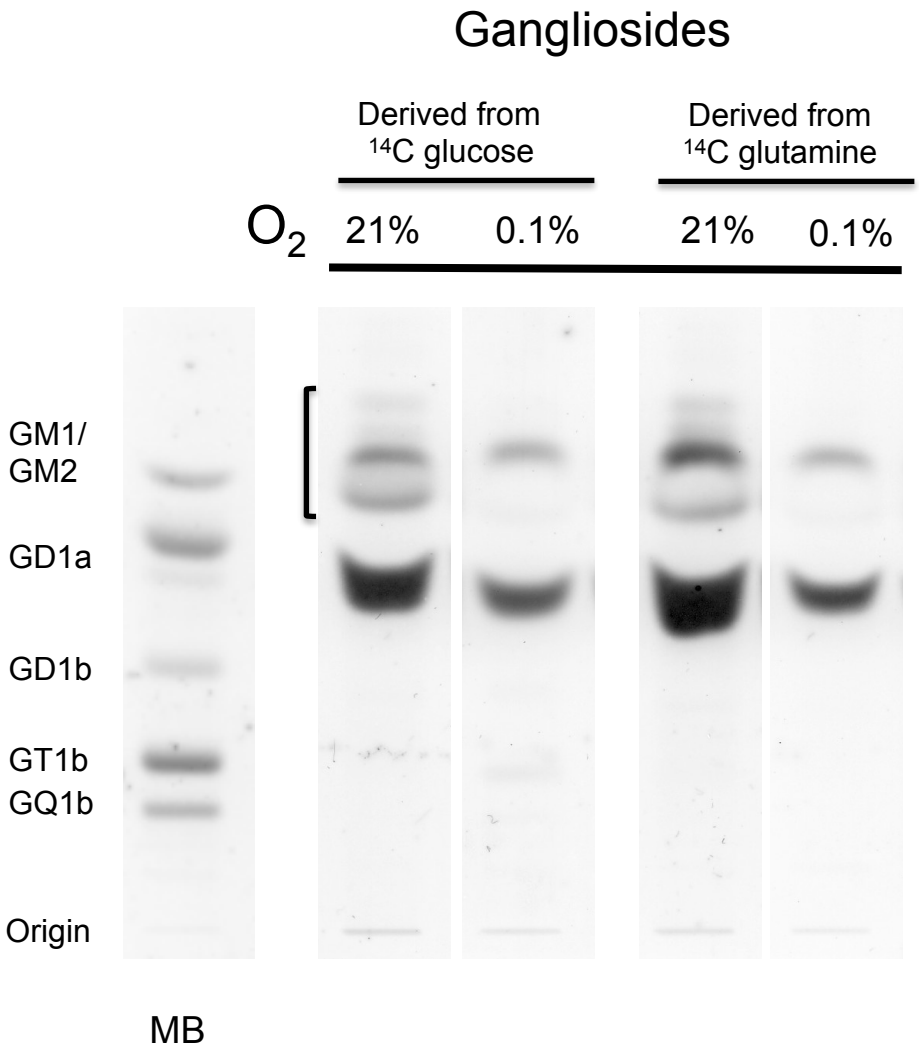
Gangliosides
Derived from
14C glucose
Derived from
14C glutamine
O2
21%
0.1%
21%
0.1%
GM1/
GM2
GD1a
GD1b
GT1b
GQ1b
Origin
MB

Table 9. Influence of O_2 on incorporation of carbons from [^{14}C] glucose and [^{14}C] glutamine into gangliosides in VM-M3 cells[a]

	[^{14}C] Glucose		[^{14}C] Glutamine	
O_2	**21%**	**0.1%**	**21%**	**0.1%**
Gangliosides[b]				
GM1/GM2	1489 ± 94	958 ± 16	1047 ± 10	1187 ± 32
GD1a	1836 ± 21	1158 ± 31	1038 ± 28	1258 ± 6
Total DPM	**3341 ± 82**	**2115 ± 45 ***	**2086 ± 56**	**2445 ± 52**

Calculated dpm were normalized to same number of cells, and expressed as means ± SEM of three independent samples. Individual lipids dpm are calculated from the percent distribution x total dpm. * indicates significant differences from 21% O_2 at $p < 0.02$.

[a] Cells were grown in DMEM with 10% FBS in the presence of 21% O_2 or 0.1% O_2 with either [^{14}C] glucose and [^{14}C] glutamine for 48hrs.

[b] The amount of lipid spotted was equivalent to 2000 dpm

Figure 23.

HPTLC analysis of endogenously synthesized (radiolabeled) gangliosides in VM-M3 tumor cell line grown in either normoxia (21% O_2) or hypoxia (0.1% O_2) using uniformly labeled [^{14}C] glucose or [^{14}C] glutamine. The amount of lipid spotted was equivalent to 2000 dpm. Radiolabeled lipids were visualized with PhosphoImager. The individual gangliosides were labeled according to the nomenclature system of Svennerholm.

Figure 23.

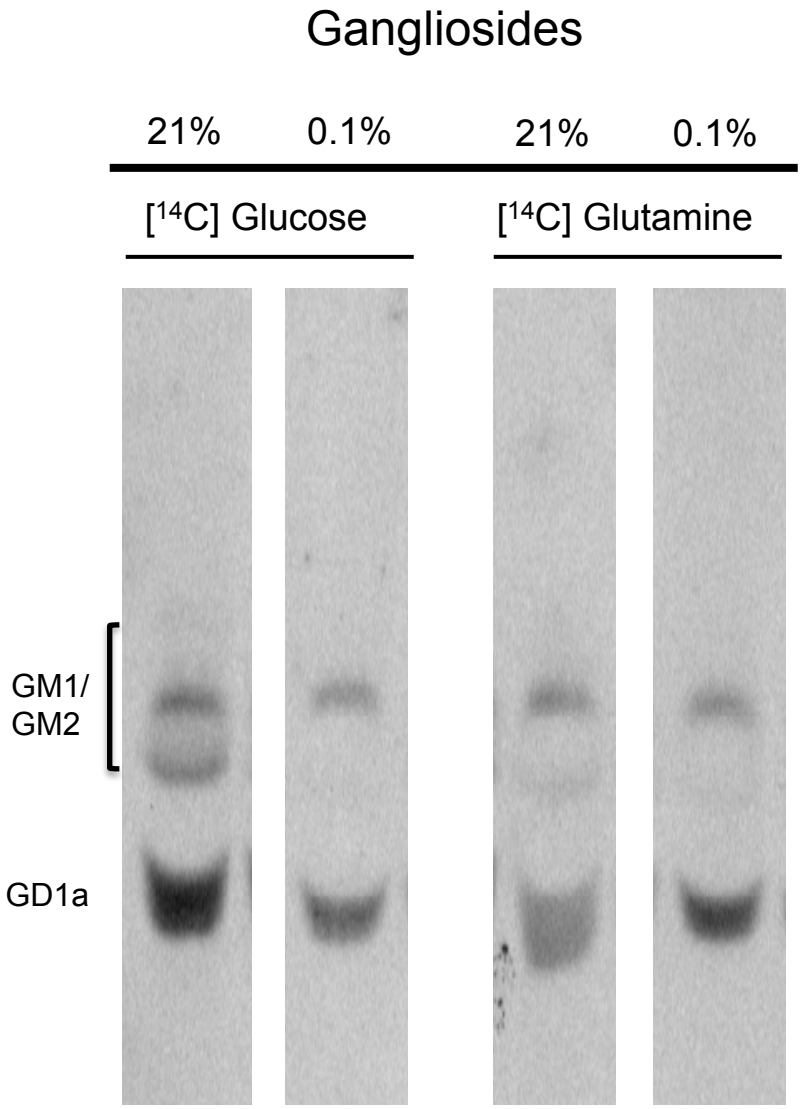
Gangliosides
21%
0.1%
21%
0.1%
[14C] Glucose
[14C] Glutamine
GM1/
GM2
GD1a

Figure 24.

HPTLC analysis of lactate derived from the media of VM-M3 grown in DMEM in either normoxia (21% O_2) or hypoxia (0.1% O_2) using uniformly labeled [^{14}C] glucose and [^{14}C] glutamine. Equal amount of 250 ul of the media was spotted (a) and data analysis was normalized to equal number of cells (b). Developing solvents is as indicated in Figure 14. Values shown in (b) represent three independent samples and are expressed as means ± SEM. Asterisk indicates significant difference from 21% O_2 at $p < 0.01$.

Figure 24.

A.

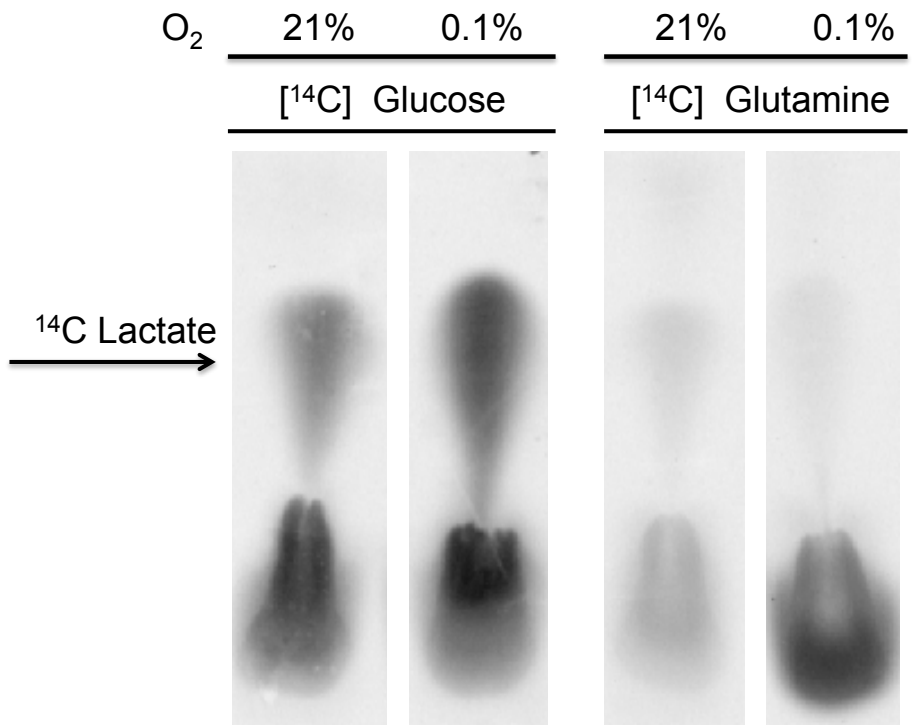
O2
21%
0.1%
21%
0.1%
[14C] Glucose
[14C] Glutamine
14C Lactate

B.

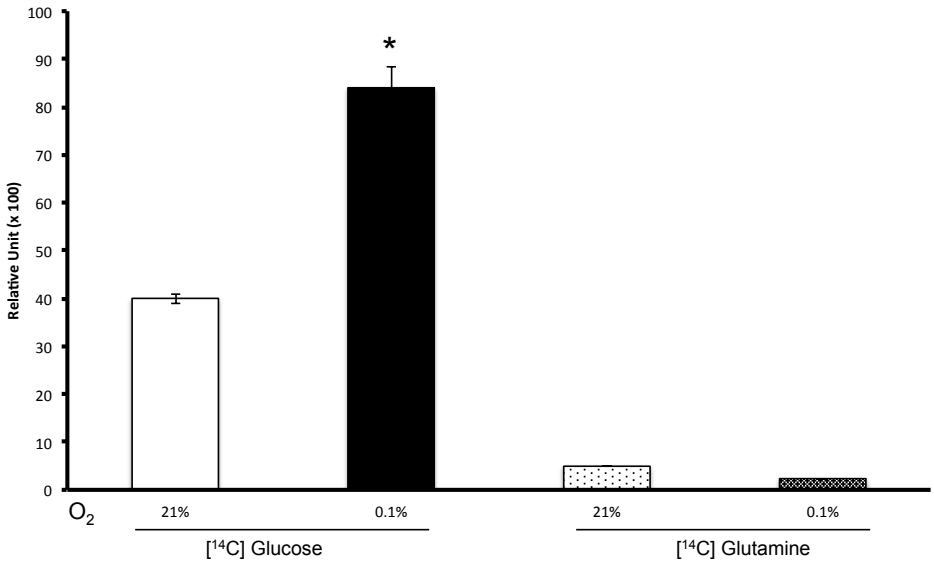
Relative Unit (x 100)
100
90
80
70
60
50
40
30
20
10
0
*
O2
21%
0.1%
21%
0.1%
[14C] Glucose
[14C] Glutamine

Figure 25.

HPTLC analysis of triacylglycerol accumulation under the influence of hypoxia or ETC inhibitor antimycin A (AA). Neutral lipids were separated according to the Material and Methods. The amount of lipids spotted was equivalent to 1 x 10^6 cells. The abbreviations used are as indicated: PL, phospholipids; C, cholesterol; TAG, triacylglycerol. The plate was developed in a single solvent system with hexanes: diethyl ether: acetic acid (70:30:1). Cells were either grown in normoxia (21% O_2), anoxia (0.1% O_2) for 24 hrs, reoxygenated at 21% O_2 for 24 hrs, or 0.1 uM antimycin A (AA).

Figure 25.

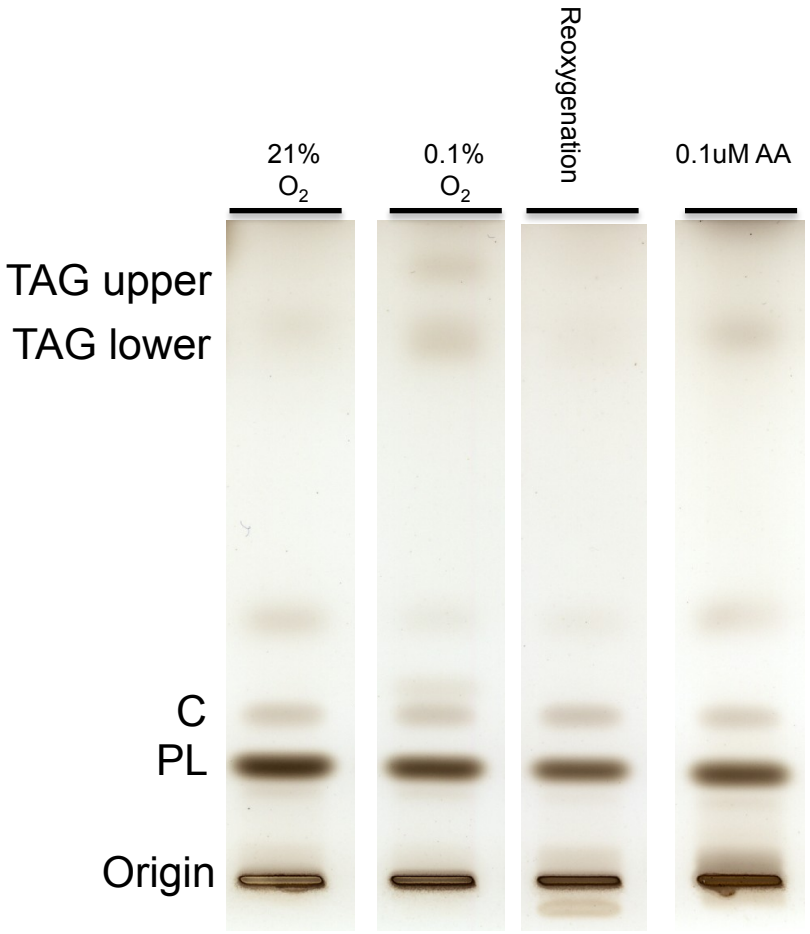
21% O_2
0.1% O_2
Reoxygenation
0.1uM AA
TAG upper
TAG lower
C
PL
Origin

Figure 26.

Oil Red O staining of triacylglycerol in normoxia (B), anoxia, (D), and 0.1% antimycin A (F) and the corresponding differential interference contrast (DIC) for normoxia (A), anoxia (C), and 0.1 μM antimycin A (E). Magnification is 63X. Three independent samples were analyzed per group.

Figure 26.

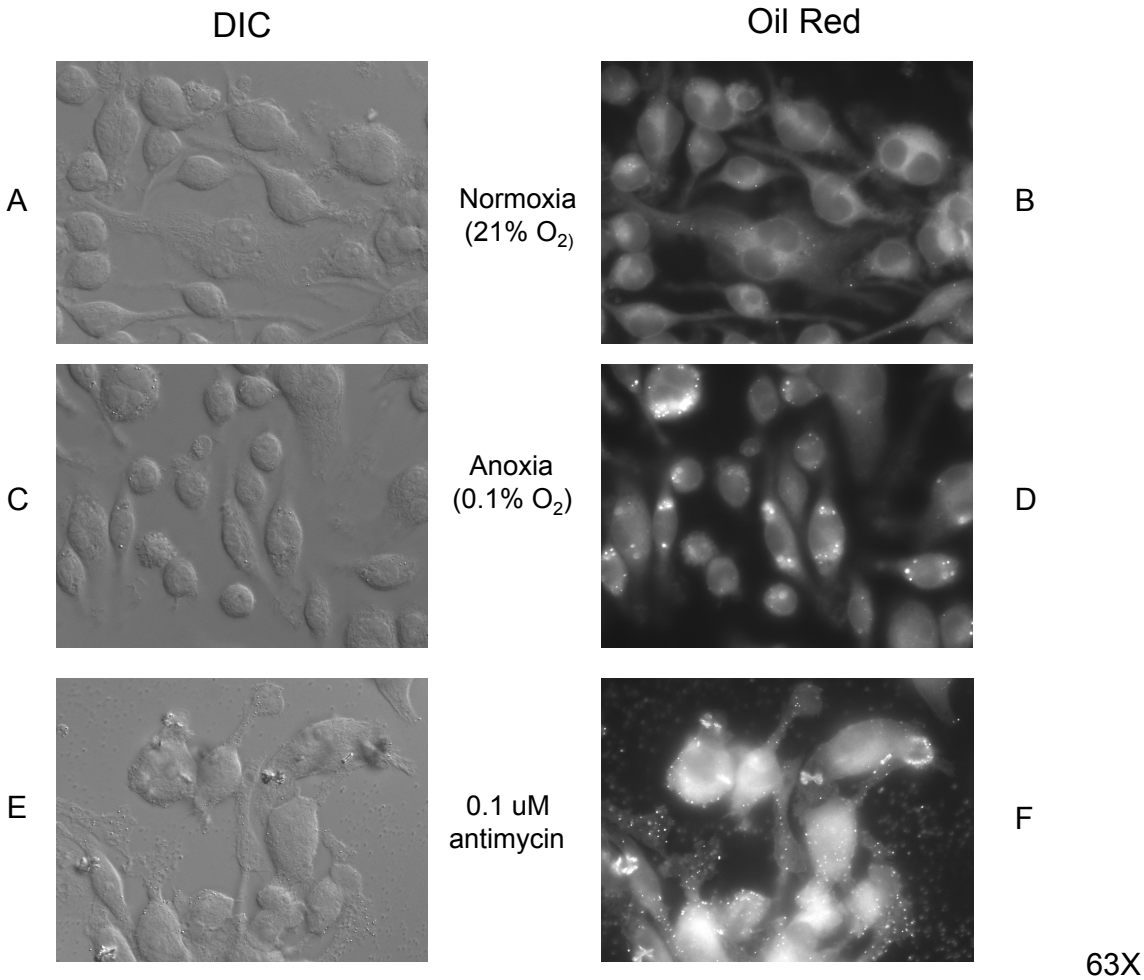
DIC
Oil Red
A
Normoxia
(21% $O_{2)}$
B
C
Anoxia
(0.1% O_2)
D
E
0.1 uM
antimycin
F
63X

Table 10. Influence of hypoxia (0.1% O_2) on the fatty acid content of triacylglycerol (ng lipid/10^6 cells)

	Fractions	
	Lower band	Upper band
Fatty acids		
14:0	0.73 ± 0.05	0.14 ± 0.02 *
16:0	3.66 ± 0.18	1.20 ± 0.11 *
16:1	1.36 ± 0.15	0.24 ± 0.03 *
18:0	0.24 ± 0.02	0.13 ± 0.00 *
18:1	2.40 ± 0.16	0.68 ± 0.04 *
C22 +	0.25 ± 0.03	0.11 ± 0.00 *

Fractions represent lower and upper triacylglyerol band similar to that seen in Figure 25. Fatty acid analysis was carried out using preparative TLC as mentioned in the Materials and Methods.

Values represent fatty acid content ± SEM from 3 independent samples using C17:0 as the internal standard. * indicates that the value in the upper band is significantly different from the value in the lower band at $p < 0.02$, as determined by ANOVA.

Table 11. Influence of hypoxia (0.1% O_2) on the relative molar percent distribution of triacylglycerol fatty acids

	Fractions	
	Lower band	Upper band
Fatty acids		
14:0	8.4 ± 1.0	5.7 ± 0.6 *
16:0	42.3 ± 0.3	47.8 ± 0.5 *
16:1	15.7 ± 1.3	9.7 ± 0.7 *
18:0	2.8 ± 0.3	5.4 ± 0.4 *
18:1	27.7 ± 0.4	27.4 ± 1.0
C22 +	2.9 ± 0.4	4.3 ± 0.4 *
SFA/UFA	1.2 ± 0.3	1.6 ± 0.1 *

Fractions represent lower and upper triacylglyerol band similar to that seen in Figure 25. Fatty acid analysis was carried out using preparative TLC as mentioned in the Materials and Methods.

Values represent mean mole percentage distribution of fatty acid ± SEM from 3 independent samples. * indicates that the value in the upper band is significantly different from the value in the lower band at $p < 0.02$, as determined by ANOVA.

SFA - saturated fatty acid; UFA - unsaturated fatty acid

Figure 27.

In vivo accumulation of triacylglycerol in subcutaneous implanted VM tumor. VM-M3 tumor was implanted subcutaneously (s.c) in VM mice for the duration of 30 days. A small tumor fragment from three sagital cross sections were obtained for triacylglycerol determination. Values represent µg lipid / 100 µg of dry tumor weight.

Figure 27.

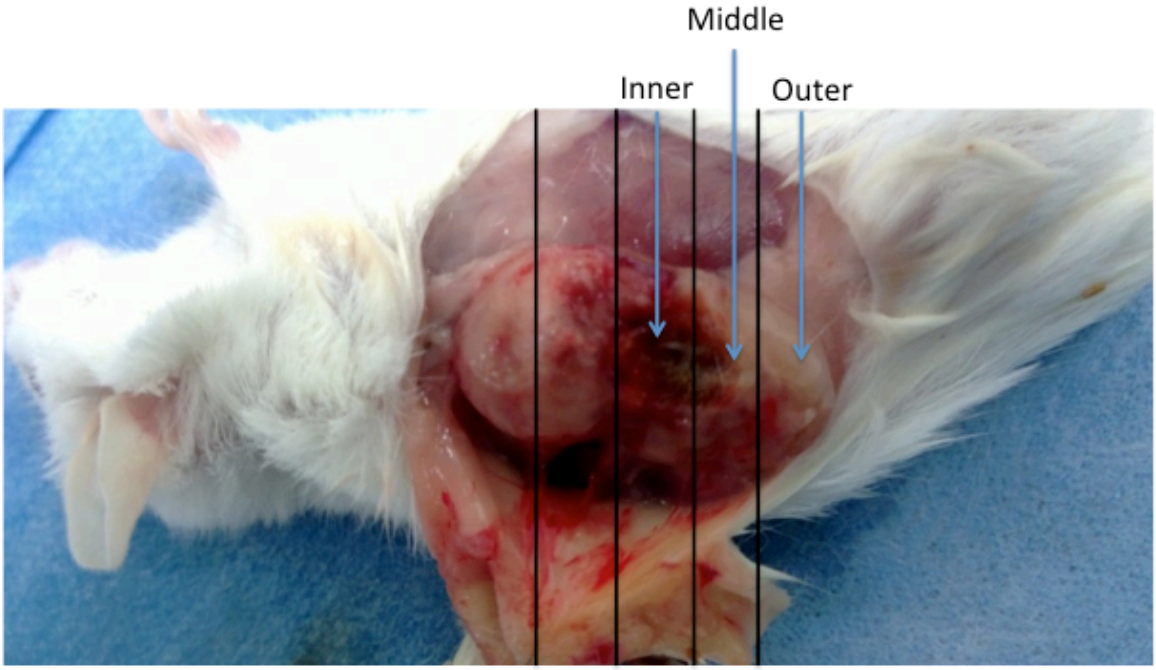
Middle
Inner
Outer

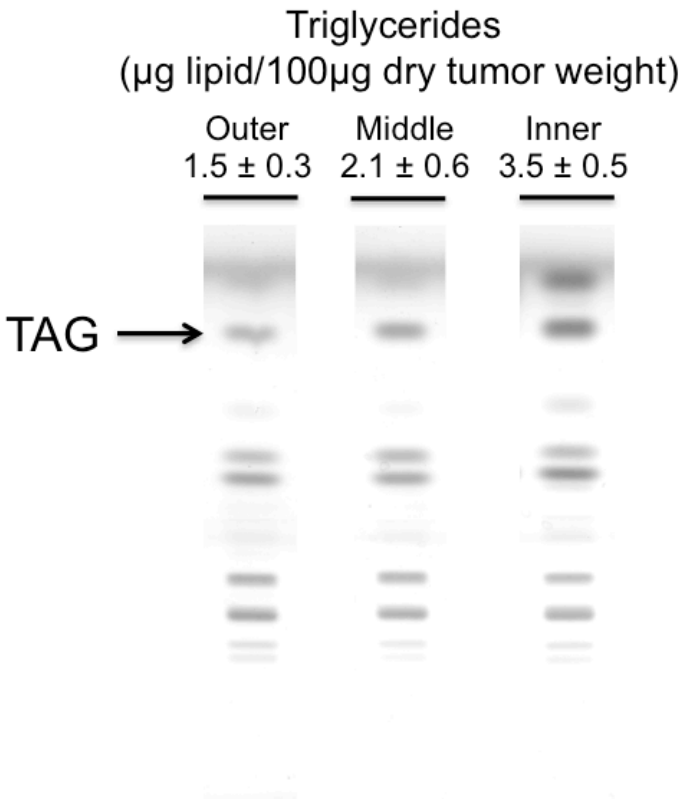
Triglycerides
(µg lipid/100µg dry tumor weight)
Outer
1.5 ± 0.3
Middle
2.1 ± 0.6
Inner
3.5 ± 0.5
TAG

Figure 28.

Summary of the relative incorporation of carbons from glucose and glutamine into lipid biosynthesis and lactate production in either normoxia or hypoxia.

Figure 28.

A.

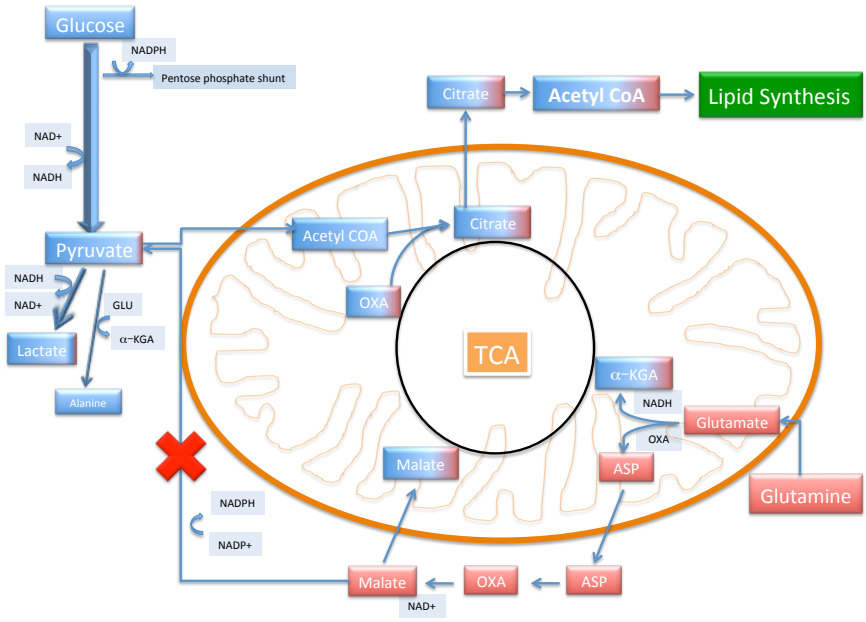
Glucose
NADPH
Pentose phosphate shunt
NAD+
NADH
Pyruvate
NADH
NAD+
GLU
α-KGA
Lactate
Alanine
Citrate
Acetyl CoA
Lipid Synthesis
Acetyl COA
Citrate
OXA
TCA
α-KGA
NADH
Glutamate
OXA
ASP
Malate
Glutamine
NADPH
NADP+
Malate
OXA
ASP
NAD+

B.

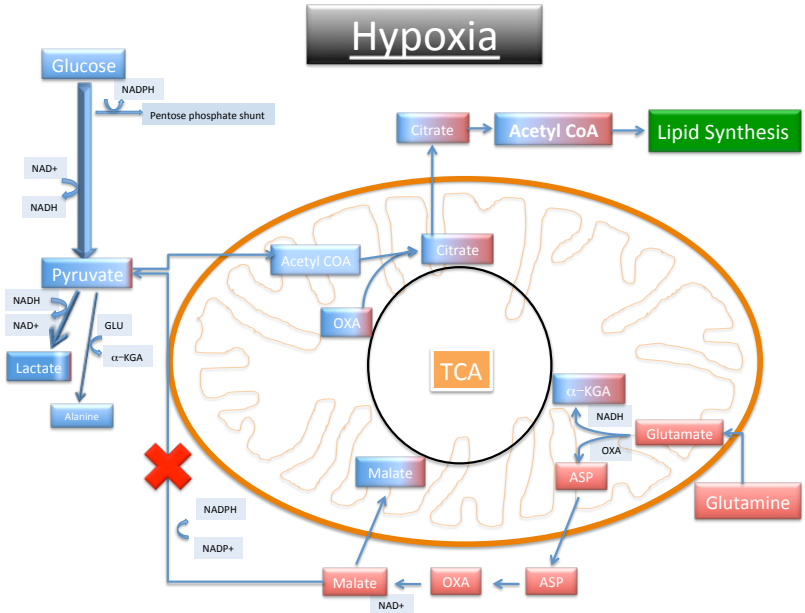
Hypoxia
Glucose
NADPH
Pentose phosphate shunt
NAD+
NADH
Pyruvate
NADH
NAD+
GLU
α-KGA
Lactate
Alanine
Citrate
Acetyl CoA
Lipid Synthesis
Acetyl COA
Citrate
OXA
TCA
α-KGA
NADH
Glutamate
OXA
ASP
Malate
Glutamine
NADPH
NADP+
Malate
OXA
ASP
NAD+

Supplemetary Figures

Figure S1.

ESI tandem mass spectrometry of triacylglycerol mass content of VM-M3 cells grown in either normoxia (21% O_2) or anoxia (0.1% O_2) for 24 hrs.

Figure S1.

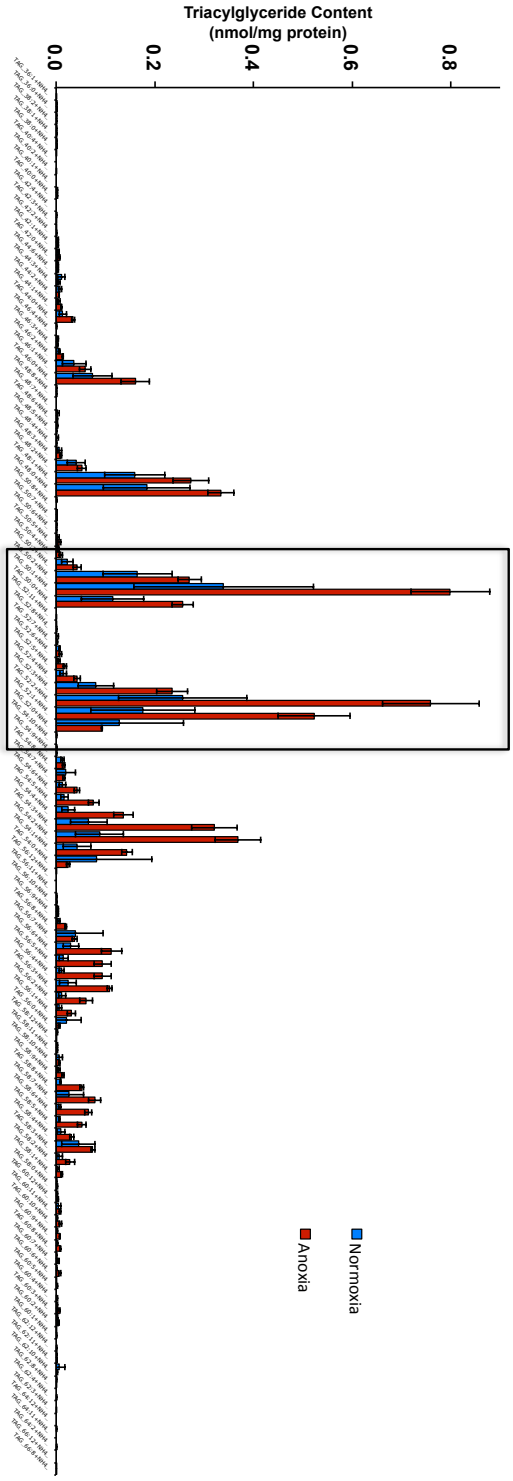
Triacylglyceride Content
(nmol/mg protein)
0.0
0.2
0.4
0.6
0.8
Anoxia
Normoxia

Figure S2.

Lipoprotein is required for cell viability and growth under hypoxia and in the absence of FBS. Cell viability and growth were assessed by trypan blue exclusion dye test. Cells were seeded at 200 (x100) cells and grew under 0.1% O_2 for 24 hrs in media containing no FBS, no FBS + 5 mg/dL lipoprotein, or 10% FBS.

Figure S2.

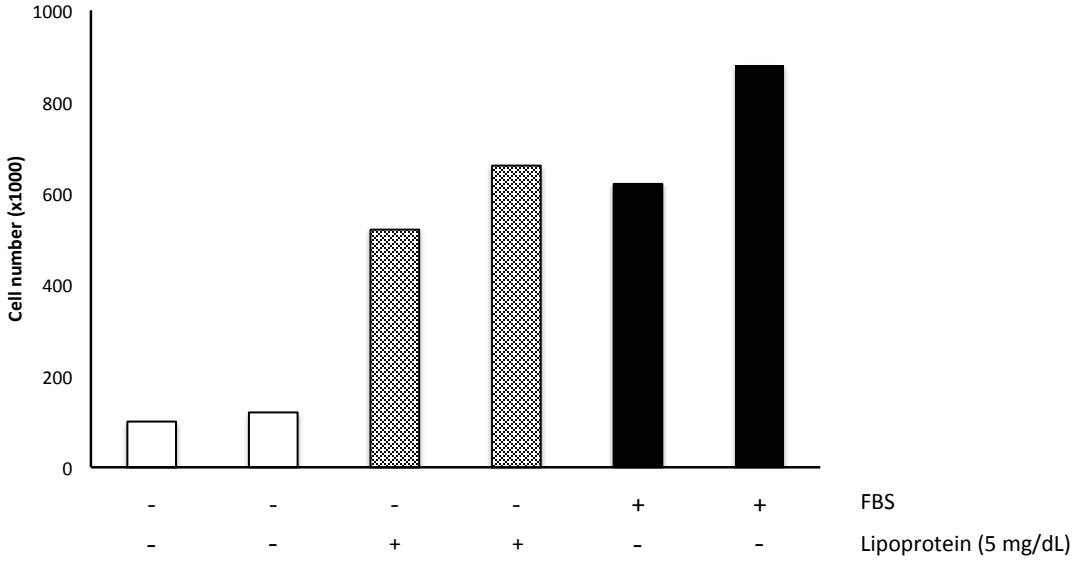
1000
800
600
400
200
0
Cell number (x1000)
- - - - + +
FBS
- - + + - -
Lipoprotein (5 mg/dL)

Figure S3.

Ceramide accumulation in cells growing under hypoxia and in the absence of FBS. Neutral lipids were separated according to the Material and Methods. The amount of lipids spotted was equivalent to 1 x 10^6 cells. The abbreviations used are as indicated in Table 1. Cells were either grown in normoxia (21% O_2) or hypoxia (0.1% O_2) and with FBS or no FBS for 24 hrs.

Figure S3.

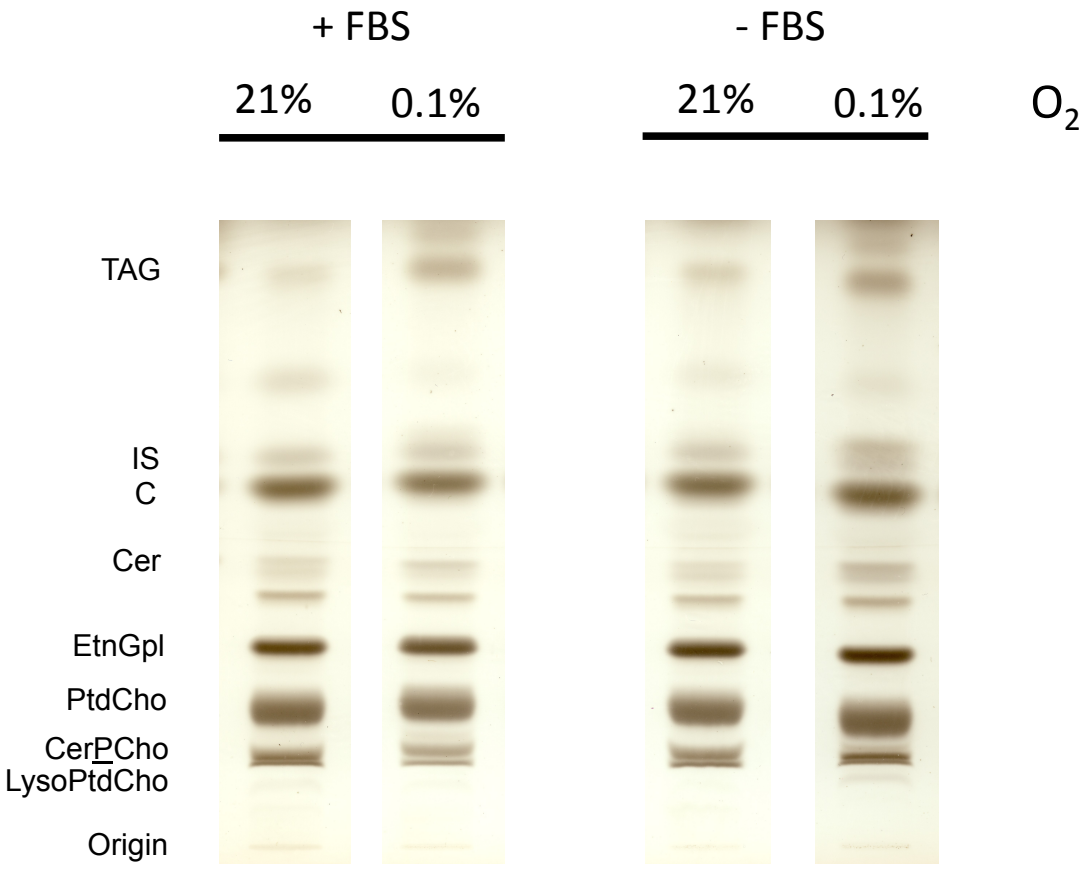
+ FBS
- FBS
21%
0.1%
21%
0.1%
O_2
TAG
IS
C
Cer
EtnGpl
PtdCho
CerPCho
LysoPtdCho
Origin

Figure S4.

Schematic representation of cholesterol biosynthesis. 11 molecules of oxygen are required to synthesize a single molecule of cholesterol.

Figure S4.

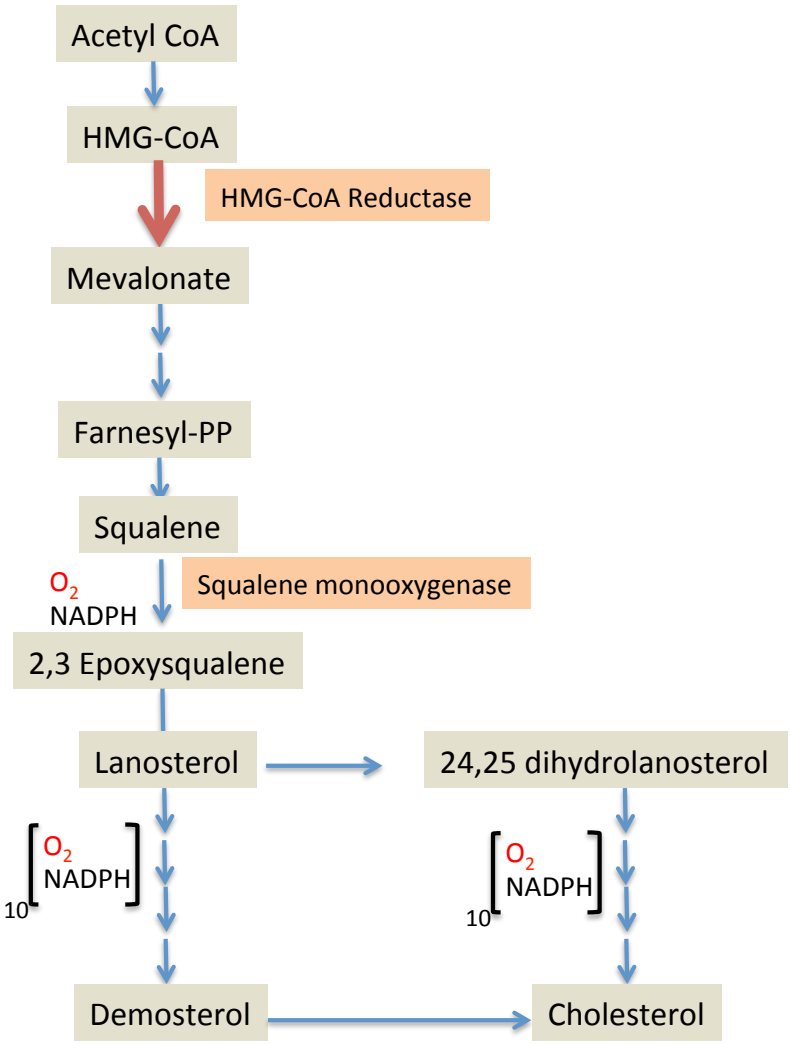
Acetyl CoA
HMG-CoA
HMG-CoA Reductase
Mevalonate
Farnesyl-PP
Squalene
O2
NADPH
Squalene monooxygenase
2,3 Epoxysqualene
Lanosterol
24,25 dihydrolanosterol
O2
NADPH
10
O2
NADPH
10
Demosterol
Cholesterol

CHAPTER THREE

Autosomal dominant inheritance of brain cardiolipin fatty acid abnormality in VM/DK mice: Association with hypoxic-induced cognitive insensitivity

Introduction

Cardiolipin (1,3-bisphosphatidyl-*sn*-glycerol, Ptd_2Gro) is a complex mitochondrial specific phospholipid that regulates numerous enzyme activities especially those related to oxidative phosphorylation and coupled respiration (Kiebish *et al.* 2008c, Berrigan *et al.* 2002, Fry *et al.* 1980, Fry *et al.* 1981, Chicco *et al.* 2007, Hoch 1992). The activities of the respiratory enzyme complexes and states 1-3 of respiration are dependent on Ptd_2Gro fatty acid species composition (Kiebish *et al.* 2008b, Chicco *et al.* 2007, Hoch 1992, Hoch 1998). Ptd_2Gro contains two phosphate head groups, three glycerol moieties, and four fatty acyl chains (Figure 29). Ptd_2Gro, like many other phospholipids in cellular membranes are continually being synthesized and degraded in a dynamic state. It represents 7-12 % of total mitochondrial phospholipids (PL) in non-neural tissues and approximately 2.5% in the brain (Schlame *et al.* 2000). Although the four possible acylated positions do provide immense diversity in molecular speciation (Schlame *et al.* 2000, Kiebish *et al.* 2008a) there is symmetry and specificity in the acylated positions. The specificity can be cell type and tissue specific or

even species specific (Schlame *et al.* 2000). It varies from rat testis consisting of predominantly tetra-palmitoyl (C16:0) to mostly tetra-linoleoyl (C18:2) in rat heart, liver and kidney (Wang *et al.* 2007). On the other hand, marine bivalves consist of predominantly tetra-docosahexaenoyl (C22:6) fatty acids (Kraffe *et al.* 2002). Mouse neural tissue constitutes primarily of C18:1, where tetra-oleoyl fatty acids represent high percentage but not the predominant molecular speciation. There is an increase in diversity in molecular speciation in neural tissue rather than the tetra-acylated structure seen in non-neural tissues (Kiebish *et al.* 2008c). Nevertheless, the symmetry of the four acylated fatty acids provide structural conformation for binding to the ETC complexes, particularly complex III, IV, ADP/ATP protein carrier, and aide in the organization of the supramolecular ETC complexes (Acehan *et al.* 2011, Wittig *et al.* 2009). The specificity in forming the mature cardiolipin in the tetra-acylated structures is seemingly the result of deacylation/reacylation or transacylase mechanisms rather than as the result of the de novo synthesis pathway. The uniqueness of this mitochondrial lipids association to the ETC enzymatic activities and membrane fluidity ultimately are responsible for the functionality and efficiency of respiration. Alterations in brain Ptd_2Gro often lead to energetic inefficiency and neurodegenerative diseases (Pope *et al.* 2008a, Daum 1985, Bayir *et al.* 2007a). Changes in Ptd_2Gro abundance or molecular species are observed in traumatic brain injury, Parkinson, diabetic cardiomyopathy, heart failure (Pope *et al.* 2008a, Ellis *et al.* 2005).

We recently identified over 100 molecular fatty acid species of Ptd_2Gro in the mitochondria from C57BL/6J (B6) brain, which was similar to the Ptd_2Gro composition of other mammalian brains (Cheng *et al.* 2008, Kiebish *et al.* 2008c). In contrast to B6 mice, mice of the VM/Dk (VM) strain have an unusual distribution of brain Ptd_2Gro molecular species consisting of a greater ratio of shorter chain saturated and monounsaturated fatty acids (C16:0; C18:0; C18:1) to longer chain polyunsaturated fatty acids (LCPUFA) (C18:2; C20:4; C22:6.) Reductions in the activity of mitochondrial respiratory Complexes I, I/III, and II/III were linked to the abnormal MUFA/LCPUFA ratio in the VM brain despite normal total amounts of total cardiolipin (Kiebish *et al.* 2008a). In addition, the incidence of spontaneous brain tumors is greater in VM mice than in B6 mice, while the onset of p53-induced lymphoma occurs significantly earlier in VM mice than in B6/129sv mice (Fraser 1986, van Meyel *et al.* 1998, Mancuso *et al.* 2009). As cancer is now recognized as a mitochondrial metabolic disease, this increased deficit in mitochondrial function associated with increased cancer incidence could be precipitated by the brain Ptd_2Gro abnormalities discovered in the VM mice (Seyfried 2012, Seyfried *et al.* 2010b).

In addition to causing energetic abnormalities in tumor cells, alterations in brain Ptd_2Gro are linked to energetic inefficiency in cardiac and neurodegenerative diseases (Pope *et al.* 2008b, Daum 1985, Bayir *et al.* 2007b). The molecular pathophysiology of cognitive deficiency is incompletely

understood. Currently, 10-15% of children express some level of cognitive deficiency that cannot be explained by genetics alone (Thomas *et al.* 2012, Petrosillo *et al.* 2013). Due to the wide array of environmental perturbations that result in decreased neural bioenergetic efficiency and are likely to alter brain mitochondrial lipid composition through peroxidation or altered remodeling, it would seem plausible that neural deficiencies might arise from alterations in the biophysical properties of the mitochondrial lipid membrane. In this report we found that the abnormal distribution of Ptd_2Gro molecular species in VM mouse brain is inherited as an autosomal dominant trait in crosses with B6 mice and that the Ptd_2Gro phenotype associates with a behavioral trait involving hypoxia-induced cognitive insensitivity.

Materials and Methods

Mice

The VM/DK (VM) strain of mice was obtained originally from H. Fraser (University of Edinburgh) and from G. Carlson (McLaughlin Research Institute, Great Falls, Montana). The C57BL/6J (B6) mice were obtained from the Jackson Laboratory (Bar Harbor, ME). The mice used for the study were maintained in the animal facility at Boston College. Mice of both strains were age matched (three months) and both sexes were used for the study. All mice were individually housed and were provided with food under *ad libitum* (AL). Water was provided *ad libitum* to all mice. Whole brain was dissected from the mice following cervical dislocation. All animal procedures were in strict accordance with the NIH Guide for the Care and Use of Laboratory Animals and were approved by the Institutional Animal Care Committee. VM and B6 mice were crossed to produce reciprocal F_1 hybrids (B6 x VMF_1 and VM x $B6F_1$ hybrids). The female parent is presented on the left in each cross.

Hypoxic Treatment

The hypoxia treatment involved placing mice in a partitioned glass chromatography jar that was flushed with 5% O_2 balanced - N_2 (containing 10

ppm of ammonia, Air Gas, Cambridge, MA, USA). The dimensions of the jar were as previously described (Seyfried 1979). The mice were treated for a maximum of 30 min. The time of exposure to hypoxia for each mouse was dependent on its cognitive sensitivity. Cognitive sensitivity was assessed by the response of a mouse to a gentle tapping sound of 70-72 decibels on the side of the glass jar. Mice responding to the tapping sound show obvious ear and head movements. Mice experiencing hypoxia insensitivity become immobile, lie flat on their stomachs, drop their tails, and close their eyes. As time under hypoxia progresses the ear response to the tapping disappears. Mice that were immobile and no longer responsive to the sound were considered cognitively insensitive. The time to insensitivity was recorded for each mouse.

Lipid extraction and fatty acid analysis

The collected mouse brains were stored at -80^{o}C and lyophilized to remove water. Total lipids were extracted with chloroform ($CHCl_3$) and methanol (CH_3OH) 1:1 by volume from the lyophilized brain tissue using modifications of previously described procedures (Seyfried *et al.* 1978, Baek *et al.* 2004, Baek *et al.* 2008). Neutral and acidic lipids were separated using DEAE-Sephadex (A-25, Pharmacia Biotech, Upsala, Sweden) column chromatography as previously described (Macala *et al.* 1983). The total lipid extract, suspended in

$CHCl_3$:CH_3OH:dH_20, 30:60:8 by volume (solvent A), was applied to a DEAE-Sephadex column (1.2 mL bed volume) that had been equilibrated prior with solvent A. Neutral lipids were eluted with two 20 ml washes of solvent A. The acidic lipids were eluted from the column with 35 mL $CHCl_3$:CH_3OH: 0.8 M sodium acetate, 30:60:8 by volume. This fraction contained Ptd_2Gro, other acidic phospholipids, and sulfatides. Preparative high performance thin-layer chromatography (20 x 20 cm) was used to separate Ptd_2Gro from the other acidic lipids. Authentic Ptd_2Gro standard, 1',3'-bis(1,2-dioleoyl-*sn*-glycero-3-phospho)-*sn*-glycerol, (Avanti Polar Lipids) was used to identify the Ptd_2Gro band from the brain samples. Ptd_2Gro visualization was observed after spraying the plate with 5% primulin (80:20 acetone: water vol/vol). The Ptd_2Gro fraction was scraped from the plate and transesterified with 0.5 N NaOH in methanol for 10 min in a sealed borosilicate tube under nitrogen at 90^{o}C (Lepage *et al.* 1984). Gas chromatography (HP 6890) equipped with flame ionization detector and splitless injector was used for the quantitative analysis of Ptd_2Gro fatty acid methyl esters. The fatty acids were resolved using a 30 m x 0.25 mm x 0.25 μm Omegawax 250 fused silica capillary column (Supelco). The temperature program ramps from 150^{o}C to 220^{o}C at 4^{o}C per minute and was held constant at 220^{o}C for 20 min.

Statistical analysis

The one-way analysis of variance (ANOVA) coupled with Tukey HSD as a *post hoc* test was used to evaluate the significance of differences among the groups of mice.

Results

The abnormal cardiolipin molecular species composition in VM mice is inherited as an autosomal dominant inherited trait

The composition of major brain fatty acid molecular species of Ptd_2Gro in the B6 and the VM parental strains and their reciprocal F_1 hybrids is shown in Figure 30. No significant differences were found between males and females in the parental strains or in the reciprocal F1 hybrids. The mole percent distribution of the major saturated and monounsaturated fatty acids (C16:0, C18:0, C18:1) was significantly higher in the VM mice than in the B6 mice. On the other hand the mole percent distribution of the major longer chain polyunsaturated fatty acids (C18:2; C20:4; C22:6) was significantly lower in the VM mice than in the B6 mice. The fatty acid composition of Ptd_2Gro was similar in the reciprocal male and female F_1 hybrids (B6 x VM F_1 and VM x B6 F_1), indicating the absence of a sex influenced or sex-linked trait. The Ptd_2Gro fatty acid distribution in the reciprocal F_1 hybrids was similar to the distribution in the VM parental strain and significantly different from the distribution in the B6 parental strain (Figure 30). Consequently the Ptd_2Gro MUFA/PUFA ratio and the ratio of shorter chain fatty acid (SCFA) to long chain fatty acid (LCFA) (C16-C18)/(C20-C22) were similar in the VM parents and F_1 hybrids and were significantly higher than the ratios in the

B6 parents (Figure 31 A, B). These findings indicate that the unusual Ptd_2Gro fatty acid pattern seen in the VM mice was inherited as an autosomal dominant trait.

Influence of hypoxia on cognitive sensitivity in the B6 and VM strains and their reciprocal F_1 hybrids

Cognitive sensitivity in the B6 and the VM parental strains and in their reciprocal F_1 hybrids under a 5% O_2 balanced - N_2 enclosed environment (hypoxia) is shown in (Figure 31 C). No differences were seen between male and female mice within each strain. The cognitive sensitivity value was significantly lower in the VM mice than in the B6 mice. The mean cognitive awareness value for the reciprocal male and female F_1 hybrids was similar to that in the VM parental strain and significantly lower than that in the B6 parental strain. The autosomal dominant pattern of inheritance described above for the distribution of Ptd_2Gro fatty acids was also seen for cognitive sensitivity under hypoxia, as the pattern of inheritance in the reciprocal F_1 hybrids was similar to that of the VM parent. Viewed together, these findings suggest a genetic association between cognitive sensitivity under hypoxia and abnormal Ptd_2Gro fatty acid composition.

Discussion

In this study, we present evidence showing that the abnormal MUFA/LCPUFA and SCFA/LCFA ratios previously reported in mice of the VM strain is inherited as an autosomal dominant trait in a cross with the B6 strain. The mole percent distribution of brain Ptd_2Gro fatty acid profile of the B6 mice was similar to previously reported values, although slightly different due to different methods of analysis (Kiebish *et al.* 2008a, Barcelo-Coblijn *et al.* 2005). The brain Ptd_2Gro fatty acid profile of the B6 mice was also similar to that reported in other mammalian brains, suggesting that the brain Ptd_2Gro fatty acid profile of VM mice is abnormal relative to profile seen in the B6 mice (Cheng *et al.* 2008, Kiebish *et al.* 2008a). Similar to Barth syndrome, where a mutation in the tafazzin gene produces Ptd_2Gro abnormalities, we suggest that the altered Ptd_2Gro fatty acid pattern in the VM mice could result from alterations in cardiolipin remodeling involving acyltransferase(s) and/or phospholipase(s) (Vreken *et al.* 2000, Kiebish *et al.* 2008a). It is also possible that the fatty acid abnormality in VM mice is due to a defect in an elongase (Jump 2009).

The autosomal dominant inheritance of the abnormal brain Ptd_2Gro fatty acid profile was also seen for cognitive sensitivity under hypoxia. Cognitive sensitivity under hypoxia was significantly less in the VM mice than in the B6 mice. The cognitive sensitivity of the reciprocal male and female $B6VMF_1$ hybrid mice was

similar to that of their VM parents and was significantly less than that of their B6 parents. The absence of differences between the male and female F1 mice for Ptd_2Gro composition and cognitive sensitivity indicate that these traits are not sex linked. These findings indicate that cognitive sensitivity under hypoxia was also inherited as an autosomal dominant trait.

It is well known that impaired cognition can arise as a consequence of impaired mitochondrial function (Mancuso *et al.* 2009, Finsterer 2008). Moreover, cognitive abnormalities were reported previously in mice with deletion of phospholipase A2, which plays a role in Ptd_2Gro remodeling (Mancuso *et al.* 2009). Ptd_2Gro fatty acid species composition is known to influence the activities of the respiratory enzyme complexes and states 1-3 of respiration. It is therefore possible that the abnormal brain Ptd_2Gro fatty acid composition and possibly that of other phospholipids in VM mice underlies the abnormal cognitive sensitivity to hypoxia in this strain and in their F_1 hybrids (Claypool *et al.* 2011). Further studies will be needed to determine if the dominant inheritance of the abnormalities in Ptd_2Gro composition and if cognitive insensitivity is due to the action of a single dominant gene or whether it is due to a multifactorial trait with dominant inheritance (Todorova *et al.* 2006, Todorova *et al.* 1999). It is unknown if the differences in Ptd_2Gro between VM, F1 hybrids and B6 occurred only specifically in the brain. Further studies will be needed to determine if the

differences could occur in other tissues and how hypoxia can influence Ptd_2Gro fatty acid composition in the brain and other tissues.

Summary

In this study we found that the abnormal brain fatty acid ratio in the VM strain was inherited as an autosomal dominant trait in reciprocal B6 x VM F_1 hybrids. Cognitive awareness (conscientiousness) under hypoxia was significantly lower in the VM parental mice and F1 hybrid mice than in the parental B6 mice, indicating an autosomal dominant inheritance like that of the brain Ptd_2Gro abnormalities. These findings suggest that impaired cognitive awareness under hypoxia is associated with abnormalities in neural lipid composition.

Tables and Figures

Figure 29.

Structure of Ptd_2Gro (1,3-diphosphatidyl-*sn*-glycerol)

Figure 29.

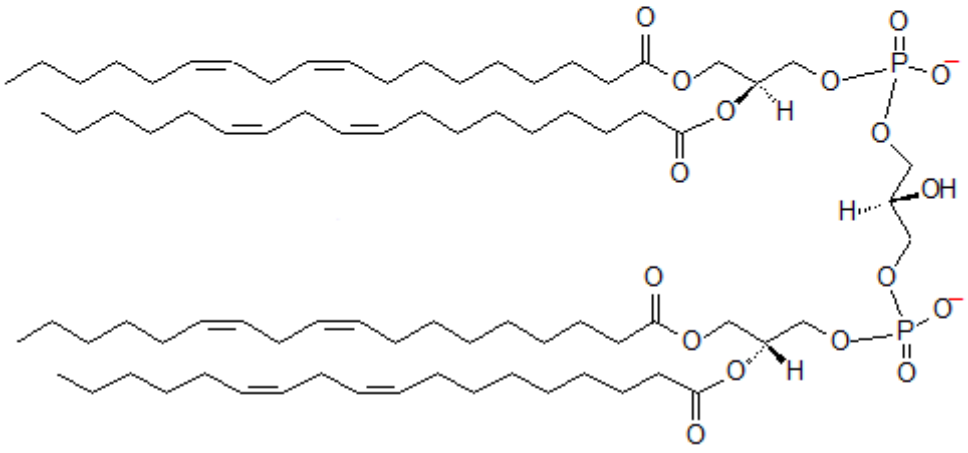

Figure 30.

The composition of major brain fatty acid molecular species of Ptd_2Gro in B6 and VM parental strains and their reciprocal F_1 hybrids. Values represent mole percent distribution of fatty acid ± SEM. Significant differences from B6 at * $p < 0.01$ as determined by ANOVA coupled with Tukey HSD as a post hoc test.

Figure 30.

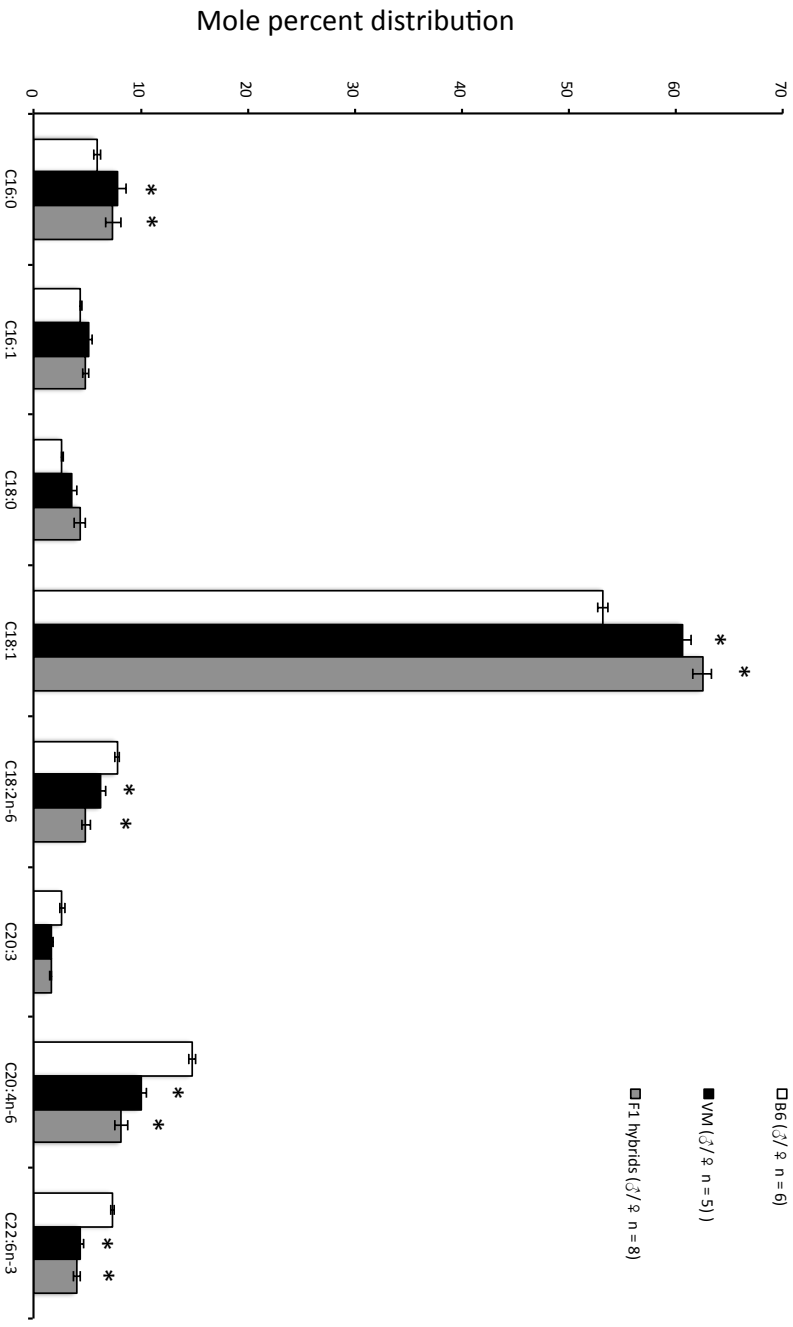
Mole percent distribution
0
10
20
30
40
50
60
70
C16:0
C16:1
C18:0
C18:1
C18:2n-6
C20:3
C20:4n-6
C22:6n-3
B6 (♂/♀ n = 6)
VM (♂/♀ n = 5))
F1 hybrids (♂/♀ n = 8)

Figure 31

The proportionality of SCFA/LCFA (A) and MUFA/PUFA (B) is associated with cognitive sensitivity (C). Shorter chain fatty acids (SCFA) represent fatty acids ranging from C16-C18. Longer chain fatty acids (LCFA) represent fatty acids ranging from C20-C22. Monounsaturated fatty acids (MUFA) represent C16:1, C18:1. Polyunsaturated fatty acids (PUFA) represent C18-2 n-6, C20:3, C20:4 n-6, C22:6 n-3. B6, VM and F_1 hybrid mice were treated for cognitive sensitivity as described in Methods. Values represent the mean ± SEM. Asterisks indicate that the values differ significantly from the values in B6 mice at $^{*}p < 0.01$ as determined by one-way ANOVA coupled with Tukey HSD as a post hoc test. n denotes number of independent mice analyzed.

Figure 31.

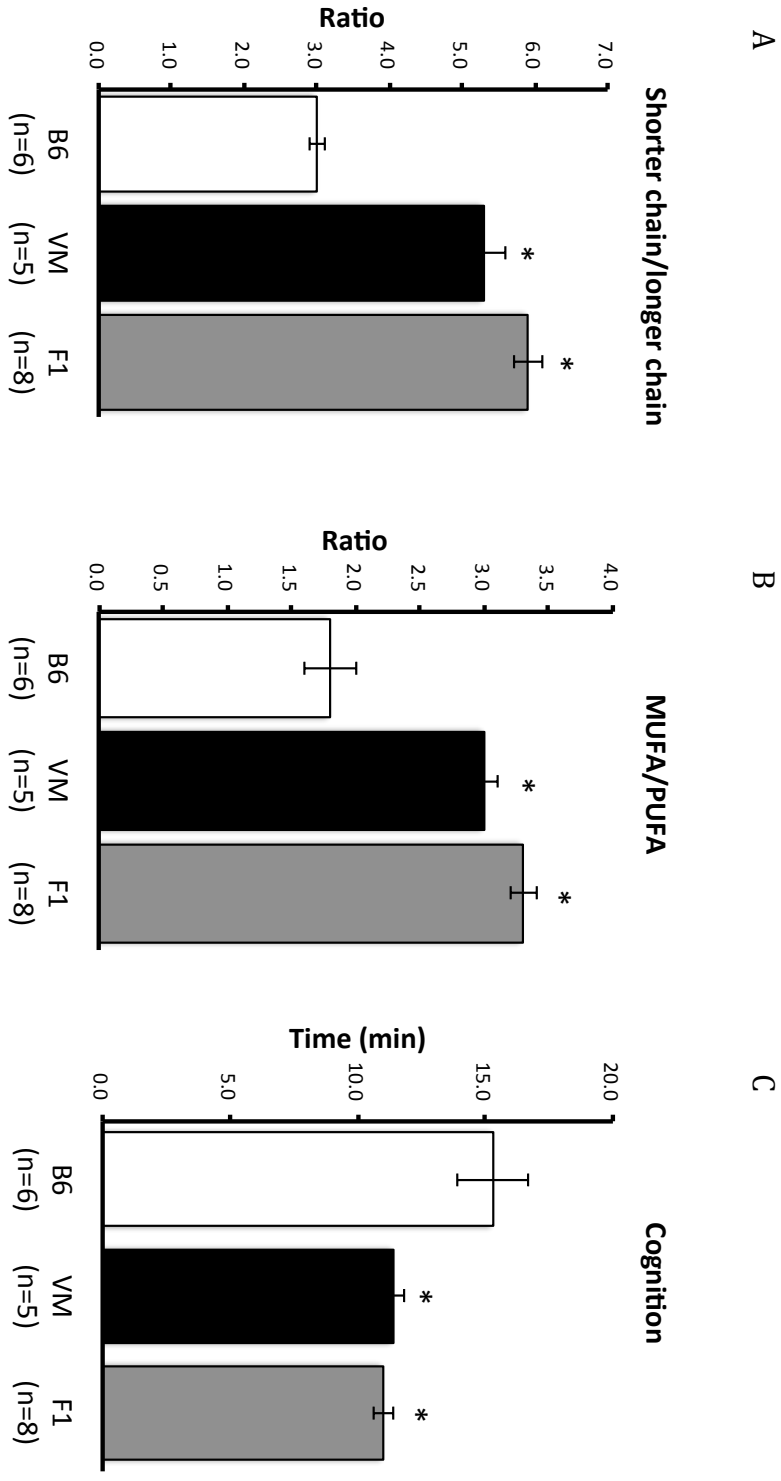
A
Shorter chain/longer chain
Ratio
0.0
1.0
2.0
3.0
4.0
5.0
6.0
7.0
B6 (n=6)
VM (n=5)
F1 (n=8)
*
*
B
MUFA/PUFA
Ratio
0.0
0.5
1.0
1.5
2.0
2.5
3.0
3.5
4.0
B6 (n=6)
VM (n=5)
F1 (n=8)
*
*
C
Cognition
Time (min)
0.0
5.0
10.0
15.0
20.0
B6 (n=6)
VM (n=5)
F1 (n=8)
*
*

APPENDIX

Publication related to Dissertation

Ta, NL, Seyfried TN. (2014) Autosomal dominant inheritance of brain cardiolipin fatty acid abnormality in VM/DK mice: association with hypoxic-induced cognitive insensitivity. *Lipids.* Jan;49(1):113-7.

Other publications

Meidenbauer JJ, **Ta N**, Seyfried TN. (2014) Influence of a ketogenic diet, fish-oil, and calorie restriction on plasma metabolites and lipids in C57BL/6J mice. *Nutr Metab (Lond).* May 22;11-23.

Dufort FJ, Gumina MR, **Ta NL**, Tao Y, Heyse SA, Scott DA, Richardson AD, Seyfried TN, Chiles TC. (2014) Glucose-dependent de novo lipogenesis in B lymphocytes: a requirement for atp-citrate lyase in lipopolysaccharide-induced differentiation. *J Biol Chem*. Mar 7;289(10):7011-24.

BIBLIOGRAPHY

Abuhusain, H. J., Matin, A., Qiao, Q. *et al.* (2013) A metabolic shift favoring sphingosine 1-phosphate at the expense of ceramide controls glioblastoma angiogenesis. *J Biol Chem,* 288, 37355-37364.

Acehan, D., Malhotra, A., Xu, Y., Ren, M., Stokes, D. L. and Schlame, M. (2011) Cardiolipin affects the supramolecular organization of atp synthase in mitochondria. *Biophys J,* 100, 2184-2192.

Alessandri, G., Filippeschi, S., Sinibaldi, P., Mornet, F., Passera, P., Spreafico, F., Cappa, P. M. and Gullino, P. M. (1987) Influence of gangliosides on primary and metastatic neoplastic growth in human and murine cells. *Cancer Res,* 47, 4243-4247.

Alli, P. M., Pinn, M. L., Jaffee, E. M., Mcfadden, J. M. and Kuhajda, F. P. (2005) Fatty acid synthase inhibitors are chemopreventive for mammary cancer in neu-n transgenic mice. *Oncogene,* 24, 39-46.

Alvarez-Tejado, M., Naranjo-Suarez, S., Jimenez, C., Carrera, A. C., Landazuri, M. O. and Del Peso, L. (2001) Hypoxia induces the activation of the phosphatidylinositol 3-kinase/akt cell survival pathway in pc12 cells: Protective role in apoptosis. *J Biol Chem,* 276, 22368-22374.

Baek, R. C., Kasperzyk, J. L., Platt, F. M. and Seyfried, T. N. (2004) N-butyldeoxygalactonojirimycin reduces brain ganglioside and gm2 content in neonatal sandhoff disease mice. *J. Neurochem (Suppl. 1),* 90, 89.

Baek, R. C., Kasperzyk, J. L., Platt, F. M. and Seyfried, T. N. (2008) N-butyldeoxygalactonojirimycin reduces brain ganglioside and gm2 content in neonatal sandhoff disease mice. *Neurochem Int,* 52, 1125-1133.

Barcelo-Coblijn, G., Collison, L. W., Jolly, C. A. and Murphy, E. J. (2005) Dietary alpha-linolenic acid increases brain but not heart and liver docosahexaenoic acid levels. *Lipids,* 40, 787-798.

Bauer, D. E., Hatzivassiliou, G., Zhao, F., Andreadis, C. and Thompson, C. B. (2005) Atp citrate lyase is an important component of cell growth and transformation. *Oncogene,* 24, 6314-6322.

Bayir, H., Tyurin, V. A., Tyurina, Y. Y. *et al.* (2007a) Selective early cardiolipin peroxidation after traumatic brain injury: An oxidative lipidomics analysis. *Ann Neurol,* 62, 154-169.

Beckers, A., Organe, S., Timmermans, L., Scheys, K., Peeters, A., Brusselmans, K., Verhoeven, G. and Swinnen, J. V. (2007) Chemical inhibition of acetyl-coa carboxylase induces growth arrest and cytotoxicity selectively in cancer cells. *Cancer Res,* 67, 8180-8187.

Benjamin, D. I., Cozzo, A., Ji, X., Roberts, L. S., Louie, S. M., Mulvihill, M. M., Luo, K. and Nomura, D. K. (2013) Ether lipid generating enzyme agps alters the balance of structural and signaling lipids to fuel cancer pathogenicity. *Proc Natl Acad Sci U S A,* 110, 14912-14917.

Bergum, C., Zoratti, G., Boerner, J. and List, K. (2012) Strong expression association between matriptase and its substrate prostasin in breast cancer. *J Cell Physiol,* 227, 1604-1609.

Berrigan, D., Perkins, S. N., Haines, D. C. and Hursting, S. D. (2002) Adult-onset calorie restriction and fasting delay spontaneous tumorigenesis in p53-deficient mice. *Carcinogenesis,* 23, 817-822.

Bifulco, M. (2005) Role of the isoprenoid pathway in ras transforming activity, cytoskeleton organization, cell proliferation and apoptosis. *Life Sci,* 77, 1740-1749.

Bloch, K. (1965) The biological synthesis of cholesterol. *Science,* 150, 19-28.

Bouterfa, H. L., Sattelmeyer, V., Czub, S., Vordermark, D., Roosen, K. and Tonn, J. C. (2000) Inhibition of ras farnesylation by lovastatin leads to downregulation of proliferation and migration in primary cultured human glioblastoma cells. *Anticancer Res,* 20, 2761-2771.

Cairns, R. A., Harris, I., Mccracken, S. and Mak, T. W. (2011) Cancer cell metabolism. *Cold Spring Harb Symp Quant Biol,* 76, 299-311.

Chang, S. H., Liu, C. H., Conway, R., Han, D. K., Nithipatikom, K., Trifan, O. C., Lane, T. F. and Hla, T. (2004) Role of prostaglandin e2-dependent angiogenic switch in cyclooxygenase 2-induced breast cancer progression. *Proc Natl Acad Sci U S A,* 101, 591-596.

Chen, H. W., Chang, Y. F., Chuang, H. Y., Tai, W. T. and Hwang, J. J. (2012) Targeted therapy with fatty acid synthase inhibitors in a human prostate carcinoma lncap/tk-luc-bearing animal model. *Prostate Cancer Prostatic Dis,* 15, 260-264.

Cheng, H., Mancuso, D. J., Jiang, X., Guan, S., Yang, J., Yang, K., Sun, G., Gross, R. W. and Han, X. (2008) Shotgun lipidomics reveals the temporally dependent, highly diversified cardiolipin profile in the mammalian brain: Temporally coordinated postnatal diversification of cardiolipin molecular species with neuronal remodeling. *Biochemistry,* 47, 5869-5880.

Chicco, A. J. and Sparagna, G. C. (2007) Role of cardiolipin alterations in mitochondrial dysfunction and disease. *American journal of physiology Cell physiology,* 292, C33-44.

Choi, H. J., Chung, T. W., Kang, S. K., Lee, Y. C., Ko, J. H., Kim, J. G. and Kim, C. H. (2006) Ganglioside gm3 modulates tumor suppressor pten-mediated cell cycle progression--transcriptional induction of p21(waf1) and p27(kip1) by inhibition of pi-3k/akt pathway. *Glycobiology,* 16, 573-583.

Claypool, S. M. and Koehler, C. M. (2011) The complexity of cardiolipin in health and disease. *Trends in biochemical sciences*.

Clendening, J. W., Pandyra, A., Boutros, P. C. *et al.* (2010) Dysregulation of the mevalonate pathway promotes transformation. *Proc Natl Acad Sci U S A,* 107, 15051-15056.

Colbeau, A., Nachbaur, J. and Vignais, P. M. (1971) Enzymic characterization and lipid composition of rat liver subcellular membranes. *Biochim Biophys Acta,* 249, 462-492.

Costello, L. C. and Franklin, R. B. (2005) 'Why do tumour cells glycolyse?': From glycolysis through citrate to lipogenesis. *Mol Cell Biochem,* 280, 1-8.

Dang, C. V., Hamaker, M., Sun, P., Le, A. and Gao, P. (2011) Therapeutic targeting of cancer cell metabolism. *J Mol Med (Berl),* 89, 205-212.

Dang, C. V. and Semenza, G. L. (1999) Oncogenic alterations of metabolism. *Trends Biochem Sci,* 24, 68-72.

Daum, G. (1985) Lipids of mitochondria. ***Biochim Biophys Acta,*** **822, 1-42.**

Deberardinis, R. J., Mancuso, A., Daikhin, E., Nissim, I., Yudkoff, M., Wehrli, S. and Thompson, C. B. (2007) Beyond aerobic glycolysis: Transformed cells can engage in glutamine metabolism that exceeds the requirement for protein and nucleotide synthesis. ***Proc Natl Acad Sci U S A,*** **104, 19345-19350.**

Ecsedy, J. A., Holthaus, K. A., Yohe, H. C. and Seyfried, T. N. (1999) Expression of mouse sialic acid on gangliosides of a human glioma grown as a xenograft in scid mice. ***J. Neurochem,*** **73, 254-259.**

Ellis, C. E., Murphy, E. J., Mitchell, D. C., Golovko, M. Y., Scaglia, F., Barcelo-Coblijn, G. C. and Nussbaum, R. L. (2005) Mitochondrial lipid abnormality and electron transport chain impairment in mice lacking alpha-synuclein. ***Mol Cell Biol,*** **25, 10190-10201.**

Fan, J., Kamphorst, J. J., Mathew, R., Chung, M. K., White, E., Shlomi, T. and Rabinowitz, J. D. (2013) Glutamine-driven oxidative phosphorylation is a major atp source in transformed mammalian cells in both normoxia and hypoxia. ***Mol Syst Biol,*** **9, 712.**

Filipp, F. V., Scott, D. A., Ronai, Z. A., Osterman, A. L. and Smith, J. W. (2012) Reverse tca cycle flux through isocitrate dehydrogenases 1 and 2 is required for lipogenesis in hypoxic melanoma cells. ***Pigment Cell Melanoma Res,*** **25, 375-383.**

Finsterer, J. (2008) Cognitive decline as a manifestation of mitochondrial disorders (mitochondrial dementia). ***Journal of the neurological sciences,*** **272, 20-33.**

Fraser, H. (1986) Brain tumours in mice, with particular reference to astrocytoma. ***Food Chem. Toxicol.,*** **24, 105-111.**

Fritz, V., Benfodda, Z., Rodier, G. ***et al.*** **(2010) Abrogation of de novo lipogenesis by stearoyl-coa desaturase 1 inhibition interferes with oncogenic signaling and blocks prostate cancer progression in mice.** ***Mol Cancer Ther,*** **9, 1740-1754.**

Fry, M., Blondin, G. A. and Green, D. E. (1980) The localization of tightly bound cardiolipin in cytochrome oxidase. ***J Biol Chem,*** **255, 9967-9970.**

Fry, M. and Green, D. E. (1981) Cardiolipin requirement for electron transfer in complex i and iii of the mitochondrial respiratory chain. ***J Biol Chem,*** **256, 1874-1880.**

Fujimoto, Y., Izumoto, S., Suzuki, T. ***et al.*** **(2005) Ganglioside gm3 inhibits proliferation and invasion of glioma.** ***J Neurooncol,*** **71, 99-106.**

Furuta, E., Pai, S. K., Zhan, R. ***et al.*** **(2008) Fatty acid synthase gene is up-regulated by hypoxia via activation of akt and sterol regulatory element binding protein-1.** ***Cancer Res,*** **68, 1003-1011.**

Gambhir, S. S. (2002) Molecular imaging of cancer with positron emission tomography. ***Nat Rev Cancer,*** **2, 683-693.**

Gorfe, A. A. (2010) Mechanisms of allostery and membrane attachment in ras gtpases: Implications for anti-cancer drug discovery. ***Curr Med Chem,*** **17, 1-9.**

Hackenbrock, C. R., Schneider, H., Lemasters, J. J. and Hochli, M. (1980) Relationships between bilayer lipid, motional freedom of oxidoreductase components, and electron transfer in the mitochondrial inner membrane. ***Adv Exp Med Biol,*** **132, 245-263.**

Hatzivassiliou, G., Zhao, F., Bauer, D. E., Andreadis, C., Shaw, A. N., Dhanak, D., Hingorani, S. R., Tuveson, D. A. and Thompson, C. B. (2005) Atp citrate lyase inhibition can suppress tumor cell growth. ***Cancer Cell,*** **8, 311-321.**

Hoch, F. L. (1992) Cardiolipins and biomembrane function. ***Biochim Biophys Acta,*** **1113, 71-133.**

Hoch, F. L. (1998) Cardiolipins and mitochondrial proton-selective leakage. ***J Bioenerg Biomembr,*** **30, 511-532.**

Hochachka, P. W., Rupert, J. L., Goldenberg, L., Gleave, M. and Kozlowski, P. (2002) Going malignant: The hypoxia-cancer connection in the prostate. ***Bioessays,*** **24, 749-757.**

Huysentruyt, L. C., Mukherjee, P., Banerjee, D., Shelton, L. M. and Seyfried, T. N. (2008a) Metastatic cancer cells with macrophage properties: Evidence from a new murine tumor model. ***Int J Cancer,*** **123, 73-84.**

Jennemann, R., Mennel, H. D., Bauer, B. L. and Wiegandt, H. (1994) Glycosphingolipid component profiles of human gliomas correlate with histological tumour types: Analysis of inter-individual and tumour-regional distribution. ***Acta Neurochir Wien,*** **126, 170-178.**

Jump, D. B. (2009) Mammalian fatty acid elongases. ***Methods Mol Biol,*** **579, 375-389.**

Kamphorst, J. J., Cross, J. R., Fan, J., De Stanchina, E., Mathew, R., White, E. P., Thompson, C. B. and Rabinowitz, J. D. (2013) Hypoxic and ras-transformed cells support growth by scavenging unsaturated fatty acids from lysophospholipids. ***Proc Natl Acad Sci U S A,*** **110, 8882-8887.**

Karmali, R. A. (1986) Eicosanoids and cancer. ***Prog Clin Biol Res,*** **222, 687-697.**

Kasperzyk, J. L., D'azzo, A., Platt, F. M., Alroy, J. and Seyfried, T. N. (2005) Substrate reduction reduces gangliosides in postnatal cerebrum-brainstem and cerebellum in gm1 gangliosidosis mice. ***J Lipid Res,*** **46, 744-751.**

Kasperzyk, J. L., El-Abbadi, M. M., Hauser, E. C., D'azzo, A., Platt, F. M. and Seyfried, T. N. (2004) N-butyldeoxygalactonojirimycin reduces neonatal brain ganglioside content in a mouse model of gm1 gangliosidosis. ***J Neurochem,*** **89, 645-653.**

Kiebish, M. A., Han, X., Cheng, H., Chuang, J. H. and Seyfried, T. N. (2008a) Brain mitochondrial lipid abnormalities in mice susceptible to spontaneous gliomas. ***Lipids,*** **43, 951-959.**

Kiebish, M. A., Han, X., Cheng, H., Chuang, J. H. and Seyfried, T. N. (2008b) Cardiolipin and electron transport chain abnormalities in mouse brain tumor mitochondria: Lipidomic evidence supporting the warburg theory of cancer. ***J Lipid Res,*** **49, 2545-2556.**

Kiebish, M. A., Han, X., Cheng, H., Lunceford, A., Clarke, C. F., Moon, H., Chuang, J. H. and Seyfried, T. N. (2008c) Lipidomic analysis and

electron transport chain activities in c57bl/6j mouse brain mitochondria. ***J Neurochem,*** **106, 299-312.**

Kiebish, M. A., Han, X., Cheng, H. and Seyfried, N. T. (2007) Mitochondrial lipid and electron transport chain abnormalities in mouse brain tumors ***J. Neurochem.,*** **102 (Suppl. 1), 64.**

Kim, W. S., Kim, M. M., Choi, H. J., Yoon, S. S., Lee, M. H., Park, K., Park, C. H. and Kang, W. K. (2001) Phase ii study of high-dose lovastatin in patients with advanced gastric adenocarcinoma. ***Invest New Drugs,*** **19, 81-83.**

Koike, T., Kimura, N., Miyazaki, K. ***et al.*** **(2004) Hypoxia induces adhesion molecules on cancer cells: A missing link between warburg effect and induction of selectin-ligand carbohydrates.** ***Proc Natl Acad Sci U S A,*** **101, 8132-8137.**

Koochekpour, S. and Pilkington, G. J. (1996) Vascular and perivascular gd3 expression in human glioma. ***Cancer Lett,*** **104, 97-102.**

Kovacevic, Z. and Mcgivan, J. D. (1983) Mitochondrial metabolism of glutamine and glutamate and its physiological significance. ***Physiol Rev,*** **63, 547-605.**

Kraffe, E., Soudant, P., Marty, Y., Kervarec, N. and Jehan, P. (2002) Evidence of a tetradocosahexaenoic cardiolipin in some marine bivalves. ***Lipids,*** **37, 507-514.**

Kridel, S. J., Axelrod, F., Rozenkrantz, N. and Smith, J. W. (2004) Orlistat is a novel inhibitor of fatty acid synthase with antitumor activity. ***Cancer Res,*** **64, 2070-2075.**

Kuemmerle, N. B., Rysman, E., Lombardo, P. S. ***et al.*** **(2011) Lipoprotein lipase links dietary fat to solid tumor cell proliferation.** ***Mol Cancer Ther,*** **10, 427-436.**

Larner, J., Jane, J., Laws, E., Packer, R., Myers, C. and Shaffrey, M. (1998) A phase i-ii trial of lovastatin for anaplastic astrocytoma and glioblastoma multiforme. ***Am J Clin Oncol,*** **21, 579-583.**

Lepage, G. and Roy, C. C. (1984) Improved recovery of fatty acid through direct transesterification without prior extraction or purification. ***J Lipid Res,*** **25, 1391-1396.**

Lersch, C., Schmelz, R., Erdmann, J., Hollweck, R., Schulte-Frohlinde, E., Eckel, F., Nader, M. and Schusdziarra, V. (2004) Treatment of hcc with pravastatin, octreotide, or gemcitabine--a critical evaluation. ***Hepatogastroenterology,*** **51, 1099-1103.**

Liu, K. and Czaja, M. J. (2013) Regulation of lipid stores and metabolism by lipophagy. ***Cell Death Differ,*** **20, 3-11.**

Liu, Y. (2006) Fatty acid oxidation is a dominant bioenergetic pathway in prostate cancer. ***Prostate Cancer Prostatic Dis,*** **9, 230-234.**

Louie, S. M., Roberts, L. S., Mulvihill, M. M., Luo, K. and Nomura, D. K. (2013) Cancer cells incorporate and remodel exogenous palmitate into structural and oncogenic signaling lipids. ***Biochim Biophys Acta,*** **1831, 1566-1572.**

Lu, W., Pelicano, H. and Huang, P. (2010) Cancer metabolism: Is glutamine sweeter than glucose? ***Cancer Cell,*** **18, 199-200.**

Lunt, S. Y. and Vander Heiden, M. G. (2011) Aerobic glycolysis: Meeting the metabolic requirements of cell proliferation. ***Annu Rev Cell Dev Biol,*** **27, 441-464.**

Macala, L. J., Yu, R. K. and Ando, S. (1983) Analysis of brain lipids by high performance thin-layer chromatography and densitometry. ***J Lipid Res,*** **24, 1243-1250.**

Maher, E. A., Marin-Valencia, I., Bachoo, R. M. ***et al.*** **(2012) Metabolism of [u-13 c]glucose in human brain tumors in vivo.** ***NMR Biomed,*** **25, 1234-1244.**

Mancuso, D. J., Kotzbauer, P., Wozniak, D. F. ***et al.*** **(2009) Genetic ablation of calcium-independent phospholipase a2{gamma} leads to alterations in hippocampal cardiolipin content and molecular species distribution, mitochondrial degeneration, autophagy, and cognitive dysfunction.** ***J Biol Chem,*** **284, 35632-35644.**

Mason, P., Liang, B., Li, L. *et al.* (2012) Scd1 inhibition causes cancer cell death by depleting mono-unsaturated fatty acids. *PLoS One,* 7, e33823.

Mathupala, S. P., Rempel, A. and Pedersen, P. L. (2001) Glucose catabolism in cancer cells: Identification and characterization of a marked activation response of the type ii hexokinase gene to hypoxic conditions. *J Biol Chem,* 276, 43407-43412.

Mazure, N. M. and Pouyssegur, J. (2009) Atypical bh3-domains of bnip3 and bnip3l lead to autophagy in hypoxia. *Autophagy,* 5, 868-869.

Mcguirk, S., Gravel, S. P., Deblois, G. *et al.* (2013) Pgc-1alpha supports glutamine metabolism in breast cancer. *Cancer Metab,* 1, 22.

Mckeehan, W. L. (1982) Glycolysis, glutaminolysis and cell proliferation. *Cell Biol Int Rep,* 6, 635-650.

Medes, G., Thomas, A. and Weinhouse, S. (1953) Metabolism of neoplastic tissue. Iv. A study of lipid synthesis in neoplastic tissue slices in vitro. *Cancer Res,* 13, 27-29.

Menendez, J. A. and Lupu, R. (2007) Fatty acid synthase and the lipogenic phenotype in cancer pathogenesis. *Nat Rev Cancer,* 7, 763-777.

Meng, M., Chen, S., Lao, T., Liang, D. and Sang, N. (2010) Nitrogen anabolism underlies the importance of glutaminolysis in proliferating cells. *Cell Cycle,* 9, 3921-3932.

Metallo, C. M., Gameiro, P. A., Bell, E. L. *et al.* (2012) Reductive glutamine metabolism by idh1 mediates lipogenesis under hypoxia. *Nature,* 481, 380-384.

Milgraum, L. Z., Witters, L. A., Pasternack, G. R. and Kuhajda, F. P. (1997) Enzymes of the fatty acid synthesis pathway are highly expressed in in situ breast carcinoma. *Clin Cancer Res,* 3, 2115-2120.

Mills, G. B. and Moolenaar, W. H. (2003) The emerging role of lysophosphatidic acid in cancer. *Nat Rev Cancer,* 3, 582-591.

Morad, S. A. and Cabot, M. C. (2013) Ceramide-orchestrated signalling in cancer cells. *Nat Rev Cancer,* 13, 51-65.

Moreadith, R. W. and Lehninger, A. L. (1984) The pathways of glutamate and glutamine oxidation by tumor cell mitochondria. Role of mitochondrial nad(p)+-dependent malic enzyme. *J Biol Chem,* 259, 6215-6221.

Nakatsuji, Y. and Miller, R. H. (2001) Selective cell-cycle arrest and induction of apoptosis in proliferating neural cells by ganglioside gm3. *Exp Neurol,* 168, 290-299.

Nguyen, A. D., Mcdonald, J. G., Bruick, R. K. and Debose-Boyd, R. A. (2007) Hypoxia stimulates degradation of 3-hydroxy-3-methylglutaryl-coenzyme a reductase through accumulation of lanosterol and hypoxia-inducible factor-mediated induction of insigs. *J Biol Chem,* 282, 27436-27446.

Nomura, D. K., Long, J. Z., Niessen, S., Hoover, H. S., Ng, S. W. and Cravatt, B. F. (2010) Monoacylglycerol lipase regulates a fatty acid network that promotes cancer pathogenesis. *Cell,* 140, 49-61.

Ookhtens, M., Kannan, R., Lyon, I. and Baker, N. (1984) Liver and adipose tissue contributions to newly formed fatty acids in an ascites tumor. *Am J Physiol,* 247, R146-153.

Opstad, K. S., Ladroue, C., Bell, B. A., Griffiths, J. R. and Howe, F. A. (2007) Linear discriminant analysis of brain tumour (1)h mr spectra: A comparison of classification using whole spectra versus metabolite quantification. *NMR Biomed,* 20, 763-770.

Park, J. B., Lee, C. S., Jang, J. H., Ghim, J., Kim, Y. J., You, S., Hwang, D., Suh, P. G. and Ryu, S. H. (2012) Phospholipase signalling networks in cancer. *Nat Rev Cancer,* 12, 782-792.

Petrosillo, G., De Benedictis, V., Ruggiero, F. M. and Paradies, G. (2013) Decline in cytochrome c oxidase activity in rat-brain mitochondria with aging. Role of peroxidized cardiolipin and beneficial effect of melatonin. *Journal of bioenergetics and biomembranes*.

Piva, T. J. and Mcevoy-Bowe, E. (1998) Oxidation of glutamine in hela cells: Role and control of truncated tca cycles in tumour mitochondria. *J Cell Biochem,* 68, 213-225.

Pizer, E. S., Chrest, F. J., Digiuseppe, J. A. and Han, W. F. (1998a) Pharmacological inhibitors of mammalian fatty acid synthase suppress DNA replication and induce apoptosis in tumor cell lines. *Cancer Res,* 58, 4611-4615.

Pizer, E. S., Lax, S. F., Kuhajda, F. P., Pasternack, G. R. and Kurman, R. J. (1998b) Fatty acid synthase expression in endometrial carcinoma: Correlation with cell proliferation and hormone receptors. *Cancer,* 83, 528-537.

Pizer, E. S., Wood, F. D., Heine, H. S., Romantsev, F. E., Pasternack, G. R. and Kuhajda, F. P. (1996) Inhibition of fatty acid synthesis delays disease progression in a xenograft model of ovarian cancer. *Cancer Res,* 56, 1189-1193.

Pope, S., Land, J. M. and Heales, S. J. (2008a) Oxidative stress and mitochondrial dysfunction in neurodegeneration; cardiolipin a critical target? *Biochim Biophys Acta,* 1777, 794-799.

Pope, S., Land, J. M. and Heales, S. J. (2008b) Oxidative stress and mitochondrial dysfunction in neurodegeneration; cardiolipin a critical target? *Biochim Biophys Acta*.

Portais, J. C., Voisin, P., Merle, M. and Canioni, P. (1996) Glucose and glutamine metabolism in c6 glioma cells studied by carbon 13 nmr. *Biochimie,* 78, 155-164.

Pyne, N. J. and Pyne, S. (2010) Sphingosine 1-phosphate and cancer. *Nat Rev Cancer,* 10, 489-503.

Qu, W., Oya, S., Lieberman, B. P. *et al.* (2012) Preparation and characterization of l-[5-11c]-glutamine for metabolic imaging of tumors. *J Nucl Med,* 53, 98-105.

Rebbaa, A., Hurh, J., Yamamoto, H., Kersey, D. S. and Bremer, E. G. (1996) Ganglioside gm3 inhibition of egf receptor mediated signal transduction. *Glycobiology,* 6, 399-406.

Reitzer, L. J., Wice, B. M. and Kennell, D. (1979) Evidence that glutamine, not sugar, is the major energy source for cultured hela cells. *J Biol Chem,* 254, 2669-2676.

Rodriguez-Enriquez, S., Marin-Hernandez, A., Gallardo-Perez, J. C., Carreno-Fuentes, L. and Moreno-Sanchez, R. (2009) Targeting of cancer energy metabolism. ***Mol Nutr Food Res,*** **53, 29-48.**

Rolin, J. and Maghazachi, A. A. (2011) Effects of lysophospholipids on tumor microenvironment. ***Cancer Microenviron,*** **4, 393-403.**

Roongta, U. V., Pabalan, J. G., Wang, X. ***et al.*** **(2011) Cancer cell dependence on unsaturated fatty acids implicates stearoyl-coa desaturase as a target for cancer therapy.** ***Mol Cancer Res,*** **9, 1551-1561.**

Rothblat, G. H., Arbogast, L. Y., Ouellette, L. and Howard, B. V. (1976) Preparation of delipidized serum protein for use in cell culture systems. ***In Vitro,*** **12, 554-557.**

Santos, C. R. and Schulze, A. (2012) Lipid metabolism in cancer. ***Febs J,*** **279, 2610-2623.**

Schlame, M., Rua, D. and Greenberg, M. L. (2000) The biosynthesis and functional role of cardiolipin. ***Prog Lipid Res,*** **39, 257-288.**

Scott, D. A., Richardson, A. D., Filipp, F. V., Knutzen, C. A., Chiang, G. G., Ronai, Z. A., Osterman, A. L. and Smith, J. W. (2011) Comparative metabolic flux profiling of melanoma cell lines: Beyond the warburg effect. ***J Biol Chem*****.**

Semenza, G. L. (2007) Hif-1 mediates the warburg effect in clear cell renal carcinoma. ***J Bioenerg Biomembr,*** **39, 231-234.**

Semenza, G. L., Artemov, D., Bedi, A. ***et al.*** **(2001) 'The metabolism of tumours': 70 years later.** ***Novartis Found Symp,*** **240, 251-260; discussion 260-254.**

Semenza, G. L., Jiang, B. H., Leung, S. W., Passantino, R., Concordet, J. P., Maire, P. and Giallongo, A. (1996) Hypoxia response elements in the aldolase a, enolase 1, and lactate dehydrogenase a gene promoters contain essential binding sites for hypoxia-inducible factor 1. ***J Biol Chem,*** **271, 32529-32537.**

Seyfried, T. N. (1979) Audiogenic seizures in mice. ***Federation proceedings,*** **38, 2399-2404.**

Seyfried, T. N. (2012) ***Cancer as a metabolic disease: On the origin, management, and prevention of cancer*****. John Wiley & Sons, Hoboken.**

Seyfried, T. N., Flores, R., Poff, A. M., D'agostino, D. P. and Mukherjee, P. (2014) Metabolic therapy: A new paradigm for managing malignant brain cancer. ***Cancer Lett.***

Seyfried, T. N., Glaser, G. H. and Yu, R. K. (1978) Cerebral, cerebellar, and brain stem gangliosides in mice susceptible to audiogenic seizures. ***J. Neurochem.,*** **31, 21-27.**

Seyfried, T. N. and Mukherjee, P. (2010a) Ganglioside gm3 is antiangiogenic in malignant brain cancer. ***J Oncol,*** **2010, 961243.**

Seyfried, T. N. and Shelton, L. M. (2010b) Cancer as a metabolic disease. ***Nutr Metab (Lond),*** **7, 7.**

Singh, R. and Cuervo, A. M. (2012) Lipophagy: Connecting autophagy and lipid metabolism. ***Int J Cell Biol,*** **2012, 282041.**

Song, W. X., Vacca, M. F., Welti, R. and Rintoul, D. A. (1991) Effects of gangliosides gm3 and de-n-acetyl gm3 on epidermal growth factor receptor kinase activity and cell growth. ***J Biol Chem,*** **266, 10174-10181.**

Souba, W. W. (1993) Glutamine and cancer. ***Ann Surg,*** **218, 715-728.**

Stoll, L. L. and Spector, A. A. (1984) Changes in serum influence the fatty acid composition of established cell lines. ***In Vitro,*** **20, 732-738.**

Summons, R. E., Bradley, A. S., Jahnke, L. L. and Waldbauer, J. R. (2006) Steroids, triterpenoids and molecular oxygen. ***Philos Trans R Soc Lond B Biol Sci,*** **361, 951-968.**

Swinnen, J. V., Brusselmans, K. and Verhoeven, G. (2006) Increased lipogenesis in cancer cells: New players, novel targets. ***Curr Opin Clin Nutr Metab Care,*** **9, 358-365.**

Tagami, S., Inokuchi Ji, J., Kabayama, K. ***et al.*** **(2002) Ganglioside gm3 participates in the pathological conditions of insulin resistance.** ***J Biol Chem,*** **277, 3085-3092.**

Teicher, B. A., Linehan, W. M. and Helman, L. J. (2012) Targeting cancer metabolism. ***Clin Cancer Res,*** **18, 5537-5545.**

Thibault, A., Samid, D., Tompkins, A. C. ***et al.*** **(1996) Phase i study of lovastatin, an inhibitor of the mevalonate pathway, in patients with cancer.** ***Clin Cancer Res,*** **2, 483-491.**

Thomas, R. H., Meeking, M. M., Mepham, J. R., Tichenoff, L., Possmayer, F., Liu, S. and Macfabe, D. F. (2012) The enteric bacterial metabolite propionic acid alters brain and plasma phospholipid molecular species: Further development of a rodent model of autism spectrum disorders. ***Journal of neuroinflammation,*** **9, 153.**

Todorova, M. T., Burwell, T. J. and Seyfried, T. N. (1999) Environmental risk factors for multifactorial epilepsy in el mice. ***Epilepsia,*** **40, 1697-1707.**

Todorova, M. T., Mantis, J. G., Le, M., Kim, C. Y. and Seyfried, T. N. (2006) Genetic and environmental interactions determine seizure susceptibility in epileptic el mice. ***Genes Brain Behav,*** **5, 518-527.**

Tugnoli, V., Tosi, M. R., Tinti, A., Trinchero, A., Bottura, G. and Fini, G. (2001) Characterization of lipids from human brain tissues by multinuclear magnetic resonance spectroscopy. ***Biopolymers,*** **62, 297-306.**

Van Den Heuvel, A. P., Jing, J., Wooster, R. F. and Bachman, K. E. (2012) Analysis of glutamine dependency in non-small cell lung cancer: Gls1 splice variant gac is essential for cancer cell growth. ***Cancer Biol Ther,*** **13, 1185-1194.**

Van Meyel, D. J., Sanchez-Sweatman, O. H., Kerkvliet, N., Stitt, L., Ramsay, D. A., Khokha, R., Chambers, A. F. and Cairncross, J. G. (1998) Genetic background influences timing, morphology and dissemination of lymphomas in p53-deficient mice. ***Int J Oncol,*** **13, 917-922.**

Vander Heiden, M. G. (2011) Targeting cancer metabolism: A therapeutic window opens. ***Nat Rev Drug Discov,*** **10, 671-684.**

Vander Heiden, M. G., Cantley, L. C. and Thompson, C. B. (2009) Understanding the warburg effect: The metabolic requirements of cell proliferation. ***Science,*** **324, 1029-1033.**

Vazquez-Martin, A., Colomer, R., Brunet, J., Lupu, R. and Menendez, J. A. (2008) Overexpression of fatty acid synthase gene activates her1/her2 tyrosine kinase receptors in human breast epithelial cells. ***Cell Prolif,*** **41, 59-85.**

Vreken, P., Valianpour, F., Nijtmans, L. G., Grivell, L. A., Plecko, B., Wanders, R. J. and Barth, P. G. (2000) Defective remodeling of cardiolipin and phosphatidylglycerol in barth syndrome. ***Biochem Biophys Res Commun,*** **279, 378-382.**

Wang, D., Wang, H., Brown, J. ***et al.*** **(2006) Cxcl1 induced by prostaglandin e2 promotes angiogenesis in colorectal cancer.** ***J Exp Med,*** **203, 941-951.**

Wang, H. Y., Jackson, S. N. and Woods, A. S. (2007) Direct maldi-ms analysis of cardiolipin from rat organs sections. ***J Am Soc Mass Spectrom,*** **18, 567-577.**

Warburg, O., Wind, F. and Negelein, E. (1927) The metabolism of tumors in the body. ***J Gen Physiol,*** **8, 519-530.**

Weljie, A. M. and Jirik, F. R. (2011) Hypoxia-induced metabolic shifts in cancer cells: Moving beyond the warburg effect. ***Int J Biochem Cell Biol,*** **43, 981-989.**

Wen, P. Y. and Kesari, S. (2008) Malignant gliomas in adults. ***N Engl J Med,*** **359, 492-507.**

Wise, D. R., Ward, P. S., Shay, J. E. ***et al.*** **(2011) Hypoxia promotes isocitrate dehydrogenase-dependent carboxylation of alpha-ketoglutarate to citrate to support cell growth and viability.** ***Proc Natl Acad Sci U S A,*** **108, 19611-19616.**

Wittig, I. and Schagger, H. (2009) Supramolecular organization of atp synthase and respiratory chain in mitochondrial membranes. ***Biochim Biophys Acta,*** **1787, 672-680.**

Wolf, A., Agnihotri, S. and Guha, A. (2010) Targeting metabolic remodeling in glioblastoma multiforme. ***Oncotarget,*** **1, 552-562.**

Yates, A. J., Thompson, D. K., Boesel, C. P., Albrightson, C. and Hart, R. W. (1979) Lipid composition of human neural tumors. ***J Lipid Res,*** **20, 428-436.**

Yin, J., Miyazaki, K., Shaner, R. L., Merrill, A. H., Jr. and Kannagi, R. (2010) Altered sphingolipid metabolism induced by tumor hypoxia - new vistas in glycolipid tumor markers. ***FEBS Lett,*** **584, 1872-1878.**

Yuneva, M. (2008) Finding an "achilles' heel" of cancer: The role of glucose and glutamine metabolism in the survival of transformed cells. ***Cell Cycle,*** **7, 2083-2089.**

Zhang, F. and Du, G. (2012) Dysregulated lipid metabolism in cancer. ***World J Biol Chem,*** **3, 167-174.**

Zhang, H., Bosch-Marce, M., Shimoda, L. A., Tan, Y. S., Baek, J. H., Wesley, J. B., Gonzalez, F. J. and Semenza, G. L. (2008) Mitochondrial autophagy is an hif-1-dependent adaptive metabolic response to hypoxia. ***J Biol Chem,*** **283, 10892-10903.**

Zhang, H., Gao, P., Fukuda, R., Kumar, G., Krishnamachary, B., Zeller, K. I., Dang, C. V. and Semenza, G. L. (2007) Hif-1 inhibits mitochondrial biogenesis and cellular respiration in vhl-deficient renal cell carcinoma by repression of c-myc activity. ***Cancer Cell,*** **11, 407-420.**

Zhong, W. B., Liang, Y. C., Wang, C. Y., Chang, T. C. and Lee, W. S. (2005) Lovastatin suppresses invasiveness of anaplastic thyroid cancer cells by inhibiting rho geranylgeranylation and rhoa/rock signaling. ***Endocr Relat Cancer,*** **12, 615-629.**

Ziche, M., Morbidelli, L., Alessandri, G. and Gullino, P. M. (1992) Angiogenesis can be stimulated or repressed in vivo by a change in gm3:Gd3 ganglioside ratio. ***Lab. Invest.,*** **67, 711-715.**